Surface Science Reports 72 (2017) 59–104

Contents lists available at ScienceDirect

Surface Science Reports

journal homepage: www.elsevier.com/locate/surfrep

Use of molecular beams for kinetic measurements of chemical reactions on solid surfaces

Francisco Zaera

Department of Chemistry and UCR Center for Catalysis, University of California, Riverside, CA 92521, USA

ARTICLE INFO

Article history:
Received 8 November 2016
Received in revised form
16 February 2017
Accepted 17 February 2017
Available online 15 March 2017

Keywords:
Molecular beams
Kinetics
Dynamics
Adsorption
Catalysis
Etching
Surface oxidation
Film deposition

ABSTRACT

In this review we survey the contributions that molecular beam experiments have provided to our understanding of the dynamics and kinetics of chemical interactions of gas molecules with solid surfaces. First, we describe the experimental details of the different instrumental setups and approaches available for the study of these systems under the ultrahigh vacuum conditions and with the model planar surfaces often used in modern surface-science experiments. Next, a discussion is provided of the most important fundamental aspects of the dynamics of chemical adsorption that have been elucidated with the help of molecular beam experiments, which include the development of potential energy surfaces, the determination of the different channels for energy exchange between the incoming molecules and the surface, the identification of adsorption precursor states, the understanding of dissociative chemisorption, the determination of the contributions of corrugation, steps, and other structural details of the surface to the adsorption process, the effect to molecular steering, the identification of avenues for assisting adsorption, and the molecular details associated with the kinetics of the uptake of adsorbates as a function of coverage. We follow with a summary of the work directed at the determination of kinetic parameters and mechanistic details of surface reactions associated with catalysis, mostly those promoted by late transition metals. This discussion we initiate with an overview of what has been learned about simple bimolecular reactions such as the oxidation of CO and H_2 with O_2 and the reaction of CO with NO, and continue with the review of the studies of more complex systems such as the oxidation of alcohols, the conversion of organic acids, the hydrogenation and isomerization of olefins, and the oxidative activation of alkanes under conditions of short contact times. Sections 6 and 7 of this review deal with the advances made in the use of molecular beams with more realistic models for catalysis, using surfaces comprised of metal nanoparticles dispersed on the oxide surfaces used as catalyst support and high-flux beams to approach the pressures used in catalysis. The next section deals with the study of systems associated with fields other than catalysis, mainly with the etching and oxidation of semiconductor surfaces and with the chemistry used to grow thin solid films by chemical means (chemical vapor deposition, CVD, or atomic layer deposition, ALD). We end with a personal assessment of the past accomplishments, present state, and future promise of the use of molecular beams for the study of the kinetics of surface reactions relevant to practical applications.

Contents

E-mail address: zaera@ucr.edu

http://dx.doi.org/10.1016/j.surfrep.2017.02.002
0167-5729/

1. Introduction

Molecular beam techniques capable of controlling the direction and energy of reactants were initially developed in response to the desire to investigate the dynamics of gas-phase reactions [1], but those setups were soon adapted to study the dynamics and kinetics of reactions on solid surfaces as well. To date, the use of molecular beams remains one of very few approaches available to surface scientists for the measurement of the kinetics of reactions on surfaces in a systematic way. Much was learned in the early studies with molecular beams about the dynamics of adsorption processes with simple molecules, as nicely summarized in early reviews [2–10]. By adding external sources of excitation, either optical or electrostatic, it also became possible to study gas-surface interactions with molecules prepared in particular excitation states [10–12]. Later, the use of molecular beams was extended to the study of the kinetics of simple reactions such as H_2+D_2 isotope scrambling and CO oxidation with O_2. Unfortunately, there has not been much research with molecular beams directed towards the study of more complex and interesting systems, perhaps because of the apparent complexity of the instrumentation required. This may be true with the supersonic beams often used for dynamics measurements, where control of the energetics of the incoming molecules is required. However, here we argue that meaningful experiments to extract kinetic information about surface reactions can also be performed with very simple effusive collimated beams [13,14]. Several modern examples from our group and others will be provided to illustrate the complexity of the problems that can be addressed with the MB approach, to illustrate the type of information that can be extracted, and to highlight its strengths and weaknesses, ending with a perspective on the (possible) future of the field.

As mentioned above, many excellent reviews have been written already on the use of molecular beams in surface science. Our emphasis here will be mainly on discussing the work on the kinetics of reactions of relevance to catalysis and other practical applications, to build up on previous reviews that we have published in the past on related themes [13–15], although reference to other applications will also be referenced. This review intends to be somewhat comprehensive, covering most of the relevant work

involving molecular beam experiments on surfaces. We initiate this review with a brief overview of the experimental setups available, and with a discussion of the two main types of molecular beam approaches possible, namely, supersonic and effusive. Next, we introduce the use of molecular beams to follow the dynamics and kinetics of adsorption processes. We follow with a brief summary of the information derived from studies of simple reactions such as H_2+D_2, $CO+O_2$, and CO+NO. A review is then offered on what has been learned from molecular beam experiments on other more complex high-probability catalytic reactions such as the oxidation of alcohols and the conversion of hydrocarbons. Next, we discuss studies of more complex systems, on surfaces comprised of metal nanoparticles dispersed on oxide films, designed to better emulate the surfaces active in heterogeneous catalysis, and of low-probability reactions, which are also pervasive in catalysis. Finally, we provide a few examples of uses of molecular beams for the study of non-catalytic systems relevant to other areas of surface science, with particular emphasis on the etching and oxidation of semiconductor materials and on the deposition of thin films by chemical means. We conclude with a brief assessment of the present and future of the use of molecular beams for the study of the surface chemistry of problems with practical applications.

2. Experimental considerations

Molecular beams are used in kinetic studies on surfaces as a way to introduce gas-phase reacting species into the ultrahigh vacuum (UHV) environment typically used in such research [7,9,16–18]. The beam is directed at the solid surface of interest, where surface reactions may lead to the formation of new products. The scattered reactants and products are then detected, identified, and quantified, usually by using mass spectrometry (which can be multiplexed to follow several masses at once in a single experiment). One key feature that makes molecular beam studies of gas–surface interactions unique is that they are carried out in a collision-free environment, which ensures that there is only a single surface interaction event per molecule. The collision-free environment affords the characterization of gas-surface dynamics, the quantitation of adsorption kinetics, the detection of products from primary surface reactions, and the measurements of both transient and steady-state kinetics. In this review, our emphasis is mainly on surveying the advances made in the last two topics of this list.

The main feature that makes molecular beams so useful is their directionality. Collimated beams can be aimed selectively at the surface of interest, creating a reacting environment above such surface while maintaining good-quality vacuum in the surroundings. Surfaces exposed to molecular beams can experience fluxes equivalent to pressures much higher than those typically used in surface-science studies. In addition, the directionality of the beams affords the investigation of reactivity on the surface as a function of the angle of incidence of the reactants. The molecular beam work may be combined with studies of the angular distribution of the desorbing species, which can be accomplished by either placing the detecting element (the mass spectrometer) on a rotating platform [19], or, in a more limited way, by rotating the surface itself.

Depending on the experimental setup used, other parameters may be controlled in molecular beam studies as well [3,11,20]. For instance, the translational energy of the beam may be narrowed and tuned via the use of supersonic expansion. The population of the different energy levels in vibrational and rotational degrees of freedom may be manipulated as well, by, for example, intersecting the gas beam with infrared light from a narrow-bandwidth tunable laser. The initial electronic, vibrational, and rotational energy states, together with the molecular orientation and the point of impact at the surface, are parameters that can greatly influence the reactivity of molecules upon collision with a surface, and these effects can be studied by state-resolved experiments involving the combination of molecular beams with photon, electron, or ion excitation and angle-resolved detection techniques.

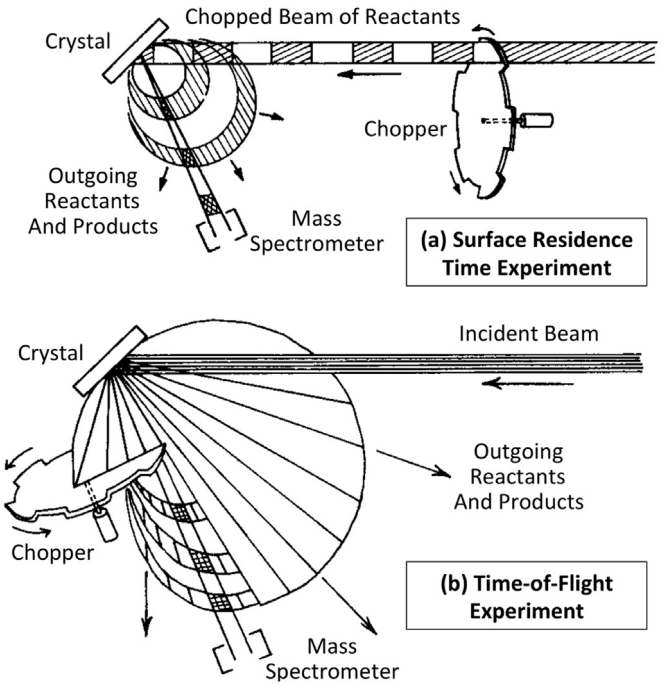

Fig. 1. Schematic representation of the two main designs available for the use of chopping in molecular beam experiments [25]. In the top diagram, the chopper is used to modulate the incoming beam in order to measure the kinetics of transient phenomena on the surface, including the residence time of adsorbates. In the lower diagram, modulation is done on the scattered or desorbing molecules in order to estimate their velocity distributions. Reproduced from Ref. [25] with permission, Copyright 1981 American Vacuum Society.

Beam modulation, using timed valves, or, more commonly, choppers, can also be added to test transient kinetic behavior, to, for instance, separate mass transport from chemical conversion steps [21–24]. This modulation can be introduced in the incoming beam, to measure surface residence times, for example, or at the exit channel, in time-of-flight experiments (Fig. 1) [25]. Several choppers can be used and synchronized to study surface dynamics at short time scales. Small modulations around equilibrium or under steady-state kinetic regimes can be used to probe the kinetic parameters of a reaction under isothermal and isosteric conditions, to separate the effects exerted by temperature and coverage on the overall kinetics of reaction [13,26].

There are, broadly speaking, two types of gas-phase beams used in kinetic studies on surfaces: supersonic (nozzle), and effusive. These are briefly described next.

2.1. Types of molecular beams

Depending on the type of gas expansion used to produce the gas beams, those can be grouped into effusive or supersonic [27]. In effusive beams, the gas is typically fed into the UHV chamber through capillary tubes under conditions where molecular flow is preserved, that is, with large Knudsen numbers ($K_n=\lambda/L>>1$, where λ is the molecular mean free path of the gas and L the characteristic dimension of the tube, typically its diameter). In supersonic beams, the gas is expanded from a high-pressure

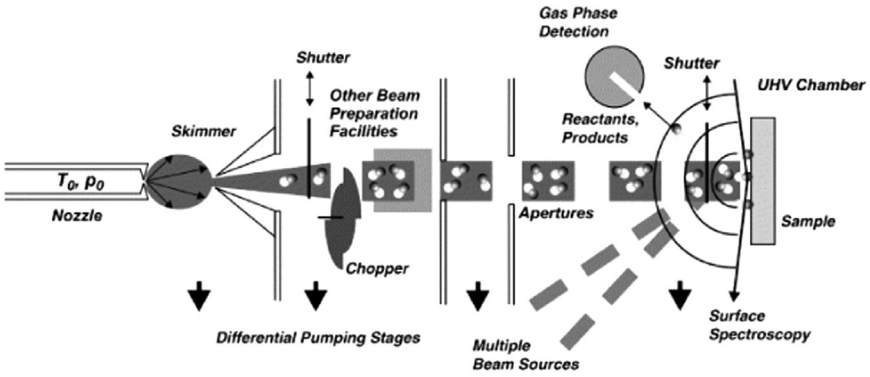

Fig. 2. Schematic representation of a typical supersonic molecular beam instrument [17,28]. Shown are, from left to right, the gas source (nozzle), the skimmer used to collimate the beam, two differentially pumped stages, the first of which has both a shutter and a chopper, the target surface, and a detector of scattered/desorbing molecules. Reproduced from Ref. [17] with permission, Copyright 2005 Elsevier B. V.

chamber through a small orifice, and collimated downstream by using a series of skimmers. Several characteristics differentiate these two types of beams, including the energy distribution of the molecules: whereas in effusive beams the gas mostly retains its kinetic and internal energy distribution, in supersonic beams significant translational and rotational cooling occurs.

Supersonic beams can provide more flexibility in terms of defining the energy distribution of the gas molecules, and have therefore been used extensively to characterize the dynamics of adsorption and scattering phenomena. Much has been learned about the design of these instruments from earlier work related to the study of gas-phase reactions [27], and new adaptations have added further versatility to experiments on surfaces. These setups have also been expanded to address issues of reactivity and reaction kinetics on surfaces, the focus of this review. The components of a typical supersonic beam arrangement for surface studies are shown schematically in Fig. 2 [17,28].

The main advantage of using supersonic beams is the great control that can be exerted on the values and distributions of energies in the different degrees of freedom of the molecules, in particular on the average and distribution of their velocity. Seeding of the beam can be combined with other methods designed to modify the energy distribution or selection of specific excited states in flight, that is, after the preparation of the beam. On the negative side, the typical velocities obtained with seeded beams are much higher than those associated with the average thermal energies of gases under most reaction conditions, and therefore not necessarily representative of realistic reactive systems. Because supersonic-expansion molecular beam instruments require several pumping stages and sophisticated alignment, they are also expensive and difficult to operate. Finally, it is difficult to generate high molecular fluxes with these instruments.

The second type of molecular beams is effusive in nature [13,29]. Effusive beams are usually generated by using capillary tubes, although other arrangements are possible. One shortcoming from using such capillary tubes is that, because the effusive regime requires large Knudsen numbers, single capillaries tend to sustain relatively small gas fluxes. Consequently, effusive molecular beams are typically made by using capillary arrays. The angular profile of the gases exiting capillary tubes are quite peaked, much more than supersonic beams, and this effect is magnified with the use of capillary arrays, so that the final beam profile in these instruments is quite directional [17,27,30–34]. A schematic representation of an effusive-beam instrument is provided in Fig. 3 [13]. In this case, a simple shutter was placed between the doser and the sample to control the time of direct exposure of the surface to the beam, and the size of the beam and position of the sample were chosen so that the single crystal only intercepts a fraction of the total gas flux

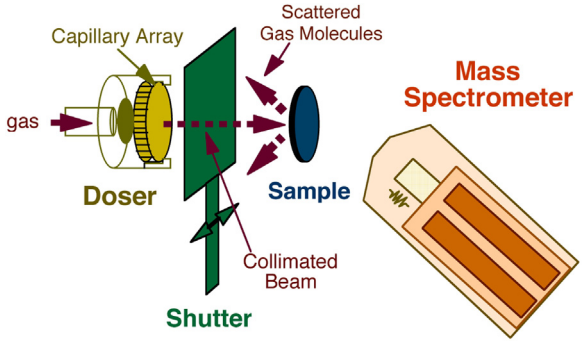

Fig. 3. Schematic representation of a typical effusive molecular beam instrument used for kinetic measurements [13]. This setup consists of a capillary-array doser, used to produce collimated beams, a shutter, used to intercept the molecular flow at will, and a mass spectrometer, used for the detection of gas molecules scattered or desorbing from the surface. The mass spectrometer is placed out of the line of sight of both the sample and the doser in order to integrate over any angular profile of the desorption process. Reproduced from Ref. [13] with permission, Copyright 2002 Taylor and Francis Ltd.

in order to ensure a homogeneous flux profile across the entire solid surface, typically a disk about 1 cm in diameter.

The advantages of effusive sources based on capillary arrays include the higher versatility on the range of beam fluxes possible, the low backing pressures required (which allows for easy beam generation with reactants having low vapor pressures), and the low amount of gas that is consumed, a factor when using rare or expensive reactants. In general, effusive sources are better suited for surface kinetics studies, whereas supersonic beams are more appropriate for the characterization of adsorption dynamics. The effusive-beam instrumentation is also easier to build and operate: simple dosers without any differential pumping are often sufficient for quantitative kinetic measurements. One drawback of effusive beam designs is the fact that, as the pressure increases, the mean free path of the gas molecules approaches the channel length, and molecular collisions lead to a broadening of the angular distribution and to deviations from the Maxwell–Boltzmann velocity distribution [35,36]. Like with supersonic beams, it is difficult to generate high-flux effusive beams, although this limitation can be circumvented at least in part by using capillary arrays [37].

2.2. Molecular beam setups for the study of chemical reactions

When the adsorption or thermal conversion of one single type of molecules is to be investigated, or, in more general terms, if dealing with an unimolecular elementary step, only one reactant is involved, and, therefore, one single molecular beam is required. As

described below, transient behavior may be investigated by following the uptake of the molecule versus time or surface coverage, and steady-state measurements may be carried out for any sustainable chemical reaction.

When two (or more) reactants are involved, however, or when bimolecular steps are being addressed, several options are available in terms of how to design the molecular beam experiments for kinetic measurements. One of the simplest approaches is to preadsorb one of the reactants on the surface and to then supply the second compound via the molecular beam. This technique offers much flexibility in terms of the preparation and characterization of the surface, since the coverage and nature of the adsorbates may be tuned by selecting the appropriate doses and temperatures. The dose ordering and choice of adsorbates may also be controlled this way. The main drawback is that this type of kinetic studies can only address transient, not steady-state, processes, because the preadsorbed reactant is consumed and is not replenished as the reaction proceeds.

A second alternative is to use the molecular beam setup to feed one of the reactants to the surface while keeping a fixed background pressure of the other in the vacuum chamber. The partial pressure of that second compound can be varied, but otherwise cannot be controlled in the same way as when using molecular beams. In particular, there is no directionality associated with this procedure (for the second reactant), so no angular dependence studies are possible. The same can be said for any experiments where the energy of any of the degrees of freedom of the molecule needs to be isolated and fixed. Of course, control of all of those parameters is possible with the first reactant, the one dosed by using the molecular beam, so in most cases the limitations mentioned above may be overcome by performing two sets of experiments, switching the reactant to be dosed with the beam. Yet, there may still be some issues with the interpretation of the data because of the very different ways in which the two gases are being dosed: the background exposure is isotropic and thermally equilibrated, whereas the molecular beam dosing is directional and possibly displaying a unique velocity distribution. Under high-flux conditions, the beam may even interfere with the accessibility of the second reactant to the surface sites in the center of the beam. Ultimately, though, all these limitations are minor; the beam-background mixed dosing approach is easy to implement and quite common, and still offers the possibility to perform both steady-state and transient or modulated measurements on bimolecular reactions.

Another option for carrying out bimolecular reactions with one single molecular beam is to feed the entire reaction mixture with it, after premixing the gases in the backing gas-handling system. This way the reactants are thoroughly intermixed in the gas phase already, a fact that avoids any transport limitations. This is also a viable and easy-to-carry-out type of experiment, even if it does require making individual gas mixtures every time the gas composition needs to be varied. In fact, this approach is not limited to just two reactants; witness, for instance, the studies reported in the literature on the conversion of $NO+CO+O_2$ [38] or $NO+H_2+O_2$ [39] mixtures. The control of the temporal and spatial parameters is limited here, as with the other approaches discussed above, as both gases are dosed on the surface with the same directionality and time modulation of the beam. Another consideration not always appreciated is the fact that the composition of the final beam may vary from that of the initial gas mixture, because most beams require diffusion through small orifices and the diffusion coefficient under those circumstances depends on molecular mass. It is advisable to check the beam composition independently in the vacuum chamber, perhaps by using the same mass spectrometer employed for the kinetic measurements.

Finally, both gases may be supplied by using a separate molecular beam for each. Some of the advantages and disadvantages of this approach are self-evident. On the negative side, such setups are complex and expensive, and also add another level of difficulty in terms of the experimental operation by requiring additional alignment and time synchronization steps. In exchange, this method offers the most flexibility when it comes to the design of time-resolved sequences or studies versus the energy or directionality of the impinging reactants. Some groups have in fact designed instrumentation that includes a third beam to be used as a probe, for He diffraction measurements, for instance [26].

Examples of the use of all these protocols will be provided throughout the course of this review.

2.3. Combination of molecular beams with other techniques

2.3.1. Isotope labeling

Often, molecular-beam kinetic studies are combined with other approaches or techniques to correlate information and extract a more detailed molecular understanding of the reactions being investigated. Given that the detection of the products in most molecular beam experiments is done by using mass spectrometry, one logical and widely used approach is to isotopically label one or more of the reactants. Isotopic substitution is a well-established method in many fields of chemistry [40], and has been used extensively in catalysis and surface science as well [14,41,42]. In the case of surface kinetics, isotope substitutions can lead to significant variations in reaction rates [43], and can even induce a change in reaction mechanism [44]. However, in molecular beam work, isotope labeling has primarily been used to keep track of the fate of specific atoms within the participating molecules, to identify particular reacting moieties within the reactants.

The most common isotope used for molecular labeling is, by far, deuterium. For instance, deuterium has been used extensively to track the chemical steps in the reversible dissociative adsorption of molecular hydrogen on solid surfaces; successful dissociation and recombination can be evaluated by following the evolution of the HD produced [45–47]. In principle deuterium can also be used to label specific positions within organic reactants and to follow its fate during reaction, as it is commonly done in other types of surface-science experiments [48,49], but this option has so far found very limited used in molecular beam studies [49–57].

Other types of atoms can be labeled isotopically as well, in particular carbon (with ^{13}C, or even ^{14}C), nitrogen (with ^{15}N) and oxygen (with ^{18}O). In such cases, the kinetic effect is small, reflected in changes on the order of only a few percent in either the rates or the equilibrium constants, and can therefore almost always be ignored. In experiments designed to explore the reactivity of mixtures that include CO, NO and/or N_2, multiple isotope labeling (using ^{13}CO and ^{15}N, for instance) may be required to unequivocally follow the evolution of the consumption or production of each of those compounds [58]. In all these isotope-labeling experiments, information can be extracted from both transient and steady-state measurements. For the latter, isotopic switching experiments can be implemented [59] where a reaction mixture is replaced during steady state by an identical but isotope-labeled beam (Fig. 4) [58,60]. These experiments will be discussed in more detail later in this review.

2.3.2. Post mortem analysis of the surface

Additional mechanistic information can also be extracted by investigating the nature of adsorbed species left on the surface after reaction via its post-mortem analysis. Different spectroscopies can be used to this end, as will be discussed in the next section. Alternatively, a simple approach can be to ramp the temperature of the surface upon termination of the isothermal section of the experiment to record temperature programmed

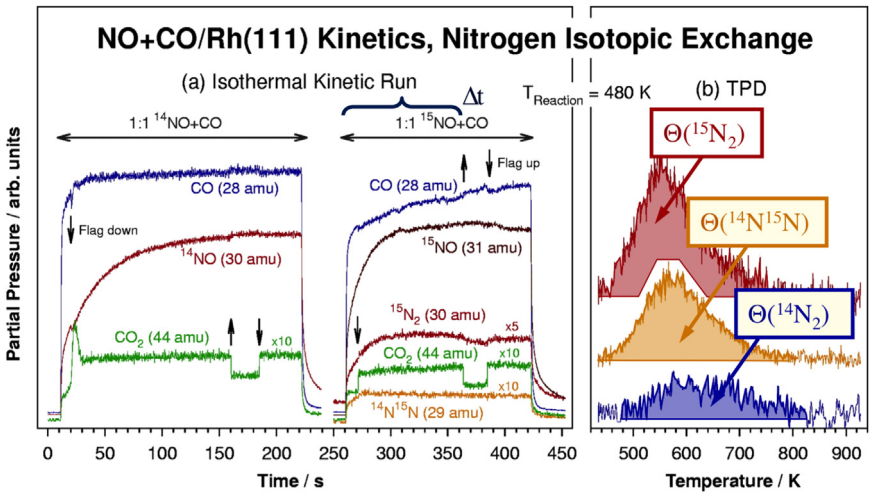

Fig. 4. Typical raw data from isotope-switching molecular beam experiments emphasizing the use of isotope labeling and post-mortem analysis of the surface species via temperature programmed desorption (TPD) [65]. This experiment was performed in three stages: (1) the reactivity of a 1:1 ^{14}NO-CO mixture on a Rh(111) single-crystal surface was followed versus time at $T_{Reaction}$ = 480 K, recording the mass spectrometer signals for CO, ^{14}NO, and CO_2; (2) the original beam was shut off and replaced with a similar reaction mixture made out of ^{15}NO+CO, and the reaction was run for an additional period of time Δt before stopping it again (recording the signals for CO, ^{15}NO, CO_2, $^{15}N_2$, and $^{14}N^{15}N$); and (3) the temperature of the surface was ramped to record the TPD traces for all the isotopologues of molecular nitrogen. The data for the rates in the second phase of the experiment were used to follow the transient isotope scrambling under steady-state reaction conditions, whereas the TPD information was useful in determining the final surface composition. Adapted from Ref. [65] with permission, Copyright 1999 American Institute of Physics.

desorption (TPD) traces of the residues left behind [15,61–63]. An interesting example of the use of this approach has been provided by Bowker and coworkers in their study of the adsorption and decomposition of acetic acid on Rh(110) surfaces, where they show that the reaction can reach a self-catalytic "explosion" state characterized by fast reactivity with highly-non-linear kinetics [64].

Post-mortem TPD analysis can also be combined with isotope labeling to extract information on the spatial distribution of adsorbates in an indirect way. We have used this approach to understand the evolution of the surface layers during the conversion of NO with CO on Rh(111) [60,65,66] The post-mortem TPD data was particularly useful in that case, because they offered a quantitative measure of the amount of atomic nitrogen present on the surface during the steady-state conversion of NO+CO mixtures. An example of the type of data acquired is provided in Fig. 4 [65]: a two-stage isotope-switching-under-steady-state molecular beam experiment of the type discussed earlier, in this case using identical ^{14}NO+CO and ^{15}NO+CO mixtures in sequence, was combined with the post-mortem TPD analysis discussed in this paragraph. By varying the delay time Δt during which the surface is exposed to the second beam, the kinetics of the exchange of atomic nitrogen on the surface was followed. These studies provided compelling evidence for the formation of atomic nitrogen islands on the surface, as discussed in more detail later.

A number of variations can be added to the TPD analysis described above. For instance, the desorption of the species left behind after reaction can be carried out isothermally instead of by ramping the temperature in order to obtain more detailed information on the kinetics of reaction of the adsorbed intermediates. In our work on the reduction of nitrogen monoxide, for instance, isothermal measurements of the rates of recombination of adsorbed nitrogen atoms allowed us to compare them with those of NO reduction to determine the role of the first reaction on the mechanism of the second [67]. Moreover, adsorbed species that do not desorb by themselves upon heating of the surface can be removed via titration with a second probe molecule. This approach is sometimes applied, using carbon monoxide, to remove residual surface oxygen [68,69].

2.3.3. *Operando mode*

More recently, molecular beams have been coupled to other surface-sensitive techniques in order to obtain both kinetic and spectroscopic information about the surface species involved in the reactions simultaneously, in *operando* mode. Perhaps the first report of an instrument combining the two is that or Rocca et al., who built an apparatus where the solid sample was placed at the focal point of both a molecular beam and the optics of a high-resolution electron energy loss spectrometer (HREELS) [70]. They tested this instrument by studying the uptake of O_2 on Ag(001), and were able to detect atomic oxygen on the surface. Unfortunately, the long acquisition times required in HREELS prevented them from being able to carry out the simultaneous analysis of the sample during the gas adsorption; the reported spectra corresponded to the final state of the surface after exposure to the beams.

The group of Freund has paired up their molecular beams with reflection-absorption infrared spectroscopy (RAIRS) in a single instrument, as shown schematically in the top half of Fig. 5 [17,28,71–73]. In general, RAIRS also requires relatively long data acquisition times, a fact that limits the temporal resolution of this type of studies, but when species with high infrared absorption cross section such as carbon monoxide are investigated, it is possible to record spectroscopic information in tandem with the kinetic experiments and to then draw appropriate correlations. This is nicely exemplified by the data in Fig. 6, where the incremental changes in adsorbed CO coverage on the surface of Pd nanoparticles dispersed on an alumina support, as measured by RAIRS, are shown to correlate with the activity toward the production of carbon dioxide seen upon exposure of the surface to successive molecular beam pulses of O_2 [72].

Pulsed molecular beams are also ideal for delivering controlled small amounts of gases to surfaces, to follow their uptake in a stepwise fashion. The doses provided by the beam pulses can be calibrated, and used in conjunction with other techniques to obtain differential information for surface processes as a function of the extent of exposure. This idea has been recently implemented for the measurement of the energetics of surface processes using microcalorimetry. The first instrument that combined molecular beams with a calorimeter capable of detecting heat changes on single-crystal surfaces was reported by the group of King and co-workers [74–76], who then provided results from studies on the energetics of chemical adsorption of a series of simple molecules

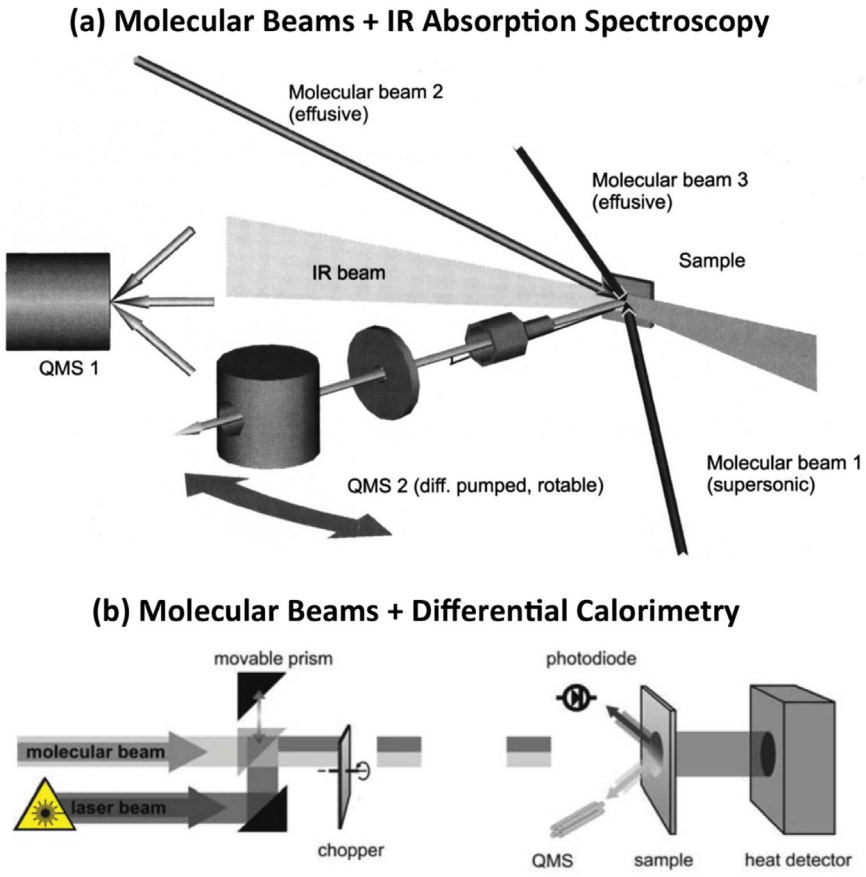

Fig. 5. Schematics of molecular beam instruments coupled with (a) a reflection-absorption infrared absorption spectrometer (RAIRS); and (b) a microcalorimeter. Adapted with permission from Ref. [71], Copyright 2000 American Institute of Physics, and from Ref. [90], Copyright 2011 American Institute of Physics.

such as hydrogen, oxygen, carbon monoxide, and nitrogen oxide [77–84], and also some data on the energetics associated with the dehydrogenation steps associated with olefin adsorption [85–87]. Both the probabilities for sticking (S, often called sticking coefficients or sticking probabilities) and the differential heats of adsorption ($\partial\Delta H_{ads}/\partial\theta$) can be followed as a function of surface coverage with this type of instrument, as illustrated by the data on the uptake of O_2 on a Ni(100) single-crystal surface at room temperature shown in Fig. 7 [80]. Particularly noteworthy in this case is the non-monotonic changes seen after saturation of the first layer, at which point the atomic deposition mechanism changes to incorporate diffusion into the subsurface. More sensitive versions of these molecular beam-microcalorimetry combined instruments have been developed and reported by the groups of Campbell [88,89] and Freund (Fig. 5, bottom panel) [90,91].

3. Dynamics and kinetics of adsorption

By and large, most of the molecular beam studies that have been performed on surfaces have been directed at the characterization of the dynamics and adsorption of simple molecules on well-defined crystals, mainly on late-transition metals. This work has been going on for several decades already, and has been thoroughly reviewed in the past by others [4,22,92–97]. The most salient features will be addressed below.

3.1. Dynamics of adsorption

Adsorption of atoms or molecules on solid surfaces, in its simplest form, takes place with preservation of the molecular structure. This process, often called molecular, or associative, adsorption, is typical with small stable molecules such as carbon monoxide and nitrogen oxide on metal surfaces. To a first approximation, the interaction can be described by a one-dimensional potential where the energy follows a Lennard-Jones type behavior versus distance from the surface: an electrostatic attraction dominates far away from the surface, until reaching an optimum (bonding) distance, beyond which a strong repulsive "wall" takes over (Fig. 8, top-left panel) [98,99]. Depending on the depth of the potential energy curve at its minimum, the adsorption is described as physical or chemical in nature. The distinction is in fact qualitative, because it reflects the type of interaction involved: weak van der Waals forces in physisorption, stronger bonding in chemisorption.

One interesting consequence of this potential energy dependence on distance is that there are no energy barriers to associative adsorption; the energy decreases monotonically as the molecule approaches the surface, until reaching the equilibrium bonding position. This means that such adsorption processes do not display the Arrhenius behavior typical of most chemical reactions. In fact, an opposite trend, that is, a decrease in sticking probability S with increasing gas or surface temperature, is what is most commonly observed, as the incoming molecules need to dissipate their excess energy. Molecular beam experiments, using supersonic expansion to control and vary the kinetic energy of the incoming molecules, have been central to the development of this picture. An example of the type of data reported in these studies is provided in Fig. 9, for the particular case of the initial sticking coefficient S_0 of CO on a Ir(110) single crystal as a function of incidence energy [100]. Also, because the surface acts as a heat bath, most desorbing molecules do not leave the surface in energetic equilibrium with the solid [101,102].

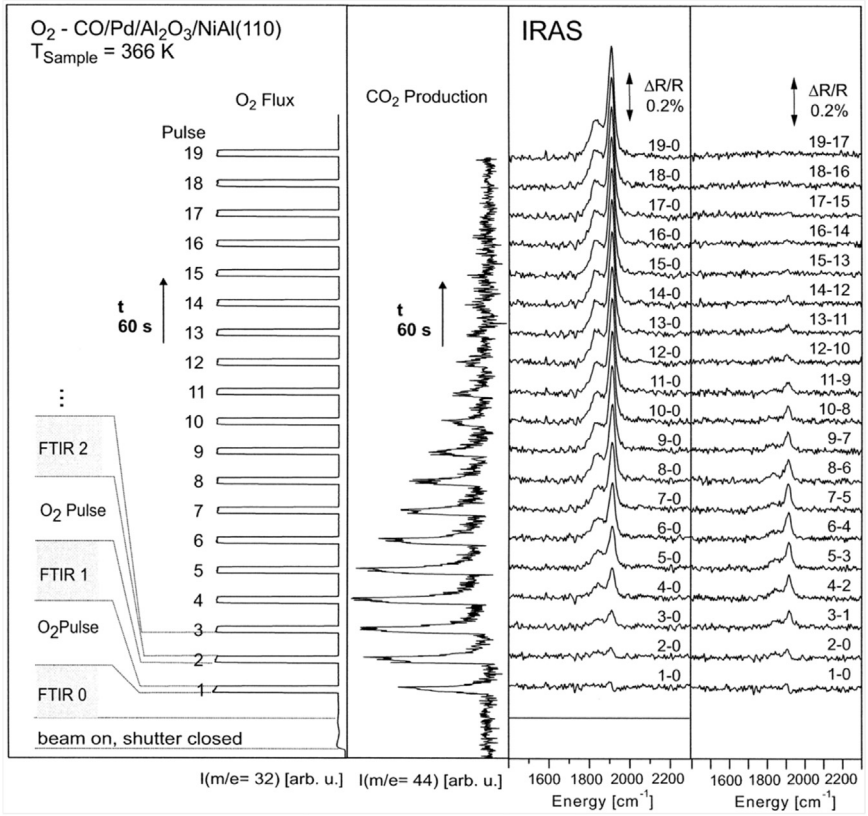

Fig. 6. Example of the information that can be acquired by correlating molecular beam kinetic data with results from RAIRS (IRAS) [72]. In this case the oxidation of carbon monoxide on a substrate consisting of Pd nanoparticles dispersed on a Al_2O_3/NiAl(110) thin film was probed by pulsing an O_2 beam on a CO-precovered surface at $T_{Surface}$ = 366 K. Shown are the oxygen (left) and carbon monoxide (center-left) partial pressures and the infrared absorption spectra, relative to that for CO saturation (center-right) and in differential mode (right), all as a function of reaction time. A nice correlation can be seen between the rate of CO_2 production (second panel) and the changes in CO surface population (last panel). Reproduced with permission from Ref. [72], Copyright 2000 Elsevier Science B.V.

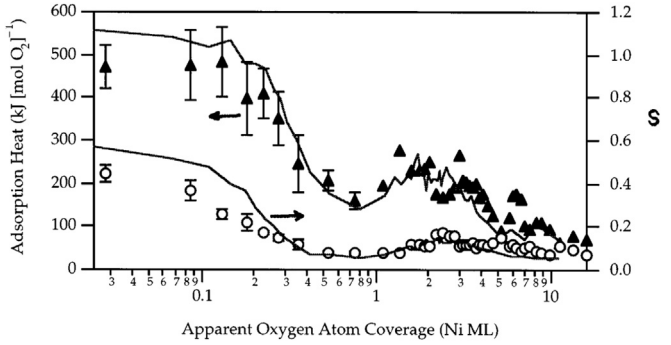

Fig. 7. Correlation between sticking probabilities S (open circles, right-hand scale) and heats of adsorption (filled triangles, left-hand scale) for oxygen on Ni(100) at 300 K. Both quantities are plotted as a function of the apparent surface coverage of atomic oxygen (in log scale) [80]. Two regimes could be clearly identified in these experiments, chemisorption on the first monolayer for oxygen coverages below unity, and the formation of a thin (~3 Ni ML) oxide film afterwards. Reproduced with permission from Ref. [80], Copyright 1997 American Institute of Physics.

3.2. Precursor state

This simple picture of adsorption on solid surfaces only applies to direct associative adsorption processes. In many instances, there are more than one adsorption states available on the surface, and in those cases each type of adsorbate may be described by its own potential curve. Those may cross paths, which means that, in their trajectory towards the surface, molecules may transition from one potential to another. One important category within this class of adsorptions is that of the crossing of physisorption and chemisorption potentials, in which case the incoming molecules may first adsorb weakly, possibly in a so-called "intrinsic precursor" state, and then transition to the chemisorption potential and end up in a stronger bonded state (Fig. 8, top-right). The transit from the precursor state to the final chemisorption state does require the overcoming of an energy barrier, which may or may not be higher than the energy required for desorption (which is described by traveling in the reverse direction of the potential energy curve). These dynamics can be manifested by a somewhat complex dependence of the sticking coefficients S on molecular energy, temperature, angle of incidence, and/or surface coverage. Again, details of this behavior have been derived thanks in great part to the availability of molecular beams [5].

The first application of a molecular beam technique to the study of precursor-mediated chemisorption was for the study of the adsorption of molecular nitrogen on a W surface [103,104]. The existence of an intermediate molecular adsorption state was identified in that study only indirectly, by following the sticking coefficient (S) behavior as a function of surface coverage (as discussed in more detail later in this review), and what was detected there is more properly described as a so-called "extrinsic precursor" state. Regardless, that report identified the most important features of precursor adsorption, namely, that S decreases with increasing beam energy, as expected by the need of energy dissipation, and also with the temperature of the surface (T_s). As mentioned above, molecules equilibrated in the precursor state can either desorb or transition into the chemisorbed state, and the relative yields of these competing processes, which ultimately are manifested in the value of S, depend on T_s. To date, the condition $\partial S/\partial T_s < 0$ is considered a strong indication of a precursor-

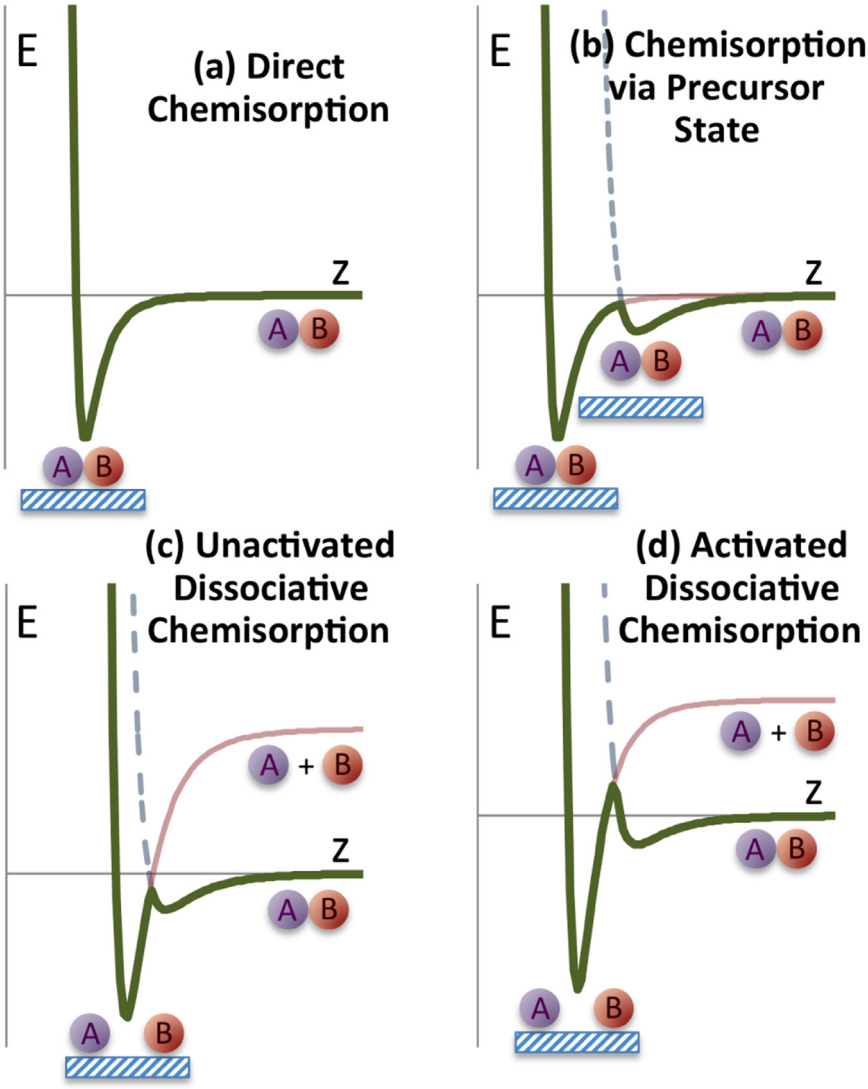

Fig. 8. One-dimensional potential energy curves for the interaction of diatomic molecules with clean solid surfaces as a function of the molecule-surface distance z. Four cases are represented here: (a) direct molecular chemisorption, without dissociation; (b), molecular chemisorption via a weakly-adsorbed internal precursor state; and (c) and (d) dissociative chemisorption via a molecular precursor state. The difference between cases (c) and (d) is in the height of the activation barrier between the precursor and chemisorbed states, which is lower in panel (c) but higher in panel (d) than the reference energy corresponding to the free molecule. In all cases, the incoming gas-phase molecules feel an initial attractive potential and ultimately settle in a potential well corresponding to the adsorption state. The energy for further approach closer to the surface becomes highly repulsive.

mediated process. Since this first report, the decrease in sticking coefficients with beam energy have been cited for a number of other systems, many involving molecular hydrogen [105,106], oxygen [107], or small alkanes [108].

Further evidence of adsorption via a precursor state can be extracted from the dependence of the sticking coefficient on the angle of incidence of the molecules: because of an expected normal energy scaling, S should actually increase with increasing angle of incidence (relative to the surface normal). Such trend has indeed been identified, at least in a qualitative sense, for several systems [105,109]. On the other hand, the quantitative description of the angular dependence of S has indicated the possible existence of an additional tangential energy component that needs to be accommodated. This can be explained by assuming that the mobile precursor state is confined to a limited surface area. It should be said that, in many dissociative adsorption processes exhibiting a precursor state, there is a second, direct, activated adsorption channel that tends to dominate at high beam energies. The existence of the two paths, and for the transition between the two as a function of beam energy, is illustrated by the data for the adsorption of N_2 on W(100) shown in Fig. 10: at low beam energies adsorption is dominated by a precursor path, as indicated by the decrease of the sticking coefficient with increasing energy, whereas at higher beam energies ($E_i > 0.5$ eV) a second, activated, adsorption path becomes dominant. Also evident from the data in Fig. 10 is the fact that lower surface temperatures enhance adsorption in the precursor state. The dissociative channel will be discussed in more detail next.

3.3. *Dissociative adsorption*

With multiatomic molecules, the molecular adsorption potential curve may also cross a second trace leading to the dissociation of one or more of the internal bonds. Depending on the exact position where the two potential energy curves cross, this transition to a dissociative adsorbed state may or may not be activated (Fig. 8, bottom two panels). The end result is the formation of two or more fragments on the surface. In the simplest cases, diatomic molecules dissociate to produce adsorbed atoms on the surface, as typically happens with H_2, O_2 and N_2 on transition metal surfaces.

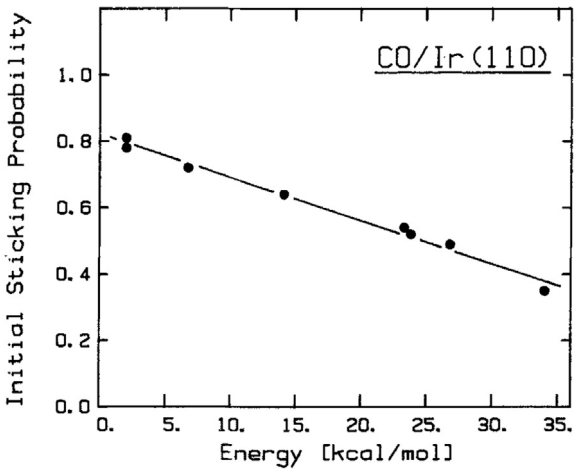

Fig. 9. Initial sticking coefficient S_0 for CO on Ir(110) as a function of the energy of the incident CO molecular beam [100]. The decrease in S_0 with increasing incident energy is common in adsorption, and reflects the requirement for the gas-phase molecules to dissipate their kinetic energy in order to bond to the surface. Reproduced with permission from Ref. [100], Copyright 1987 Elsevier Science B.V.

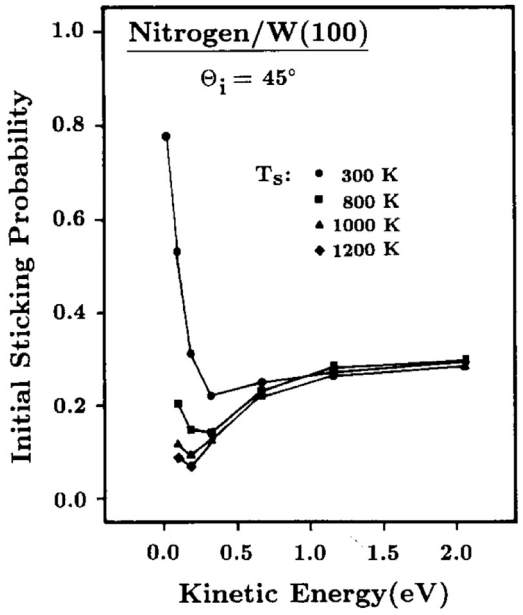

Fig. 10. Initial sticking probability for N_2 on W(100) versus the kinetic energy of the N_2 incoming beam [5]. Several traces are provided for different surface temperatures T_s, between 300 and 1200 K. These results exemplify the competition often encountered between direct and precursor-mediated adsorption pathways: at high energies the sticking probability decreases with decreasing beam energy and does not depend on surface temperature, trends characteristic of direct adsorption, but a lower incident energies the value of the sticking coefficient goes back up and also increases significantly with decreasing surface temperatures, a signature behavior for the intervention of a precursor state. Reproduced with permission from Ref. [5], Copyright 1994 Elsevier Science B.V.

3.3.1. Molecular hydrogen on metals

The adsorption of molecular hydrogen has received quite extensive attention by the molecular beam surface-science community, especially on transition-metal surfaces [110]. Several adsorption states have been identified or inferred from molecular beam measurements, in combination with the use of other spectroscopies and with quantum mechanics calculations. First, it is believed that in most cases hydrogen first goes through a weakly adsorbed physisorbed state. In this phase, which has been quite difficult to characterize, the adsorption energy is low, typically between 3.5 and 15 kJ/mol, and molecular properties such as the H–H bond distance and the rotational spectrum are barely perturbed from the gas-phase values [110]. Virtually no evidence is available for molecular H_2 adsorption above 20 K; perhaps the best data proving the existence of the physisorbed state comes from studies on the velocity distribution of specularly scattered D_2 molecules from Cu(111) and Au(111) surfaces, which shows a series of sharp dips and peaks with widths below 0.25 meV [111].

Next, there is the possible existence of a deeper well in the potential energy curve signifying molecular chemisorption. In this state, a clear reduction in the H–H bond strength and a concurrent elongation of the molecular bond is estimated. Direct proof for this state has also been elusive, but such adsorption is expected to be reminiscent of the stable H_2-metal discrete complexes known to form with transition metals in inorganic chemistry [112–114]. Regardless, in most cases the ultimate result of exposure of metals to molecular hydrogen is its dissociative adsorption and the formation of atomic hydrogen on the surface [6,110,115]. On most metals the dissociation of the H–H bond is unactivated (Fig. 8, bottom-left panel), especially on high-Miller-index defective surfaces, but in some coinage metals the adsorption is activated (Fig. 8, bottom-right panel). This difference is discussed in more detail below.

Two mechanisms have been identified for the dissociative adsorption of H_2: a direct process, in which the incoming molecules have enough kinetic energy to overcome any possible activation barrier and break up upon impingement on the surface to produce the final H(ads) species, and a second indirect channel in which molecularity is retained for a certain amount of time, in either the physisorbed or the molecularly-chemisorbed states mentioned above, before proceeding to dissociation. In the direct path, exemplified by the case of H_2 on Ni(111) [101,105,116], the decisive parameter is the translational energy of the incoming molecules: the surface temperature T_s plays no major role on defining the sticking and dissociation probabilities. In the path involving the molecular precursor, on the other hand, the activation barrier in the exit channel consists mainly of the stretching of the H–H bond, for which vibrational excitation is necessary. Also, T_s does play a role in this precursor-mediated dissociation channel, via a phonon-assisted vibrational excitation of the trapped molecule. Examples here include hydrogen adsorbed on Pt(111) and Cu(111). Interestingly, the metal–H binding energies are similar, between 115 and 150 kJ/mol, in all cases, even if wider differences exist in the corresponding heats of adsorption [110]. This points to a fairly similar binding mechanism for hydrogen on many metals. For all metals in or near the platinum group except Pd, bulk absorption of atomic hydrogen via diffusion into the bulk is endothermic.

It is interesting to note that, in many cases, the initial sticking probability S_0 for molecular hydrogen (as well as for other diatomic homonuclear molecules such as N_2 or O_2) on flat surfaces, on the (111) planes of fcc transition metals for instance, is substantially smaller than unity [116]. Such conclusion had been controversial for a long time because dissociation does occur readily on defects [45,117,118], which are difficult to avoid entirely even on well-characterized single crystal surfaces, but has been proven convincingly, and has been explained on the bases of a small activation energy barrier for adsorption. In support of this idea, molecular beam studies on the adsorption of H_2 on Ni(111) have identified a two-state character with thermally activated sticking and an activation energy for the low-energy state showing a strong dependence on the density of surface defects [119,120].

More clear cases of activated adsorption, where the intersection of the two potential energy curves occurs above the zero-energy line (Fig. 8 bottom-right), have been reported for hydrogen adsorption on late transition metals, typically coinage metals. Perhaps the best-studied metal in this regard is copper. Early indications of an unusual dependence of the initial sticking coefficient S_0 on temperature, pointing to the existence of an adsorption activation

barrier of a few kJ/mol, were later confirmed by molecular beam experiments. Indeed, both the groups of Cardillo and of Rendulic concluded that a threshold translational energy, of between 10 to 20 kJ/mol, is needed for the sticking of H_2 on several planes of copper surfaces, including Cu(111), Cu(100), Cu(110), and Cu(310) [6,109,121,122]. More recently, molecular beam experiments with H_2 and D_2 on Cu(110) have shown that higher sticking probabilities can be reached with molecules exhibiting particular combinations of translational and internal energies [11,123]. For instance, Hayden et al. have shown that the translational energy onset for H_2 sticking amounts to 130 meV for molecules in the $\nu=1$ vibrational state but only 60 meV for $\nu=2$ [124]. A more detailed analysis by Michelsen et al. for the case of the uptake of D_2 on Cu(111) provided the estimated curves of S_0 versus kinetic energy for specific vibrational and rotational molecular states shown in Fig. 11 [125].

3.3.2. Other diatomics and surfaces

So far our discussion has centered on the adsorption of molecular hydrogen on metals, but similar qualitative conclusions have been reached from experiments on other surfaces and with other molecules. In particular, evidence has been found in many systems for the existence of both direct and precursor-mediated dissociative adsorption channels [126]. For instance, the dissociative adsorption of H_2 on silicon, which is considered to be prototypical for activated chemical reactions on semiconductor surfaces, has been shown to depend strongly on T_s and to involve phonon excitation of the silicon substrate [127].

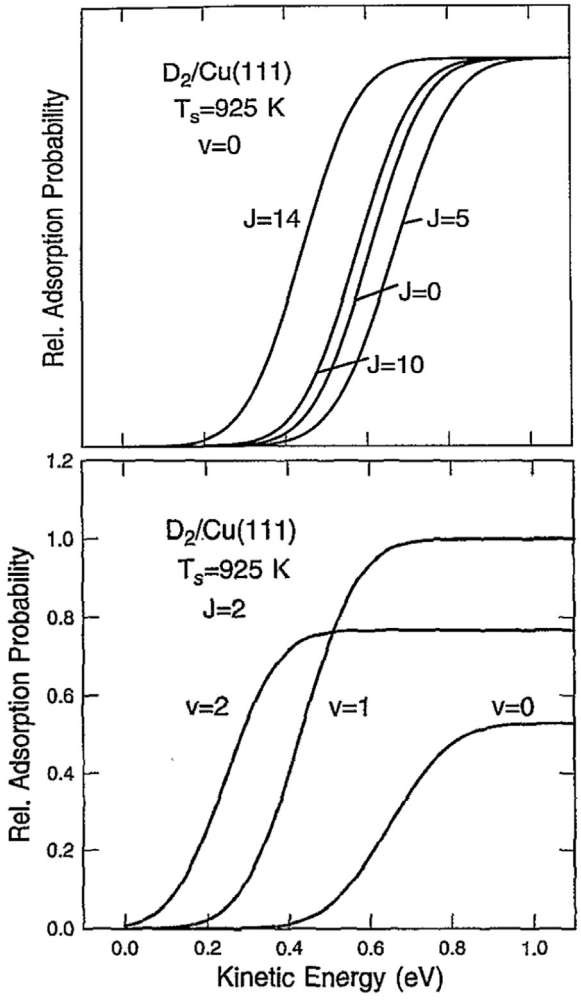

Fig. 11. Results from a energy-state-resolved molecular beam study of the dynamics of the adsorption of D_2 on a Cu(111) single-crystal surface [125], in the form of the dependence of the adsorption probability on the kinetic energy of the beam. Top: Data for several rotational excited states, J=0, 5, 10 and 14, within a single vibrational state ($\nu=0$). Bottom: Equivalent data for several vibrational states ($\nu=0$, 1, and 2) at a single rotational state (J=2). All the data were acquire at a surface temperature of $T_s=925$ K. Adapted with permission from Ref. [125], Copyright 1993 American Institute of Physics.

In terms of the reactants, much of what has been learned with hydrogen can be extended to other diatomics, even if there may be some unique features associated with particular systems. For instance, a study of the adsorption probability of O_2 on Pt(111) as a function of initial energy, angle of incidence, and surface temperature provided evidence for dissociative chemisorption via both precursor mediated and quasi-direct mechanisms, the latter made evident by a steep increase in sticking probability with initial energy [128]. By combining the use of molecular beams with post-CO titration experiments, it was determined that the molecular-precursor pathway is operational even at relatively high incidence kinetic energies, at least as high as 1.1 eV [129]. On both Pd (111) [130] and Rh(111) [131], the adsorption mechanism of molecular oxygen also evolves continuously from molecular precursor-mediated to a direct adsorption pathway with increasing incident energy. Yet, on other metals such as Ag(110), the dependence of S on the temperature of the surface indicates that adsorption takes place directly into the molecular well and that dissociation is eventually induced thermally, at $T_s \geq 150$ K, without the participation of any physisorbed precursor state [132].

Even the highly stable N_2 molecule can be dissociated on surfaces. In one case, Auerbach and co-workers [133–135] showed that the dissociative adsorption of N_2 on W(110) is activated, with a barrier of roughly 80 kJ/mol. The initial sticking probability is relatively insensitive to the angle of incidence of the beam, in contrast to the H_2/Cu system, so S_0 scales approximately with the total kinetic energy rather than with the component normal to the surface. Such behavior is inconsistent with a quasi-one-dimensional activation barrier, and shows that the reaction is primarily translationally activated. The same scaling of S with total energy was reported on W(100), but in that case the dissociative adsorption probability falls rapidly with increasing kinetic energy and with surface temperature, strongly suggesting dissociation via a precursor state [136]. The primary difference for N_2 dissociation between the W(110) and W(100) surfaces was found to be a higher energy barrier to dissociation on the former [137].

3.3.3. Methane and other alkanes

Additional complications arise when considering multiatomic adsorbates. Much work has been focused on the study of the activation of small alkanes, starting with methane, on metal surfaces. It has been concluded that, as with diatomics, the promotion of C–H bond-scission steps in alkanes by metal surfaces may occur either directly upon collision of the incoming gas molecule with the solid or via the formation of weakly adsorbed intermediates trapped on the substrate [108,138–159]. It has also been shown that the critical factor for alkane activation is the efficiency with which energy is transferred from the translational and internal degrees of freedom of the gas molecules to the particular C–H bond to be broken; the energy stored by the surface is often of little importance for this process. In some instances it has been reported that it is the normal component of the translational energy of the alkane that is important for the C–H bond-breaking step, as summarized in Fig. 12 [147,158,160,161], but Stewart and Ehrlich have shown that the vibrational modes of the incoming molecules may be the most likely to provide energy for the dissociation of methane [162]. Combinations of translational and vibrational energy excitations can also add up to provide the total energy needed to surpass the energy barrier for activation, as discussed above for hydrogen [163].

On the basis of theoretical calculations, it has been estimated

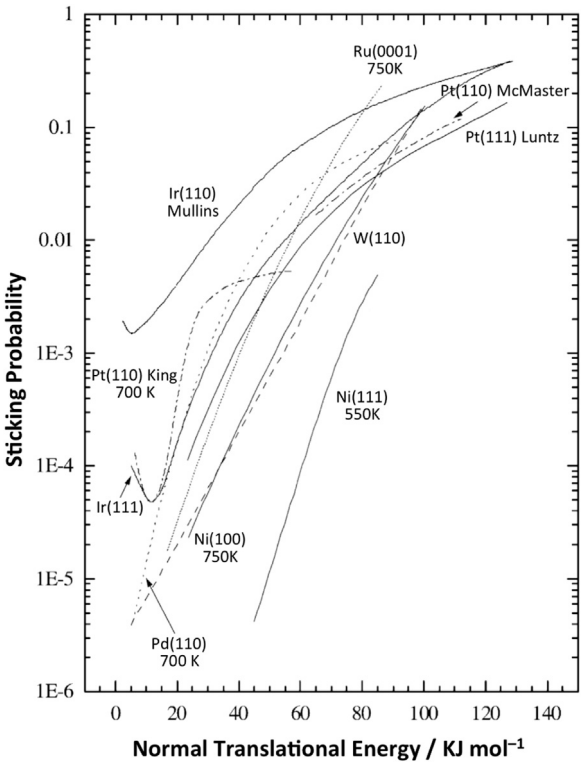

Fig. 12. Initial dissociative sticking probability S_0 for CH_4 on various metal surfaces, plotted as a function of the normal component of the translational energy, $E_{Normal} = E_i \cdot \cos^2\theta_i$ (where θ_i is the angle of incidence of the beam on the surface) [158]. Most cases show the exponential relationship typical of activated processes, corroborating the scaling with the normal component rather than the total energy, but some deviations are seen in a few instances. In particular, the reversal in S_0 with decreasing energy observed with Pt(111), Ir(111), and Ir(110), where higher values are seen at lower energies, signifies the participation of a precursor state. Reproduced with permission from Ref. [158], Copyright 1995 Elsevier Science B.V.

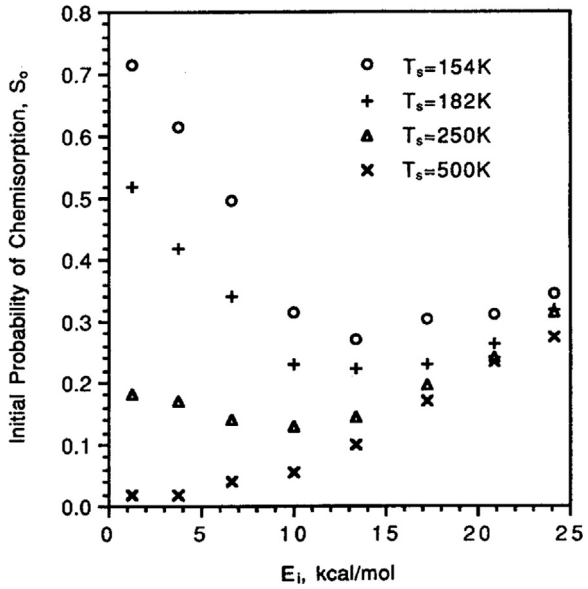

Fig. 13. Initial probability for the dissociative chemisorption of ethane S_0 on Ir (110)-(1 × 2) as a function of incident kinetic energy at surface temperatures of T_s = 154, 182, 250, and 500 K [168]. All measurements were made at normal incidence. Like in Fig. 10, two components are clearly seen in these data, the low-energy region where S_0 depends strongly on T_s and increases with decreasing energy, as expected from a precursor-mediated process, and the high energy end where all curves converge and the values are proportional to the incident energy, the sign of direct dissociative chemisorption. Reproduced with permission from Ref. [168], Copyright 1990 American Institute of Physics.

that direct alkane activation may occur via a tunneling mechanism [164,165], at least at the high kinetic energies associated with supersonic beam experiments. Alkane sticking probabilities often increase monotonically with increasing kinetic energy, not in a stepwise fashion at a given threshold energy value as expected if the kinetics were dominated by an activation barrier. Also, the observed shifts in the translational energy needed to activate CH_4 vs. CD_4 (or C_2H_6 vs. C_2D_6) are usually on the order of 20 kJ/mol, much larger than the differences in the zero-point energy due to isotopic substitution [166]. On the other hand, the dependence of the sticking probability of methane seen on some metals as a function of either the energy or the angle of incidence of the molecular beam may be more appropriately explained by a classical model based on the microscopic reversal of the trajectory of a reductive elimination step between methyl and hydrogen adsorbed species [167]).

Other molecular beam work has provided evidence for a precursor-mediated alkane activation mechanism: the trapping probability of ethane on Ir(110)-(1 × 2), for instance, shows only a weak dependence on the angle of incidence of the beam, suggesting that the momentum of the incoming molecules is rapidly transferred to the surface [168]. In yet other cases, the dissociation of alkanes has been shown to be assisted by a reverse energy transfer from the surface to the molecule. This appears to be the case on both platinum and rhodium, where S_{CH4} displays an Arrhenius temperature dependence in the limit of low kinetic energy, with an activation energy between approximately 20 and 40 kJ/mol [169]. Finally, the mechanism of activation may change with varying incident energy. For instance, studies with low-energy beams have indicated that the probability of dissociation of methane on platinum decreases with increasing incoming kinetic energy [170], a result that is counterintuitive and that has yet to be properly explained but that may reflect intermediate molecular-adsorption steps. A similar behavior, plus a strong dependence of S on T_s, has been reported for ethane on Ir(110)-(1 × 2), as shown in Fig. 13 [168].

Molecular beam work on the dissociative adsorption of heavier alkanes corroborates some of the same general features observed with methane. For instance, in the case of cyclopropane on Ir(110), a precursor-mediated mechanism dominant at low energies gives way to direct activation for $E_i > 40$ kJ/mol [153]. The absence of any isotope effects upon substitutions of the hydrogen atoms with deuteriums suggests that the initial reaction coordinate involves a C–C bond cleavage. Further studies with C_3H_8, C_3D_8, and $(CH_3)_2CD_2$ led to similar conclusions, with the added observation that primary C–H bonds may be easier to activate than secondary C–H bonds [151,154].

3.4. Surface corrugation

In the preceding discussion, the dynamics of adsorption has been described by a one-dimensional potential that focus the attention on the effect of the distance between the adsorbate and the solid but neglects the other two dimensions, along the plane of the surface. Certainly the distance of the incoming molecules from the surface is the primary dimension determining their interaction, but the energy potential does display some corrugation in the other dimensions as well, especially with open planes or on defective surfaces. One of the basic conclusions on adsorption from modern surface-science studies is that bonding to surfaces is localized and takes place on specific surface ensembles and with specific geometries [93,99]. This is true even on metals, where the electron density is highly delocalized. Such localization of surface bonding can only be explained if the 2D potential energy surface along the plane of the surface displays well-defined minima.

One consequence of this corrugation of the 2D surface potential along the surface plane is that, because open surfaces display a higher degree of corrugation, they can further facilitate adsorption. It is particularly noteworthy that the dissociative adsorption of H_2, which as mention above has been shown to display low sticking coefficients on close-packed metal surfaces such as Pt(111), typically shows S_0 values close to unity on more open planes [110]. In addition, a combination of molecular beam and angle-resolved desorption studies have indicated total energy accommodation of the adsorbate with the surface, which shows up as cosine distributions. This is in contrast with the highly peaked desorption profiles obtained on (111) planes of fcc metals such as Ni [101,116]. Detailed quantum-mechanics calculations have shown that the corrugation of the 2D surface potential should manifest itself in detailed sticking coefficient measurements as a function of incidence angle and energy excitation levels in the different molecular degrees of freedom [171]. One nice experimental example of the effect of surface corrugation on adsorption dynamics was provided by Vattuone et al., who showed that, for O_2 on Ag(110), the initial sticking coefficient S_0 is different along each of the two high-symmetry azimuthal directions, [001] and [1$\bar{1}$0], of the surface; a clear anisotropy was seen as a function of the total energy and the angle of incidence of the molecules, and also as a function of the crystal temperature, for both low and room-temperature adsorption [132].

It is well known that surfaces are dynamic and may reconstruct to minimize their surface tension [172]. It has also been repeatedly established that such reconstructions can be removed upon the adsorption of molecules [173]. This type of reconstructions is expected to alter the surface potential, and with that the dynamics of adsorption. The dynamics of surface reconstruction upon exposure of surfaces to specific adsorbates can be studied with the aid of molecular beams. In one example, by combining molecular beams with calorimetric measurements, the group of King and coworkers determined that, with CO or NO, adsorbate–adsorbate interactions determine the formation of different ordered structures [79,174]. In a related study, they followed the growth of (1×1) islands upon exposure of a hexagonal-reconstructed Pt(100) surface to deuterium: by measuring sticking coefficients at desorption temperatures, they found that island growth follows a highly nonlinear rate law, with a forth-power dependence on the local deuterium coverage on the surface [175,176]. Interesting, a different behavior was seen with Ir(100) [177]. Ultimately, it appears that these adsorbate-induced reconstructions follow complex dynamics not easy to describe with mean-field kinetic equations.

3.5. Effect of steps

Steps and other types of defects on surfaces expose atoms with low coordination numbers, and those are expected to be particularly reactive. Molecular beam measurements of sticking coefficients of simple adsorbates have in general bear this out. Perhaps the earliest demonstration of the role of steps on chemical reactivity using such beams came from the elegant set of experiments reported by the Somorjai group on the isotope scrambling of H_2+D_2 beams on stepped platinum surfaces [45,117,178–180]. In studies on the Pt(332) (Pt(S)−[6(111)×(111)]) and Pt(553) (Pt(S)−[5(111)×(111)]) planes, measurements of reactivity as a function of both polar and azimuthal angles highlighted a strong variation versus the direction of approach of the gas molecules, with the production of HD being highest when the reactants strike the open side of the step and decreasing by approximately a factor of two when the inner corner of the step is shadowed (Fig. 14). They also found that the exchange reaction is first-order in deuterium flux and half-order in H_2 background pressure. Combined with subsequent measurements of the angular and velocity distributions of the HD product [181], these results indicated that a

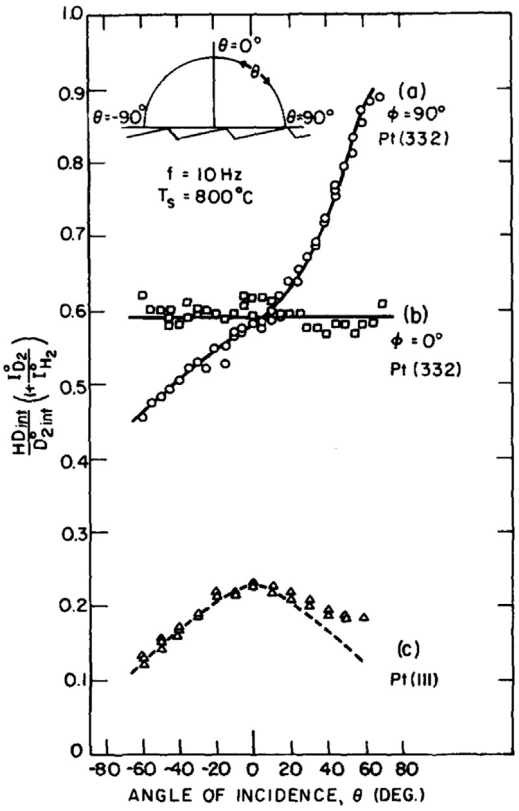

Fig. 14. HD production (HD_{int}) from reaction of H_2+D_2 mixed molecular beams on platinum single-crystal surfaces as a function of the angle of incidence θ, normalized to the intensity of the incident D_2 signal ($D_2°_{int}$) [117,585]. The expression in parentheses in the y-axis label, $1+I°_{D2}/I°_{H2}$, is a correction factor introduced to account for the relative proportions of H_2 and D_2 in the beam. Data are provided for experiments on: (a) Pt(332), also known as Pt(S)-[6(111)×(111)], with its step edges perpendicular to the incident beam (φ=90°); (b) the same Pt(332) surface, but where the projection of the beam on the surface is parallel to the step edges (φ=0°); and (c) Pt(111). The data clearly show that the isotope scrambling reaction occurs preferentially at the open side of the steps. Reproduced with permission from Ref. [586], Copyright 1990 American Chemical Society.

Langmuir-Hinshelwood atom-atom recombination on the surface must be the rate-limiting step of the overall process.

The H_2/Pt system has been studied extensively since, and the general conclusions arrived to by the Somorjai group have in general been confirmed. In one study with D_2 and a Pt(533) (Pt(S)−[4(111)×(100)]) crystal, the initial dissociative sticking probability S_0 was found to first decrease with increasing kinetic energy E_i, up to about 9 kJ/mol, but to then increase [182–184]. Comparison with D_2 dissociation on Pt(111), where S_0 increases linearly with E_i, suggests that it is the step sites that are responsible for the low-energy dissociation on the Pt(533). In another example, the initial sticking probability was found to increase with surface temperature [185]. More recent work with curved surfaces, which has afforded a more systematic characterization of the adsorption process as a function of step density on the surface [186,187], has again shown that the initial reaction probability increases significantly at low kinetic energies when steps are introduced, but markedly decreases for all stepped surfaces (at the expense of an increase in reactivity on the (111) surface) above 10 kJ/mol. With the aid of quantum-mechanics calculations, the low-energy step-mediated pathway has been described as a non-activated precursor-mediated reaction channel due to molecular chemisorption at the bottom of the steps [184]. Two more direct-activation routes have been proposed for H_2 dissociation at higher energies, on the terraces and on the steps, respectively [118,184].

Comparable conclusions have been reached from studies on other surfaces and with other reactants [5]. For instance, Karner et al. have reported non-activated adsorption on step sites but activated adsorption for hydrogen on the flat terraces of Ni(997) (Ni(S)−[9(111)×(111)]) [188–190]. With the beam aimed in the step-up direction adsorption was found to proceed via a precursor state ($\partial S/\partial T_s < 0$ and $\partial S/\partial E_i < 0$), whereas aiming the beam in the opposite direction was determined to lead to an activated adsorption ($\partial S/\partial T_s > 0$) ascribed to reactivity on the (111) terraces. The first route was found to dominate at low energies ($E_i < 0.1$ eV), but the direct activation on terraces was seen to take over at higher energies.

Comsa and coworkers have developed an interesting approach for the characterization of adsorption on terraces versus defect sites based on measurements of the cross section for He scattering, and applied it to the case of CO adsorption on platinum surfaces with planes of orientations slightly off the (111) plane [191,192]. The large scattering cross section seen with small amounts of carbon monoxide adsorbed on those surfaces, $\sim$250 Å^2 (much larger than expected from the Van der Waals radii of He and CO), was taken as an indication of preferential CO occupation at defect sites [193].

Some reports are also available on the dynamics of molecular adsorption. For instance, for either CO or NO scattered from either Pt(111) or Pt(557) (Pt(S)−[6(111)×(100)]) surfaces, the molecular beam scattering data obtained for temperatures above 500 K could be well described by using an adsorption-desorption model with a constant sticking coefficient but a higher activation energy for desorption from the stepped sites [194]. However, below 525 K, the NO scattering results were quite different from those of CO, and could not be simulated with the simple models that were tried. What can be said is that NO does not dissociate upon adsorption, and that its sticking coefficient decreases with increasing coverage.

For the O_2/Pt(533) case, it was found that the steps dominate the dissociative adsorption process, with initial sticking coefficients significantly larger than on Pt(111) (even though the two surfaces show similar dependences of S_0 on E_i) [195]. Strong and asymmetric angular dependences were identified, containing contributions from separate activated dissociative adsorption channels for the chemisorbed precursors on the (111) terraces and the steps, respectively. A rapid decrease in S_0 was seen below 0.15 eV on both Pt(533) and Pt(111), consistent with a trapping mechanism followed by unactivated dissociation of the physisorbed precursor. Additional studies with different stepped surfaces led to the conclusion that the most reactive sites for O_2 dissociation are at the top of Pt steps [196].

Finally, molecular beams have also helped understand the dynamics of the dissociative adsorption of alkanes on stepped surfaces. In one case, with methane on Pt(533), it was found that, for beam incident kinetic energies between 26 and 1450 meV, the initial dissociation probability is higher than on Pt(111) at all surface temperatures investigated because of additional direct sticking mediated by the steps [197]. No evidence for any additional indirect dynamical channel to dissociation induced by the steps was seen, but the S_0 dependence on both E_i and incident angle could be deconvoluted into two contributions, from the (111) terraces and the (100) steps, respectively, the latter with an effective activation barrier for dissociation approximately 300 meV lower than that for the former. An enhanced dependence on T_s was also observed on the Pt(533) surface versus on the Pt(111), and ascribed to a more effective coupling of the energy from the surface into the reaction coordinate.

3.6. Assisted adsorption

The adsorption of molecules on surfaces can be assisted via an additional external excitation channel, especially if it involves a precursor state or requires the dissociation of one or more bonds. Particularly relevant to studies with molecular beams is an approach where the molecules are excited with the aid of lasers in the gas phase, prior to their impingement on the surface, to prepare them in vibrational and/or rotational hot states. An example of the effect of molecular excitation on reactivity upon adsorption is that of the dissociation of NO on Cu(111) surfaces [198]. By preparing the NO molecules in single quantum states with vibrational energies as high as 300 kJ/mol, the dependence of the vibrationally elastic and inelastic scattering probabilities could be mapped out. Highly excited NO (ν=13 and 15) was found to react with a probability of 0.87 ± 0.05, more than three orders of magnitude greater than the reaction probability of ground-state NO.

Molecular excitation to activate adsorption can also be performed on larger polyatomic molecules. In fact, in those cases specific vibrational modes may be promoted by using narrow-band infrared lasers. For instance, in studies using vibrationally-hot CD_4 and C_2D_6 supersonic beams directed at an Ir(110) surface, it was shown that the extra vibrational energy leads to a decrease in the translational energy required for the onset of measurable dissociative chemisorption [199]. The main vibrational mode contributing to the dissociative adsorption was found to be the asymmetric C–D stretching motion. Interestingly, a similar energy compensation effect between translation and vibration modes appears not to be operational with CH_4 or C_2H_4 [152,166]. These observations were explained by a direct chemisorption mechanism with quantum-mechanic tunneling. In the case of the uptake of methane on Ni(100), excitation of the ν_3 C–H stretching vibration to its first excited level led to an increase in dissociative adsorption by a factor of 1600 compared to the unexcited molecules [10,200,201]. In beams with high translational energy, though, the ν_3 was found to be responsible only in part for vibrational activation.

Another interesting mechanism for the augmentation of reactive adsorption is the excitation of molecules adsorbed molecularly in a weakly-bonded precursor state by collision with other atoms or molecules incoming from the gas phase. This "chemistry with a hammer" was pioneered by the Ceyer group, and shown to be operative for the case of the dissociation of methane on nickel surfaces [143,202,203]. As shown in Fig. 15, the cross section of the collision-induced dissociation displays a complex dependence on the energy of the impinging atom (an inert gas such as Ar or Ne, the "hammer") that does not scale with either the total or the normal energy. It was concluded that the activation occurs via the impulsive transfer of kinetic energy upon collision of the projectile with the physisorbed CH_4 followed by translationally activated dissociative chemisorption of the latter upon its subsequent collision with the Ni surface.

Information on the reactivity of specific excited states can also be extracted, thanks to the principle of microscopic reversibility, from detailed characterization of the energetics and angular dependence of the desorbing molecules. For instance, in a study of the associative recombination of deuterium atoms chemisorbed on Cu (111), the dependence on rotational J and vibrational ν states of the translational energy of the D_2 molecules desorbing from the surface after recombination were mapped out in a quantum-state-specific manner using three-photon resonance-enhanced multiphoton ionization (2+1 REMPI); the kinetic energies were obtained by measuring the flight time of D_2^+ ions in a field-free region [125]. It was found that the mean kinetic energies depend strongly on the rotational and vibrational states, and it was concluded that the vibrational energy is effective, though not as effective as the

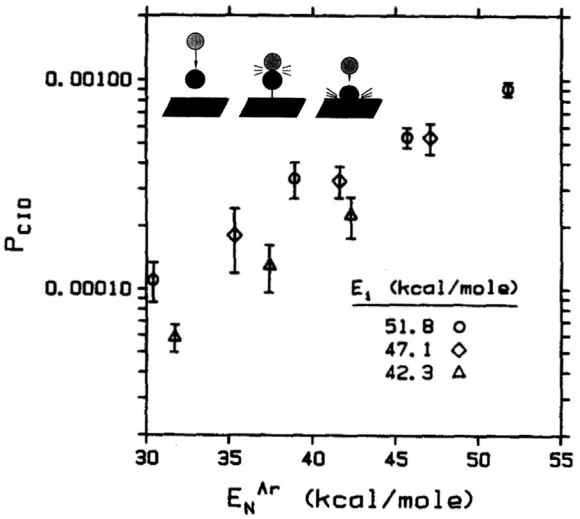

Fig. 15. Probability of collision-induced dissociation events per incident Ar atom, P_{CID}, for methane physisorbed on a Ni(111) surface ($\theta_{CH4}=0.03$ monolayers) as a function of the normal component of the kinetic energy of the Ar atoms, $E_N^{Ar}=E_i\cdot\cos^2\theta_i$ [202]. Experiments were carried out at three different argon kinetic energies, $E_i=42.3$ (triangles), 47.1 (diamonds), and 51.8 (circles) kcal/mol, and several angles of incidence, $\theta_i=0°$, 20°, 30°, and 40°. The probability for methane activation is seen to increase exponentially with the normal component of the incident Ar atoms, suggesting a methane activation mechanism via impulsive collisions as depicted schematically in the inset. Adapted with permission from Ref. [202], Copyright 1989 American Institute of Physics.

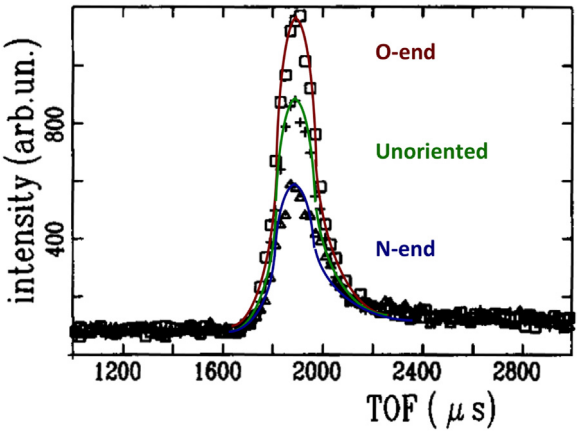

Fig. 16. Time-of-flight (TOF) spectra of NO molecules scattered from a Pt(111) surface [209]. The characteristics of the incoming NO molecular beam and surface were as follows: $E_i=0.24$ eV, $\theta_i=47.5°$, $\theta_r=61.5°$ (angle of detection), $T_s=575$ K. In these experiments, the orientation of the NO molecules was aligned with the aid of electrostatic focusing; data are shown for the intensity of the scattered molecules in O-end (red), random orientation (green) and N-end (blue) collisions. The N-end collisions were shown to lead to less scattering, and therefore more molecular trapping, than the O-end collisions. Adapted with permission from Ref. [209], Copyright 1990 Elsevier Science Publishers B.V. (For interpretation of the references to color in this figure legend, the reader is referred to the web version of this article.)

translational energy, in promoting adsorption. Rotational motion was found to hinder adsorption for low rotational states ($J\leq 5$) but enhance adsorption for high rotational states ($J\geq 5$), and also to never be as effective as either the vibrational energy, which is 30–70% more effective than the rotational energy, or the translational energy, which is 2.5–3 times more effective than the rotational energy, in promoting adsorption.

3.7. Steering

In the preceding section we discussed the possibility of enhancing adsorption via the excitation of molecular vibrational states within the incoming adsorbates. The sticking of molecules on surfaces may also be affected by molecular orientation, and that may be aided by molecular steering [204,205]. This idea has been invoked to explain some of the results obtained in molecular beam work on adsorption. For instance, for D_2 on Pt(100), the fact that on the reconstructed hexagonal phase the initial sticking coefficient decreases sharply in the range of initial energies between 5 and 10 meV was interpreted as the result of dynamical steering [206].

Steering may be characterized by evaluating the scattered molecules selectively as a function of their rotational excitation level J, by using optical detection that relies on resonant excitation. Using 2+1 REMPI, it was determined that, in the case of hydrogen on Pd(111), the sticking is sensitive to the rotational quantum number, first decreasing as J is raised from 0 to 3, then increasing again for $J=4$ and $J=5$ [207]. It was also established that some of the H_2 incident molecules in the $J=0$ and $J=1$ states are excited directly upon collision with the surface, without any involvement of dissociation or recombination states, to the $J=2$ and $J=3$ states, respectively, with probabilities that increase strongly with surface temperature and that are roughly independent of incident translational energy. Steering has also been identified indirectly from the need to include such effect in theoretical calculations to be able to reproduce data from molecular beam experiments, as in a recent paper on the adsorption dynamics of O_2 adsorption on Cu(100) [208].

An alternative methodology for controlling steering is to manipulate the rotational state of the incoming gas molecules in the gas phase. This can be accomplished with polar molecules such as NO by using electrostatic focusing. Orienting NO molecules this way with the N-end versus the O-end towards the surface led to different results on Pt(111) and Ag(111): N-end collisions showed lower scattering yields and larger trapping probabilities than O-end collisions on the first surface (Fig. 16), whereas the opposite was seen with the second [209]. Paramagnetic molecules can also be aligned using hexapoles. For instance, it was determined using such approach that, at translational energies below 0.2 eV, O_2 sticking on Al(111) occurs predominantly when the molecular axis is parallel to the surface [210]. Similar experiments have been carried out on Ni(111) and Si(100) [211]. In another study, the initial sticking coefficient of CH_3Cl on Si(100) was found to be the largest when the molecules are oriented with their chlorine atom pointing toward the surface [212]. The opposite preference for sticking via the methyl side was reported for CH_3F on graphite (0001) [213,214].

More recently, a methodology has been developed to collisionally align non-polar molecules in molecular beams [215]. Application of this technique to the study of the sticking of ethylene on oxygen-predosed Ag(001) versus surface coverage has shown that, interestingly, the sticking is not affected by the degree of molecular alignment at the very early stages of the uptake but develops a large difference in S, by a factor of up to 3.5, starting at ethylene coverage of only a few per cent of a monolayer (Fig. 17) [215].

3.8. Kinetics of adsorption uptake

As already implied in the previous sections of this review, adsorption is often described in terms of sticking coefficients, that is, in terms of the fraction of molecules impinging on a surface that adsorb instead of scatter back into the gas phase [13,216]. The sticking coefficient for adsorption depends on the coverage of adsorbed species on the surface, and that can be measured by recording the adsorbate uptake as a function of time of exposure.

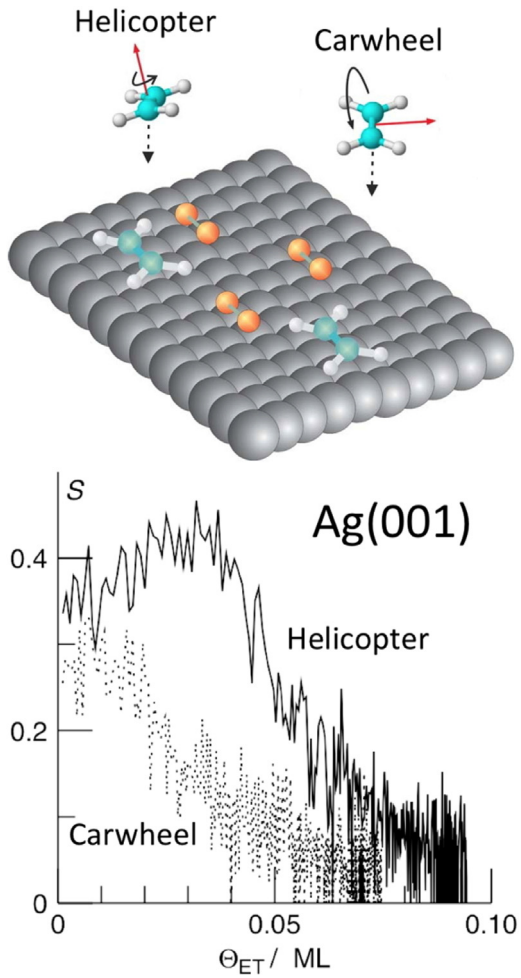

Fig. 17. Bottom: Plot of the sticking coefficient S versus coverage θ_{ET} during the uptake of ethylene on a Ag(001) surface pre-covered with molecular oxygen [215,587]. In these experiments the molecular beam energy was fixed at E_i=0.36 eV, and, like in Fig. 16, the rotational states of the incoming ethylene molecules were controlled; data are reported for the interaction of randomly orientated (mostly helicopters, solid line) and aligned (mostly cartwheels, dotted line) ethylene projectiles (the molecular motions are shown schematically in the top scheme). Differences in sticking probabilities are obvious from the data, especially at high ethylene surface coverages, with the uptake of the helicopters being more effective than that of the cartwheels. Adapted with permission from Ref. [215], Copyright 2006 The Royal Swedish Academy of Sciences, and Ref. [587], Copyright 2005 American Institute of Physics.

This methodology, which was initially described simultaneously by King and Wells [103] and Madey [217], is exemplified for the case of carbon monoxide adsorption on Pt(111) in Fig. 18, which was studied by using the setup described in Fig. 3 [218]. The top left panel (a) shows the raw data, in the form of the partial pressure of CO versus time. An initial jump in signal is seen at t = −8 s, as the beam is turned on. With the beam still blocked from impinging directly on the surface, the CO partial pressure rises to a new steady-state value because of scattering of the molecules from the intercepting flag, a process that takes a few seconds. Then, at t=0 s, the flag is removed to allow the beam to strike the surface directly, an action that causes the CO partial pressure to drop instantly because of the removal of some of the CO molecules from the gas phase upon adsorption on the Pt(111) surface. After some time, the platinum surface becomes saturated and therefore incapable of adsorbing any more CO, at which point the CO partial pressure in the vacuum chamber returns to its steady value.

These data can be processed to extract the desired information. The measured CO partial pressure is subtracted from that expected if the beam would not have been blocked, the dashed line in Panel (a) of Fig. 18, and calibrated to values of sticking coefficient by determining the maximum drop in pressure expected if S=1 (typically determined by independent studies with a condensable gas). The resulting sticking probabilities (s(t) in the figure) are plotted versus time in Panel (b) of Fig. 18. Next, the signal from that plot is numerically integrated versus time to obtain the dependence of surface coverage on time (Θ(t) in Panel (c), Fig. 18). Finally, the sticking coefficient data in Panel (b) are collated with the coverage data in panel (c) to develop a plot of sticking coefficient versus coverage, Panel (d).

The results from this type of analysis can then be fitted to different adsorption models. The simplest analysis is based on Langmuir isotherms, where all surface sites are assumed to be identical, and where adsorption on a given site renders it inactive for further uptake [219,220]. For a molecular process, this model predicts that the sticking coefficient, that is, the probability for the impinging molecules to adsorb on the surface rather than to scatter back to the gas phase, should decrease linearly with coverage because more and more surface sites become blocked and inactive for further uptake as the population of the adsorbates on the surface increases, whereas in the case of dissociative adsorption the dependence of S on Θ is quadratic (for two resulting adsorbates). The Langmuir model can also be easily extended to competitive and non-competitive adsorption of two or more species.

Langmuir uptake kinetics has been seen in some instances but are not very common, so a number of adsorption isotherms have been developed to describe the uptake on surfaces with a distribution of sites, and several approaches have also been advanced to include the role of adsorption on precursor states, the most common perhaps been that proposed by Kisliuk [221,222]. Two types of precursors need to be considered: the intrinsic precursor state described in Section 3.2, a physisorbed species associated with a shallow minimum in the potential energy surface as the molecule approaches the chemisorbed state on the clean surface [223], and an extrinsic precursor, due to weak adsorption on top of a surface site that is already occupied by another adsorbate [130,224–226]. Further refinements include the consideration of coverage-dependent adsorption energies [227–230], something that is fairly common because of adsorbate-adsorbate interactions [231], and the inhomogeneous distribution of adsorbates, seen in cases such as when surface islands are formed [232,233]. The latter is difficult to reproduce with mean-field kinetic equations, but may be simulated with Monte Carlo kinetic algorithms [234–243].

The so-called King and Wells method described above for sticking coefficient measurements is vastly popular, and has been used in numerous studies, too many to survey here. Its usefulness can be illustrated by a recent study from our group focused on identifying enantioselectivity on surfaces. Our general idea, borrowed from the pioneering work of Tysoe and coworkers [244,245], is that a chiral molecule such as propylene oxide (PO) can be use to titrate enantioselective surface sites made by building a controlled coverage of another chiral adsorbate, the chiral modifier [246–248]. During the characterization of the adsorption of PO by itself on Pt(111), it was found that the saturation monolayer of a racemic (50:50) mixture is approximately 20% less dense than a similar layer made out of one single PO enantiomer (either S- or R-PO). Molecular beam measurements (Fig. 19, left panel), combined with temperature programmed desorption (TPD) and scanning tunneling microscopy (STM), and also with kinetic Monte Carlo simulations (Fig. 19, right), helped identify the reason for this behavior as the result of adsorption kinetics assisted by adsorbates previously dosed on the surface. Different probabilities for homo- versus hetero-enantiomeric pairs needed

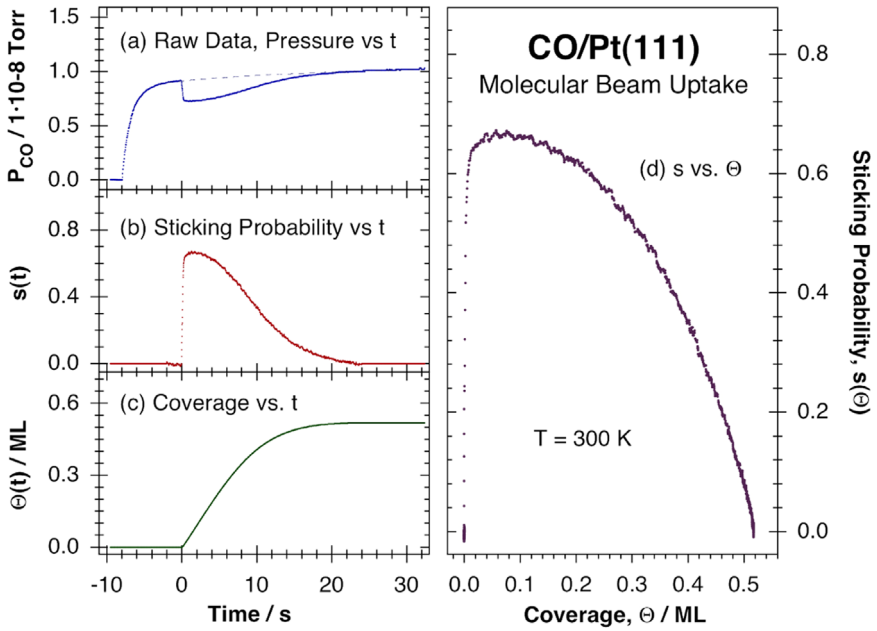

Fig. 18. Typical kinetic data from experiments using an effusive molecular beam to measure sticking coefficients as a function of coverage, following the so-called King and Wells method [13,218]. This case corresponds to the uptake of carbon monoxide on a Pt(111) surface at 300 K. (a) Raw data, in the form of CO partial pressure (P_{CO}) versus elapsed time. The beam is turned on at t=–8 s, but the shutter is kept in place at that time in order to avoid direct exposure of the crystal to the beam. The observed rise in signal corresponds to the increase in pressure due to CO scattering off the intercepting flag. That flag is removed at t=0 s, at which point the partial pressure of CO drops because of its removal from the gas phase via adsorption on the surface. The P_{CO} eventually returns asymptotically to the value seen before the flag is removed, as the platinum surface becomes saturated with CO. (b) Plot of the CO sticking probability, s(t), versus time, calculated directly from the data in the first panel after appropriate calibration. (c) CO surface coverage Θ(t) versus time, obtained by integration of the temporal evolution of the sticking coefficient. (d) Sticking probability versus coverage for CO adsorption on Pt(111) at 300 K, obtained by combining the data in panels (b) and (c). Adapted with permission from Ref. [13], Copyright 2002 Taylor & Francis Ltd.

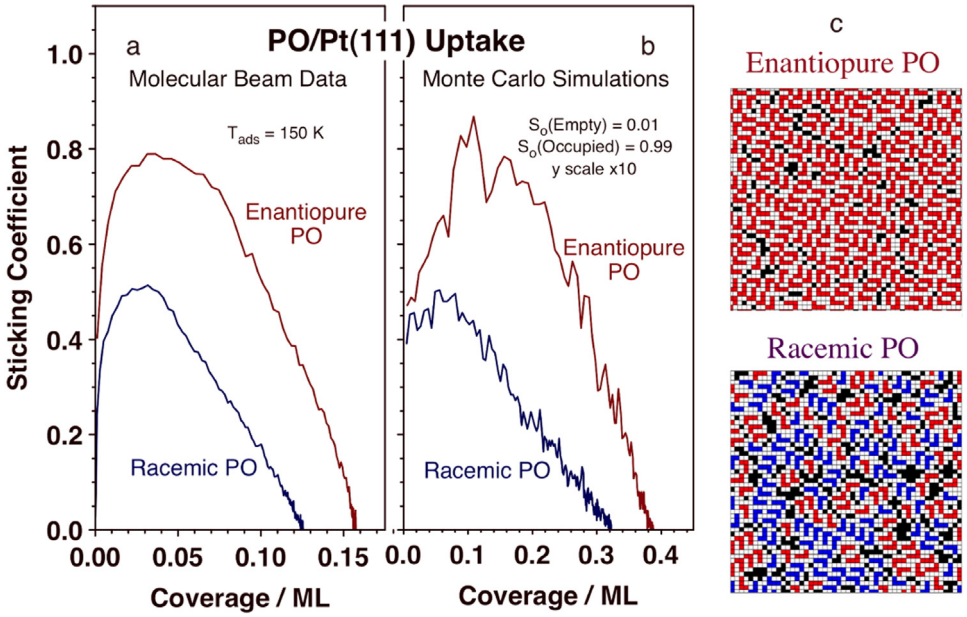

Fig. 19. Experimental (molecular beam) (a) and Monte-Carlo-simulated (b) isothermal uptake curves for propylene oxide (PO) on Pt(111) at 150 K, in the form of sticking coefficient versus PO surface coverage [249]. PO is a chiral molecule, and in this study it was demonstrated that the uptake depends on the enantiomeric composition of the incoming molecules. Two traces are shown in each panel, for the uptake of enantiopure (red) and racemic (blue) PO. Higher saturation coverages and sticking coefficients are always seen with the enantiopure molecules. In addition, there is always an initial increase in sticking coefficient with coverage, reproduced in the Monte Carlo simulations by considering an adsorbate-assisted process with a higher sticking coefficient on occupied sites, S_0(Occupied)=0.99, than on empty sites, S_0(Empty)=0.01. Panel (c) shows snapshots of the simulated surfaces obtained at saturation with enantiopure (top) and racemic (bottom) PO. The red and blue elements represent the two enantiomers of PO, the white squares the buffer zones between adsorbates, and the black areas unfilled empty spaces. Reproduced with permission from Ref. [249], Copyright 2013 American Chemical Society.

to also be considered in this explanation [249,250].

Adsorbate-assisted adsorption has been known from past experiments [224,251] but is not common. The molecular beam uptake experiments have been particularly valuable in this research, as the adsorbate-assisted kinetics is clearly manifested by an initial increase in sticking coefficient with increasing coverage; this is seen in Fig. 19 for coverages below about 0.03 monolayers (ML). In the end, two separate effects were identified in these studies, a kinetic preference for homochiral adsorption dominant at the initial stages of the uptake, and a second thermodynamic

bias towards racemic mixtures at saturation [252]. It was also established that the enantioselectivity of the surface can be amplified from that bestowed by a small amount of adsorbed homochiral PO by subsequently adsorbing a second non-chiral (but prochiral) molecule such as propylene [253]. All these conclusions have relied in great part on results from measurements of sticking coefficient versus coverage acquired with an effusive molecular beam system.

4. Kinetics of reactions: Early examples

In the previous section, the focus of the discussion was on either molecular or dissociative adsorption. In either case, the kinetics refers to the association of one single species with the solid surface, and involves a set of unimolecular reaction steps. It is possible, and more common in practical applications such as in heterogeneous catalysis, to have two or more species adsorb and react on solid surfaces. These systems are, from a kinetic point of view, much more complex to describe. At the very least, the question arises as to what is the dynamics of the reaction. In general, such dynamics can be described in terms of either the so-called Langmuir-Hinshelwood mechanism, where the reactants interact and undergo chemical conversion once they are all adsorbed on the surface, or the Eley-Rideal mechanism, in which case one of the reactants impinges directly from the gas phase on the second adsorbate. To distinguish between these two possibilities, there is a need to pinpoint the details of the dynamics and kinetics of the adsorption of the reactants and the desorption of products. Molecular beam experiments, in particular those that use pulsed and time-resolved techniques to extract transient information, have been quite informative in this area. Many details about the dynamics of catalytic reactions have been obtained for simple systems, as discussed in this Section. Data relevant to reaction kinetics have also been collected for more complex chemical transformations, as described in the next Section.

4.1. $CO+O_2$

The oxidation of carbon monoxide with molecular oxygen on late-transition-metal single-crystal surfaces is perhaps the reaction that has been studied to the largest extent by using molecular beams [22,254,255]. Most combinations of experimental setups, as discussed in Section 2.2, have been applied to this system. For instance, on Pt surfaces, Fair and Madix used background oxygen fluxes sufficiently high to nearly saturate the surface and combined that with modulation of an incident CO beam to extract kinetic parameters for this reaction, specifically focusing on the role of terraces and defects in promoting CO_2 formation [256]. Ertl and coworkers, on the other hand, utilized a modulated O_2 beam with a small CO background pressure to obtain rate constant for cases where the coverages of both CO and atomic oxygen on the surface (Θ_{CO} and Θ_O, respectively) are small, and also performed transient measurements on oxygen-presaturated surfaces by alternatively using a continuous or a modulated CO beam to measure the residence time of CO as a function of Θ_O [257]. These modulated experiments were conducted in two different regimes to allow for the linearization of the reaction, namely, at a high constant value of Θ_O and with a modulated CO beam, and with a modulated O_2 beam at surface temperatures such that CO desorption is rapid compared to oxidation so that Θ_{CO} is approximately constant. On Rh(110), Bowker performed three types of experiments: (1) under steady-state by using a mixed beam of CO and oxygen, (2) in a transient where the crystal was predosed with oxygen and then exposed to a beam of CO, and (3) under conditions where the reaction was allowed to reach steady state at one temperature (usually 370 K) and the crystal temperature then ramped to a second, higher, value [258].

One important conclusion derived from the time-resolved experiments designed to probe the transient states is that, in general, the oxidation of CO with O_2 on the surfaces of late transition metals such as Pt or Pd takes place via a Langmuir-Hinshelwood mechanism, that is, by recombination of two surface species. The general consensus is that the metals adsorb oxygen dissociatively, and that it is the resulting adsorbed oxygen atoms that react with adsorbed CO to produce CO_2 [256,257,259,260]. For instance, on Pd(111), surface residence times measured by modulating one of the two (O_2 or CO) beams while keeping the other constant yielded results for the phase dependence of the signals consistent only with a reaction between chemisorbed CO molecules and chemisorbed O atoms; no evidence for an Eley-Rideal mechanism could be found [260]. One possible exception to the general conclusion that CO oxidation takes place via the Langmuir-Hinshelwood mechanism is the case of oxygen-precovered Ru(0001), where CO molecules with a translational energy of 1.2 eV are oxidized with reaction probabilities below 0.05; this result is consistent with the activation barrier derived from density functional theory (DFT) calculations for a reaction by direct collision from the gas phase [261].

Regarding the dynamics of the CO oxidation reaction, on Pt (111) the dependence of the CO_2 yield on the angle of the beam, studied by phase analysis and time delay measurements with modulated CO beams (Fig. 20), led to the conclusion that the uptake of incident CO from the gas phase on O-presaturated surfaces goes through a weak precursor state [257]. Desorption from this state causes a decrease in chemisorption probability with temperature, but once chemisorbed, the CO molecule shows almost unit probability for its conversion to CO_2 below 540 K. The CO_2 angular distribution in that case varies from cosine-like (thermally accommodated) to highly peaked depending on the coverages of the adsorbed reactant [257,262,263]. Curiously, no such effects have been seen on Pd; the CO_2 angular distribution from Pd(111) is diffuse [259]. The peaked CO_2 angular distributions on Pt suggest high translational energies of the product under specific reaction conditions not seen on Pd.

The structure of the surface is an important parameter in determining reaction rates. On rhodium, for instance, the surface was found to be covered with atomic oxygen under steady state and at temperatures above those needed for CO desorption, at which point the reaction becomes structure sensitive: it is markedly faster on the more open Rh(110) plane than on the close-packed Rh(111) [264]. On Pd(110), the production of CO_2 was seen to show two rate maxima at 375 K, likely reflecting changes in reactivity upon reconstruction of the surface [265]. Steps and other defects on the surface can alter the dynamics of the surface in significant ways as well. On the one hand, Fair in Madix, experimenting with a Pt[9(111) × (100)] surface, showed that the steady-state reaction occurs primarily on the terraces, at least at high coverages, because both oxygen and CO bind preferentially to step and kink sites and block those for further reaction [256]. In contrast, Campbell et al. showed that, on Pt(111) surfaces treated to create some subsurface oxygen, the channel that produces thermally accommodated CO_2 becomes less important with increasing O or CO coverages, presumably because the added oxygen blocks the defects where that reaction may take place [266]. On oxygen-precovered Ru(0001), the formation of a thin ($\geq$ 3 ML thick) oxide layer leads to a two-orders-of-magnitude increase in CO oxidation reaction probability because of a further destabilization of the surface oxygen by the onset of oxide formation [261].

In terms of the kinetics of the CO oxidation reaction, those are difficult to describe with a simple rate law over the entire range of temperatures and pressures under which the reaction can proceed

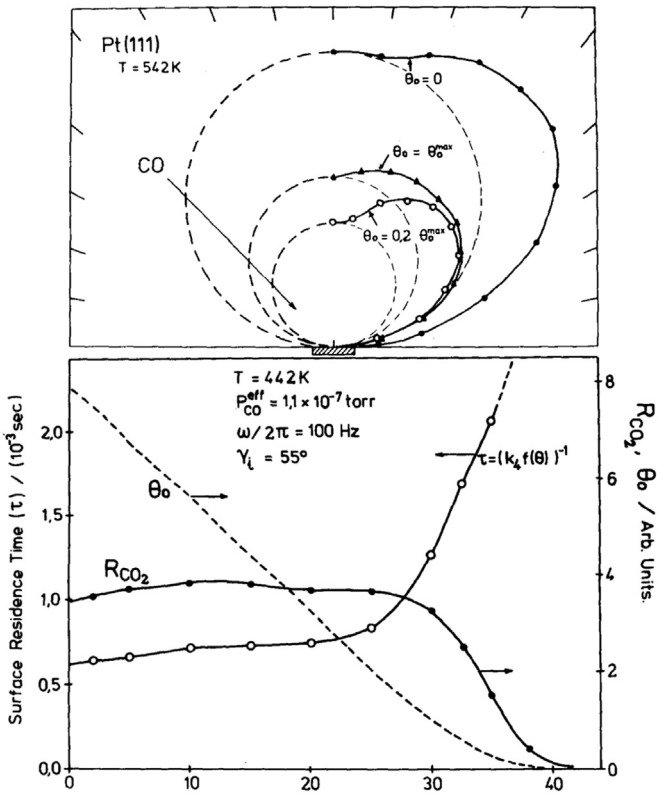

Fig. 20. Top: Signal intensity for scattered CO versus outgoing angle from molecular beam experiments where a layer of atomic oxygen was titrated off a Pt(111) surface at 542 K [257]. The angle of incidence was 45°. Angular profiles are shown for three different times during the titration corresponding to three different oxygen coverages, θ_O/θ_O^{max}=0, 0.2, and 1. Two components can be identified in these desorption angular profiles, a cosine part indicated by the dashed lines, corresponding to molecules that have fully accommodated their energy with the surface via a precursor state, and an extra, peaked, signal, indicated by the solid lines and symbols, from specular reflection. Bottom: Results from a modulated CO titration at 442 K in the form of CO surface residence time (open circles, left scale) and rate of CO_2 production (solid circles, right scale) as a function of titration time (which reflects decreasing oxygen surface coverage). The relatively long residence times for CO attest to a Langmuir-Hinshelwood mechanism for the formation of CO_2. That residence time increases as the oxygen reaches a threshold value (about 25% of saturation), at which point the production of CO_2 dies down and the data reflect CO adsorption on clean Pt. Reproduced with permission from Ref. [257], Copyright 1980 American Institute of Physics.

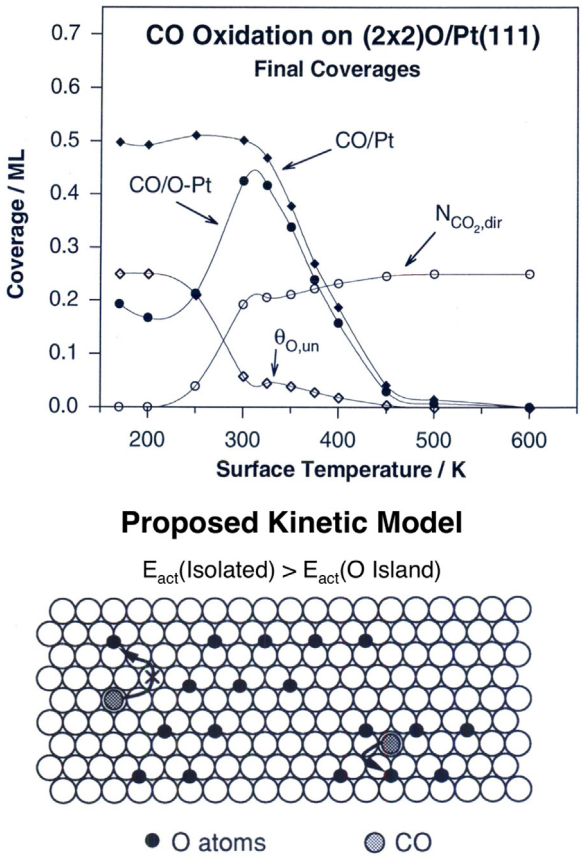

Fig. 21. Results from isothermal CO titration experiments on oxygen-saturated Pt (111) surfaces using an effusive molecular beam [68,270]. The data correspond to the measured temperature dependence of the CO_2 yield, $N_{CO2,dir}$, the final CO coverages (on both oxygen-saturated and clean Pt surfaces), and the oxygen coverage, $\theta_{O,un}$. Below 300 K no reaction is observed and above 400 K oxygen removal is complete, but in the intermediate 300–400 K temperature regime the reaction never reaches completion. This was explained by invoking two kinetically distinct types of oxygen atoms, as illustrated schematically in the bottom diagram: isolated atoms, which are difficult to remove, and those associated with surface islands, where the activation barrier for CO_2 production is lower [68,271]. Adapted with permission from Ref. [271], Copyright 1996 American Institute of Physics.

because of changes in the adsorption rate for O_2, the effects due to coadsorption of CO and atomic oxygen, the role of possible limited diffusion of the adsorbates within the adlayer, and the possible non-homogeneous distribution of adsorbates on the surface, which may vary with varying coverage. In particular, chemisorbed CO is known to inhibit the adsorption of O_2, whereas the sticking probability of CO is largely unaffected by adsorbed oxygen [254,267,268]. It is also known that the interaction among adsorbed oxygen atoms is attractive, a fact that leads to the formation of surface islands at coverages as low as 5% of a monolayer and at surface temperatures as low as 300 K [22]. Typically, it has been stated that CO adsorbs preferentially outside of the oxygen surface islands, but at sufficiently high coverages the oxygen islands may be compressed [267–269], and even form a mixed CO (ads)+O(ads) phase [268,269]; transient measurements on oxygen-presaturated surfaces have indicated that the activation energy for CO oxidation changes with coverage because of these effects [22,259].

We have explored the kinetics of CO oxidation on Pt(111) in an intermediate regime where these oxygen islands play a critical role by using effusive molecular beams in several of the modalities discussed in Section 2.2 (Fig. 21, top) [68,270,271]. Above 400 K, the rate of CO_2 production was found to be determined by the impinging rate of the carbon monoxide molecules on the surface as long as the CO:O_2 ratio is low, but the CO steady-state coverage was seen to increase and to poison the adsorption of oxygen and the overall CO_2 production as that CO:O_2 ratio is increased [68,270]. At the other end, below 300 K, no reaction is observed, and the presence of preadsorbed atomic oxygen on the surface does not significantly affect the initial sticking coefficient of CO but only reduces its saturation coverage by less than half, which it does by preferentially blocking the bridge sites [68]. In between, however, the rate of surface recombination of CO with oxygen competes with that of CO adsorption, giving raise to a fairly complex overall dynamic behavior where the reaction rates not only depend on the coverages of the reactants but also on how the surface is prepared. Two kinetically distinct types of oxygen atoms were identified between 300 and 400 K even though they all sit in identical sites at the start of the reaction, and the isothermal removal of the adsorbed oxygen by incoming CO molecules is incomplete [68,271]. This was explained by a lowering in the reaction activation barrier within the oxygen islands that form on the surface (Fig. 21, bottom).

Similar experiments have been carried out on Pd(111). Some common features were observed, but the CO poisoning typically

observed on virgin surfaces could in this case be partially lifted by modifying the surface via the addition of subsurface oxygen, to the point of allowing for ambient CO oxidation [272–274]. A significant time delay was also observed between the onset of oxygen adsorption and that of CO adsorption and CO_2 production. Even more complex kinetics have been seen on Pd(110), where CO oxidation exhibits an isothermal 'light-off' in which the rate autocatalytically increases with time. This is believed to be due to the desorption of CO, which releases extra sites for O_2 dissociation and in turn removes more CO (hence the self-acceleration) [275]. Finally, on surfaces prone to reconstruction, the non-linearity of the rate of that process on surface coverage can cause, under specific conditions, chemical oscillations, both in time and in space [276–278].

4.2. H_2+O_2

Another well-studied reaction catalyzed by transition metals is the oxidation of molecular hydrogen to produce water. This reaction shares some common steps with the $CO+O_2$ process discussed above, in particular the dissociative adsorption of molecular oxygen, but it offers additional complexity in the form of the possible formation of an hydroxide surface intermediate as the result of the sequential addition of atomic hydrogen to adsorbed oxygen. In fact, many studies have focused on trying to answer this specific mechanistic issue.

In one of the earliest reports on this reaction, the group of Dumesic et al. used a steady-state molecular beam technique to obtain kinetic data for the conversion of H_2+O_2 mixtures on polycrystalline Pt that they found consistent with a Langmuir-Hinshelwood mechanism involving a direct 2H(ads)+O(ads) recombination step to form H_2O(g), with an activation energy of ~80 kJ/mol [279]. However, those authors could not rule out other possible mechanisms. On Pt(111), Smith and Palmer measured apparent reaction orders between 0.8 and 1 in O_2 flux and between 1 and 2 in D_2 flux, a result that led them to suggest a direct reaction with O_2(ads) [280]. However, they did not offer a detailed mechanism that indicated the intervening elementary steps for this process. Water formation was found to be activated, but, interestingly, so was D_2 adsorption under the reaction conditions. On the basis of the kinetic parameters measured, the authors suggested a mechanism involving an equilibrium between adsorbed oxygen atoms, hydrogen atoms, and an adsorbed OH intermediate, the latter with a short lifetime, and a rate-limiting step consisting of a reaction between H(ads) and OH(ads) to form H_2O(g). On the other hand, Gdowski and Madix found that the rate of H_2O formation on Pt(S)-[9(111)×(100)] is second order in H(ads), which precludes OH(ads) formation as the rate-limiting step and suggests a quasi-equilibrium among O(ads), H(ads), and OH(ads) surface species [281]. Nevertheless, neither a direct 2H(ads)+O(ads)→H_2O(g) recombination nor a disproportionation of OH(ads) groups, 2OH(ads)→O(ads)+H_2O(g), could be excluded. These authors also determined that above 700 K a second parallel process associated with oxygen atoms at the steps becomes operative.

Padowitz et al. designed a modulated molecular beam reactive-scattering technique involving three beams, namely, a continuous O_2 source, a modulated H_2/D_2 beam, and a third low-flux H_2/D_2 beam (used to induce small perturbations on the steady state of the reaction), to measure kinetic parameters around steady-state conditions (Fig. 22, left) [282]. With this technique, the authors were able to vary the surface oxygen coverage, use isotopic substitution, and linearize the HDO reaction. The reaction orders were found to display a complex interdependence, as indicated by the data in the right side of Fig. 22. They determined that, on Rh(111), the formation of water takes place via sequential atomic-hydrogen addition steps, with apparent activation energies of 10 ± 4 and 40 ± 4 kJ/mol for the OH(ads) and H_2O(g) formation, respectively [282]. This is perhaps the most comprehensive kinetic study available for this reaction, and the one that contributes the most convincing arguments for the determination of the reaction mechanism.

The need to activate molecular hydrogen to produce water becomes more evident on surfaces on which the dissociative adsorption of hydrogen is itself activated. For instance, on a Cu(110) surface predosed with oxygen, no water can be produced until the normal component of the energy of the H_2 beam reaches a value of about 200 meV, at which point H_2O is made via Langmuir-Hinshelwood kinetics [283]. The results from that study suggest that the dissociative barrier for hydrogen adsorption is rate determining, and itself insensitive to oxygen coverage.

The water-formation reaction on palladium can be further complicated by the ability of that metal to absorb atomic hydrogen. On Pd(111), Engel and Kuipers determined that the reaction product, H_2O, is emitted from the surface with a cosine distribution [284]. Under excess H_2, large H_2O phase lags were observed even at high temperatures, indicating a Langmuir-Hinshelwood mechanism and the presence of bulk diffusion effects. The rate-

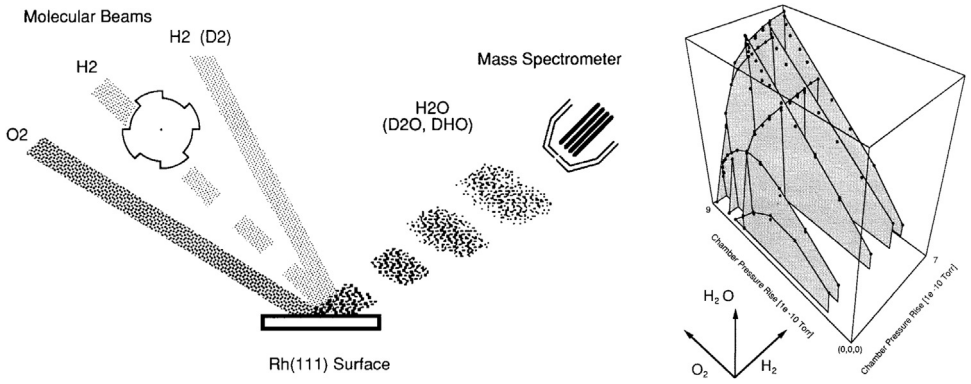

Fig. 22. Left: Schematics of an instrument with a multiple molecular beam configuration used for the study of water formation from the reaction between hydrogen and oxygen on Rh(111) [282]. In addition to continuous oxygen and modulated hydrogen beams, a third continuous beam of hydrogen or deuterium was incorporated to control the surface coverages and linearize the reaction, to study its kinetics under steady state via the induction of small transients. Right: Product (H_2O) mass spectrometer signal as a function of the beam fluxes of the reactants at 650 K. The sections running from the lower right to the upper left correspond to experiments with varying oxygen fluxes at a constant hydrogen flux, whereas the second axis in the bottom plane is associated with variations in hydrogen flux at constant oxygen flux (the third, vertical axis reports the results in terms of water partial pressure). The kinetics of this reaction are quite complex: sections taken at constant O_2 flux show that the reaction rate increases rapidly with H_2 flux but then levels off, indicating a reaction order in H_2 below one, whereas at constant high H_2 flux the response to O_2 flux is linear. Moreover, at low H_2 flux, the rate is not monotonic with O_2 flux. Instead, as the O_2 flux is increased, the rate of water production first rises but then declines to zero. Consequently, no global reaction order can be specified in terms of reactant pressures. Reproduced with permission from Ref. [282], Copyright 1991 Elsevier Science Publishers B.V.

determining step in that case was determined to be the formation of OH(ads) from O(ads)+H(ads), a step with an activation energy of 30 kJ/mole. With O_2 in excess, however, the phase lag decreases to zero at high temperatures, indicating that a high oxygen coverage blocks H diffusion into the bulk, and that the hydrogen reservoir available for reaction at the surface is therefore decreased by several orders of magnitude. This results in a drastic reduction of the reaction rate that can be reversed by increasing the partial pressure of H_2.

Studies on the dynamics of the water-forming reaction have also identified some surprising facts. In terms of the angular distribution of the desorbing products, the H_2+O_2 reaction on Pt(111) shows similar characteristics to those seen in the oxidation of CO in that there is a substantial amount of energy to be disposed of as the final activation barrier is surmounted. However, whereas peaked CO_2 angular distributions were observed with CO, only diffuse H_2O distributions have been reported with H_2 [280,284,285]. Moreover, the D_2O molecules produced from D_2+O_2 have been seen to desorb cold independently of the desorption angle, presumably because of losses to the surface due to molecular diffusion [285].

4.3. CO+NO

A third related system to the two discussed above is the reduction of nitrogen oxide by carbon monoxide. The main channel for this chemistry on late transition metals is N–O bond dissociation, after which further conversion involves both the nitrogen and oxygen atoms adsorbed on the surface. The removal of adsorbed oxygen follows a reaction similar to that seen with $CO+O_2$ mixtures (discussed above), and is typically fast. Therefore, the key chemistry defining the reactivity of the surface in this case is that related to the nitrogen atoms. Typically, the main product is N_2, but in some cases small amounts of N_2O have been seen as well [286–288]. Most of the molecular beam research on this system has been carried out on rhodium surfaces because that is the metal of choice for the three-way catalyst, and therefore we will review that work first. Some research has been performed on Pd and Pt as well, as mentioned later, and that will be reviewed later. The reaction is even feasible on Cu(110) surfaces [289].

Some aspects of the dynamics of this reaction have been characterized with a supersonic molecular beam apparatus that affords the control of the molecular orientation of the incoming NO molecules. Experiments on CO-precovered Rh(100) surfaces indicated a marked preference for CO_2 production with N-end collisions that cannot be explained solely by an orientation-dependent sticking coefficient (Fig. 23) [290]. The authors interpreted their data in terms of a transition in the reaction mechanism from a direct Eley-Rideal step to an indirect surface reaction channel via a Langmuir Hinshelwood pathway. A similar N-ended reactivity preference was also detected on Pt(100), but in that case the cosine angular distribution seen for the desorbing CO_2 suggested that neither direct nor precursor-mediated reaction mechanism are probable [291]. An additional shift of the CO_2 peak as a function of NO translational energy was observed that could be modeled by assuming an energy-dependent NO dissociation. The authors concluded that the best mechanism that explains their results is one where NO adsorption is dissociative and depends on both the orientation and the momentum of the incoming molecules. A large steric effect on the production of CO_2 was seen at high translational energies, justified by a second channel involving orientation-dependent dissociative NO adsorption.

We have investigated the kinetics of this reaction extensively on Rh(111) with the aid of an effusive molecular beam [13,292]. We found that the adsorption of NO is precursor mediated (by previously adsorbed NO) at low temperatures, and that it is

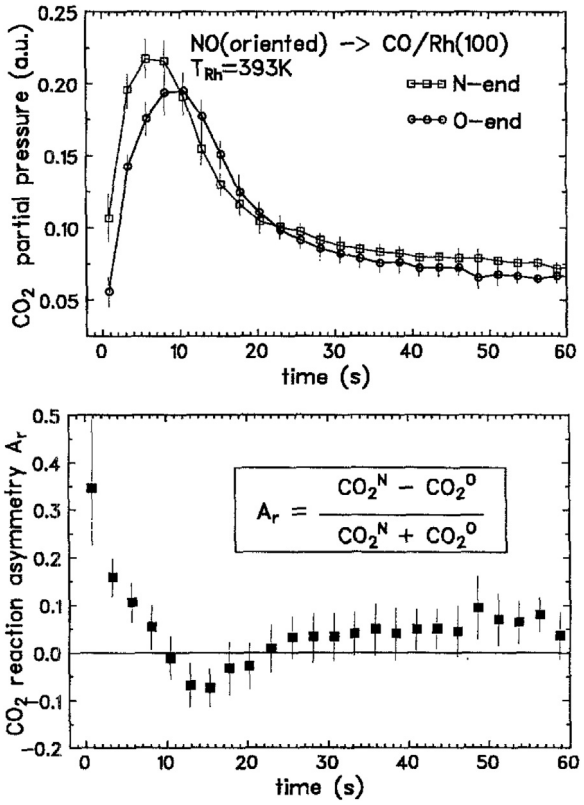

Fig. 23. Results from molecular beam experiments on the reaction of CO with NO on Rh(100) studied with oriented NO molecules [290]. Top: CO_2 partial pressure for both extreme spatial orientations of the NO molecule, namely, with either the N (open squares) or the O (solid circles) end oriented towards the surface, as a function of time at a surface temperature of 393 K. Bottom: corresponding CO_2 reaction asymmetry parameter, A_r, calculated from the raw data provided above, as a function of time. The changes in orientation preference seen as a function of time are interpreted as a switch in the dominant mechanism, from a direct Eley-Rideal step at early times to an indirect surface reaction channel via a Langmuir Hinshelwood pathway later on. Reproduced with permission from Ref. [290], Copyright 1996 Elsevier Science B.V.

not affected significantly by the presence of coadsorbed nitrogen and/or oxygen atoms on the surface at any temperature below 900 K [293]. In the absence of CO, molecular nitrogen is produced above 450 K, in a reaction controlled by the recombination of atomic nitrogen below 600 K but with an order in nitrogen coverage below unity, indicating slow diffusion of nitrogen atoms across the surface prior to their recombination. A strong additional effect due to lateral repulsions between nitrogen and/or oxygen atoms was also inferred from the data. With CO+NO beams, it was determined that the maximum in reaction rate occurs between 450 and 900 K, the exact temperature depending on the NO:CO beam ratio because of a synergistic behavior where the lost in reactivity induced by increasing the CO concentration in the beam is partly compensated by a higher surface temperature [69,294,295]. The NO+CO conversion rate is directly proportional to the coverage of atomic oxygen on the surface, but shows an inverse relationship with nitrogen coverages in most cases.

The build-up of a critical coverage of atomic nitrogen was found to be necessary to trigger the nitrogen recombination step to N_2 [65], causing a time delay between the start of the reaction and the evolution of N_2 [296]. This critical coverage of strongly-held nitrogen was determined to not depend in any significant way on the composition of the beam, but to decrease with reaction temperature, and to display an inverse correlation with the steady-state reaction rate. In fact, two types of kinetically different nitrogen atoms were identified on the surface, with an additional

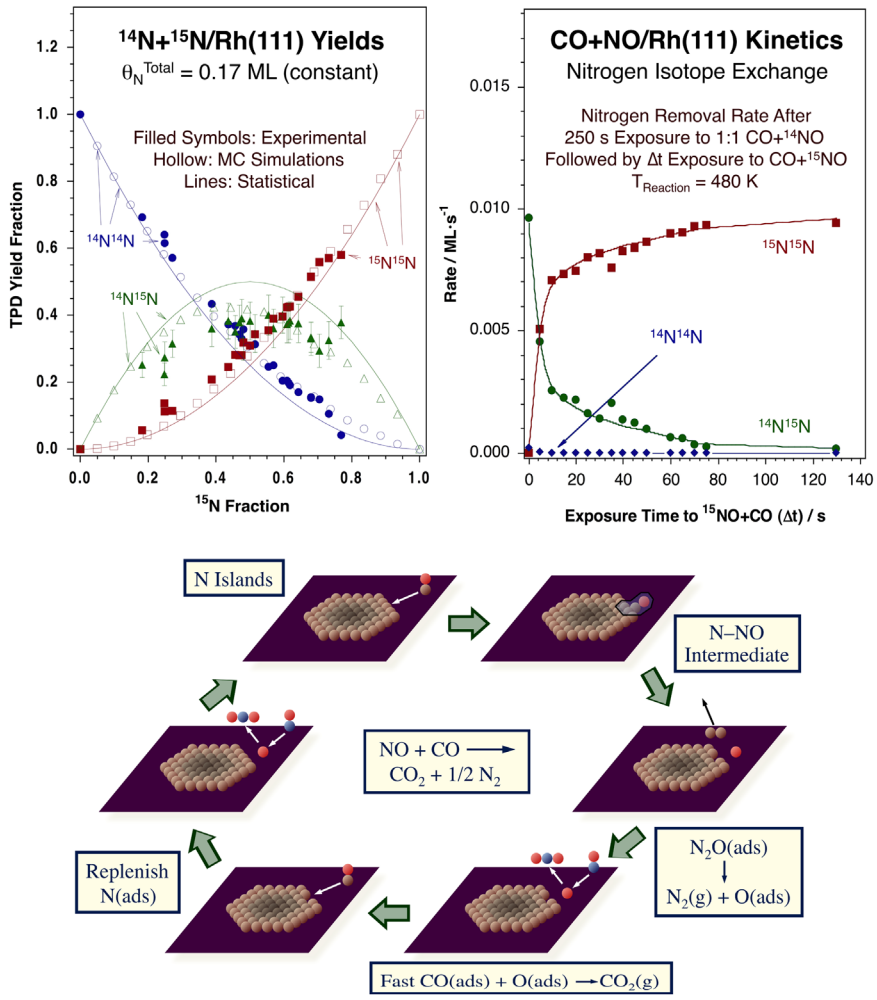

Fig. 24. Data from isotope-labeling molecular beam experiments with CO+NO mixtures on Rh(111). Top, left: $^{14}N^{14}N$,$^{14}N^{15}N$, and $^{15}N^{15}N$ TPD yield fractions as a function of the fraction of ^{15}N within the total surface atomic nitrogen measured in experiments such as that illustrated in Fig. 4 [66]. The filled symbols correspond to the data obtained experimentally, whereas the open symbols come from a Monte Carlo simulation based on surface islanding; the lines, which correspond to the yields expected on statistical grounds, do not fit the data. Top, right: Evolution of the $^{14}N^{14}N$, $^{14}N^{15}N$, and $^{15}N^{15}N$ production rates as a function of the time Δt a ^{14}N-covered surface is exposed to a ^{15}NO+CO beam (in the isotope-switching experiments described in Fig. 4) [58]. The original ^{14}N is slowly replaced by new ^{15}N, but only via the formation of $^{14}N^{15}N$; no $^{14}N^{14}N$ is ever detected, indicating that molecular nitrogen must be produced via the formation of an N–NO intermediate. Bottom: Schematic depiction of the kinetic model proposed to explain these results [297]. Two key features are worth highlighting from this model, namely: (1) the formation of nitrogen islands; and (2) the preferential reaction of the N atoms at the edges of those islands with incoming NO molecules to form a N–NO surface intermediate. Adapted with permission from Ref. [66], Copyright 2001 American Chemical Society, Ref. [58], Copyright 2000 Elsevier Science B.V., and Ref. [297], Copyright 2002 American Chemical Society.

small amount of adsorbed nitrogen present during catalysis that desorb rapidly after the removal of the gas-phase reactants. The NO reduction rate displays an approximately first-order dependence on the coverage of these latter labile N atoms.

Isotope switching experiments led to the proposal of a model in which the nitrogen atoms form surface islands and where only the atoms at the perimeter of those islands are reactive [294]. This is supported by the non-statistical distribution of the ^{14}N and ^{15}N in the N_2 produced in isotopic labeling experiments where ^{14}N-dosed surfaces were subsequently exposed to ^{15}NO+CO gas mixtures for varying times (Fig. 4): the yield of the mixed $^{14}N^{15}N$ isotopologue were found to be significantly lower than that expected from statistical considerations (Fig. 24, top-left panel) [66]. In addition, the replacement of surface ^{14}N by ^{15}N upon switching the isotopic nitrogen label in the incoming NO reactant (from ^{14}NO to ^{15}NO) was determined to occur via the exclusive formation of $^{14}N^{15}N$; no $^{14}N^{14}N$ was detected in these experiments (Fig. 24, top right). This result provided direct kinetic evidence for a mechanism where the production of molecular nitrogen involves the formation of an N–NO intermediate (Fig. 24, bottom) [58,297,298]. Our interpretation was supported and expanded by a series of theoretical studies using Monte Carlo simulations [60,299–303].

Further corroboration of the formation of an N–NO intermediate was acquired by studying the kinetics of N_2O decomposition with the same molecular beam approach [304]. Such decomposition was determined to occur at temperatures as low as 120 K, to follow first order kinetics, and to lead to the stoichiometric production of N_2(g) and atomic adsorbed oxygen. Steady-state reaction rates were found to be limited by the rate of oxygen removal (with CO), not by the decomposition of the N_2O molecules. Curiously, lower rates and total yields were observed with increasing reaction temperatures, presumably because of the increased importance of N_2O desorption and surface mobility to the overall kinetics. In fact, it was seen that after the rhodium surface is rendered inactive by N_2O decomposition at high (520 K) temperatures, significant activity is still possible at lower (350 K) temperatures [305]. Monte Carlo simulations helped explain these observations by assuming that the surface sites required for the activation of adsorbed N_2O increase in size with increasing reaction temperature.

Addition of oxygen to the reaction mixture inhibits both NO reduction to N_2 and CO_2 production, not because of the consumption of CO by the added O_2 but because of poisoning toward

CO adsorption by adsorbed atomic oxygen [38]. In fact, NO always competes favorably against O_2 for the consumption of CO. Optimum reaction rates for the production of both N_2 and CO_2 are reached at temperatures around 500–600 K and under conditions leading to stoichiometric coverages of all reactants. An interesting consequence of this conclusion is the fact that with CO-rich mixtures the addition of oxygen to the reaction mixture sometimes facilitates rather than poisons NO reduction, presumably because that helps in the removal of the excess CO from the surface. A synergy was observed in terms of the reaction-rate maxima between temperature and beam composition, CO-richer mixtures requiring higher temperatures to reach comparable reaction rates. Finally, Bowker and coworkers found that there is a structure sensitivity to the CO+NO and N_2O decomposition reactions, with reaction rates on Rh(110) being much lower than on Rh(111) [306–308]. The group of Matsushima has offered further support for the structure sensitivity of the CO+NO conversion in the form of an angular dependence of the desorption of N_2 that implies an intermediate N_2O oriented along the [001] direction [19].

The reaction of CO with NO on palladium surfaces share many of the features identified on rhodium. On Pd(111), for instance, NO decomposition starts at 425 K, selectively produces N_2 (although a minor amount of N_2O is also detected), and reaches maximum rates between 475 and 500 K [309,310]. These conclusions all mimic those reported on Rh(111). However, data from CO titration experiments after NO dosing on Pd have identified some diffusion of oxygen into the subsurface region and the start of surface oxidation at $\geq$475 K. Addition of O_2 to the reaction mixture suppresses the reduction of N_2 [311].

On Pd(110), thermal decomposition of NO starts around 440 K and leads to the formation of molecular nitrogen and nitrous oxide gas products [312]. This conversion leaves only oxygen adatoms on the surface, which can be cleaned off by hydrogen or carbon monoxide. At the low-temperature end more nitrous oxide is produced than nitrogen, but this ratio falls with increasing temperature until, above 600 K, there is a 100% selectivity toward the production of nitrogen. The authors of that study suggested that the change in selectivity observed relates to the low lifetime of molecular NO on the surface, even if at such high temperatures the reaction only occurs on a few sites, probably on defects. Angle-resolved studies of the desorbing N_2 yielded similar results to those reported for Rh(110) and Rh(100) [19].

The structural dependence of the CO+NO reaction can, in an extreme, lead to non-linear kinetics, as with the other oxidation reactions. On Pd(110), isothermal light-off due to autocatalysis is seen, as with $CO+O_2$ (Section 4.1), starting at the onset of NO dissociation, around 400 K [313]. Once NO dissociates into adsorbed nitrogen and oxygen atoms, N_2O production is immediate, and accelerated by the creation of vacant sites for both NO and CO adsorption, the latter removing additional O(ads) as CO_2(g). On the whole, the self-acceleration is proposed to take place following the overall reaction $2NO(ads)+CO(g)+{}^{*}\rightarrow N_2O(g)+CO_2(g)+3{}^{*}$, which produces more adsorption sites (*) for both CO and NO that it consumes as it proceeds. On Pt(100), oscillations can be driven by the interconversion between the native (1×1) and hexagonal-reconstructed phases [174]. Two temperature regimes were identified: a main pathway related to the growth of (1×1) islands, with an apparent reaction order of 4.1 in the local CO coverage on the hexagonal phase, and a second high-temperature regime associated with the interconversion between the two surface structures.

N_2O decomposition by itself has been studied on a few other surfaces. In a contrasting study of the steady-state N_2O decomposition on polycrystalline Pt versus Rh, a dependence of the rate of the reaction on surface temperature was observed on the first but not on the second metal, indicating a more prominent role of a precursor-mediated pathway on Pt [314]. On Ni(100), two weakly adsorbed species were identified below 200 K, on clean and oxygen-covered sites. However, above 200 K, decomposition to N_2(g) and adsorbed oxygen atoms was found to dominate [315] .

4.4. Others

The kinetics of other simple reactions on transition metals have also been studied with molecular beams and single-crystal surfaces, albeit with a lesser degree of detail. One example is the thermal decomposition of ammonia. On polycrystalline W, data from molecular beam studies have been explained by the formation of an NH(ads) intermediate and by the disproportionation of that species with extra ammonia to yield N_2 and H_2 [316]. Experiments with polycrystalline Pt at high temperatures detected N_2 produced in vibrationally excited states, with energies as high as 2.4 eV [317], presumably originating from disproportionation of two NH(ads) surface intermediates. In spite of the unique mechanistic interpretations put forward in these two examples, however, a stepwise disproportionation is the accepted mechanism in most cases. Evidence for such mechanism on Pt single crystals include [318]: (1) an increase in the probability for decomposition with increasing temperature, going from 500 to 800 K, followed by a decrease at higher temperatures; (2) a first-order dependence in incident beam intensity; (3) a large phase lag for the H_2 and N_2 product signals at lower temperatures; and (4) a first-order dependence on incident beam intensity for the H_2 signal phase lag and a higher-order dependence for the N_2 signal phase lag. A strong dependence of reactivity on surface structure has also been identified: contrasting experiments on the flat Pt (111) plane versus a Pt(557) stepped surface pointed to a large enhancement in reactivity on the latter case [318]. On Pt(100), dissociation was observed on the original (1×1) surface but not on the hexagonal reconstructed phase [319].

Oxidation of ammonia with molecular oxygen can produce NO. Two different kinetic channels for NO formation were observed on Pt(111), both producing molecules cooler than the surface but each with a different activation energy [320]. These two kinetic pathways were ascribed to reactions between atomic oxygen and either N(ads) (slow) or NH(ads) (fast) on the surface. On Pt(100), N_2 is the major product below 600 K, from recombination of N(ads) produced by ammonia dehydrogenation, but NO dominates above 600 K because of a relative increase in the rate of its desorption over that of its decomposition [321].

In the conversion of $NO+H_2+O_2$ mixtures on Pd(111), the major products are N_2 and H_2O, but small amounts of NH_3 and N_2O are also detected (Fig. 25) [39,322]. O_2-rich compositions inhibit deNO_x activity, but some NO reduction to N_2 is possible as long as the atomic oxygen from both O_2 and NO decomposition can be consumed by the hydrogen added to the mixture. NO was proven to compete favorably against O_2 for the consumption of H_2 (as previously shown with CO on Rh, as discussed before), especially at temperatures below 550 K, and to produce N_2 and H_2O. However, the formation of the latter appears to be the rate limiting reaction. Again, the dissolution of oxygen into the palladium subsurface plays an important role in the NO reduction catalysis with this metal, enhancing reactivity and lowering the threshold temperature to values near ambient temperatures [323].

5. Kinetics of reactions: More complex reactions

In this section we discuss molecular beam studies involving more complex reactants and more elaborate surface chemistry. The number of examples here is relatively small, a fact that highlights the limited use of molecular beams in studies of the

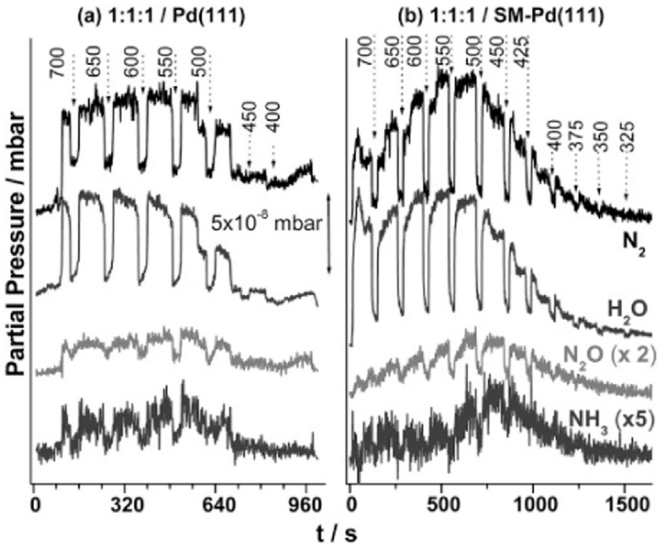

Fig. 25. Comparison of kinetic results from experiments with $NO+H_2+O_2$ effusive molecular beams, produced using a capillary array, on (a) a clean Pd(111) surface, and (b) a Pd(111) surface modified by dissolving oxygen into the subsurface (SM-Pd (111)). These experiments were designed to emulate the reactions that take place in three-way automobile catalytic converters [323]. The surface temperature was decreased in a stepwise manner to various values between 700 and 325 K during a single kinetic run, as indicated by the labels in the figure. All products, namely, N_2, H_2O, N_2O, and NH_3, are seen with both surfaces, but the addition of subsurface oxygen enhances the overall reactivity and decreases the threshold temperature at which the conversion starts. Reproduced with permission from Ref. [323], Copyright 2016 Académie des sciences.

kinetics, rather than the dynamics, of complex chemical processes involving surfaces reported in the literature to date. It should also be noted that much of the advances discussed above in connection with simple reactions was accomplished several decades ago. The interest in this field appears to have waned in more recent times. We will revisit this issue in the last section of our review.

5.1. Alcohol oxidations, organic acid conversions

Several molecular beam studies have been carried out on the thermal decomposition of small oxygenated organic compounds on late-transition metals, mostly to investigate the transient behavior versus exposure starting with clean surfaces. The most common reactants probed in this category are alcohols such as methanol and ethanol, aldehydes such as formaldehyde and acetaldehyde, and organic acids such as formic acid and acetic acid, and the most common metals researched have been Pd and Pt. In many instances, the main observation has been the evolution of decomposition products, most often CO and H_2. This is, for instance, what was reported by Steinbach and Spengler in an early study with methanol on polycrystalline Ni [324], and also by the Madix group with D_2CO, CH_3OD, and HCOOH on Pt(110) and with D_2CO on $Pt(S)-[9(111)\times(100)]$ [325]. In the latter case, the kinetics was determined to be rate limited by the desorption of the products.

In other cases, more complex chemistry has been reported during the decomposition of oxygenated organic molecules, and more mechanistic details have been provided. For example, the decomposition of HCOOH on Ni(110) was shown to lead to the formation of H_2 and CO_2 as primary products, H_2O and CO as minority products, and surface carbon and oxygen [326,327]. Large phase lags were measured in that system, suggesting the participation of a weakly-adsorbed state and of surface diffusion/migration steps in the reaction mechanism. On polycrystalline Pt, the decomposition of HCOOH have been shown to exhibit a much more complex behavior than on Pt(110), with the main CO_2 and H_2 products being accompanied by the evolution of a small amount of CO, and, probably, some H_2O [328]. An unusual transient high activity was seen in that case, an observation that led the authors to propose a five-step mechanism. An acetate surface intermediate was suggested for the conversion of acetic acid on Rh(110), and corroborated by other spectroscopic techniques [64].

Molecular beam studies of the reaction of DCOOD on polycrystalline Pt led to the proposal of the formation of a similar surface formate intermediate [329]. The data, some of which are shown in Fig. 26, illustrate the kinetic arguments made to interpret this type of experiment. First, a maximum in reaction rate was seen at about 550 K (Fig. 26, left). Because there is no equivalent maximum in the phase shift data (Fig. 26, right), this must be attributed to the adsorption step; with increasing temperature, which decreases the lifetime of the molecular adsorption state, molecular desorption prevails over the dissociative adsorption step. Second, reaction orders could be extracted from these data. The facts that the phase shifts for CO_2 are independent of beam intensity and that the product intensities are proportional to beam intensities indicate a first order dependence of the rate on CO_2 flux. In contrast, the square dependence of product intensity on beam intensity and the inverse relationship between the phase shift and the signal intensity for the case of D_2 point to a second-order rate law for that product. It was concluded that the decomposition of DCOO is a monomolecular process, whereas the desorption of D_2 is a bimolecular step (via the recombination of two D atoms).

The addition of isotope labeling to molecular beam experiments is particularly useful with organic molecules, because it affords the extraction of additional regional and steric details on the surface steps associated with the conversion of those molecules. The most common approach is to label specific positions within the organic molecules with deuterium to determine their ultimate fate, often in either the molecular hydrogen or water products [50]. Alternatively, carbon and/or oxygen positions can be tagged by using ^{13}C or ^{18}O, respectively, as in the case of the study be the Yates group where they used mixtures of $^{13}CH_3{}^{16}OH$ and $^{12}CH_3{}^{18}OH$ to probe the possible scission of the C–O bond on Ni (111) [330]. In the end, no isotopic scrambling was observed in that case unless an adsorbed mixture of methanol isotopes was activated by Ar^+ ion sputtering. Dehydrogenation was also reported to be fast, and H_2 production to be desorption limited.

Some molecular beam research has been directed at establishing that the surface reactivity toward organic oxygenates can be modified by preadsorption of oxygen atoms. This has been reported on Rh(110) [64], and is particularly critical on copper (and possibly other coinage metals), where virtually no adsorption is possible on the clean surface [50,97,331]. On oxygen-precovered Cu(110), for instance, the surface chemistry of oxygenates can be rich. Reactivity is only seen below certain coverages of atomic oxygen, however, typically half of monolayer saturation, since oxygen saturation often renders the surface inert again; only the oxygen sites at the short sides of the oxygen islands that form on the (110) surfaces appear to participate in these conversions [50,332]. The uniqueness of this reaction site can lead to unusual kinetic behavior: for methanol on oxygen-predosed Cu(110), for instance, the reaction rate is initially low but accelerates in an autocatalytic fashion as vacancies are created in the oxygen layer [332].

A more comprehensive molecular beam study of these systems led to the conclusion that the conversion of alcohols on Cu(110) surfaces predosed with intermediate coverages of atomic oxygen typically display reactivity that can be grouped into three temperature regimes [50,97,331]. At low temperatures, typically below room temperature, adsorption is not followed by any surface reactions, and the uptake stops once saturation is reached. It is

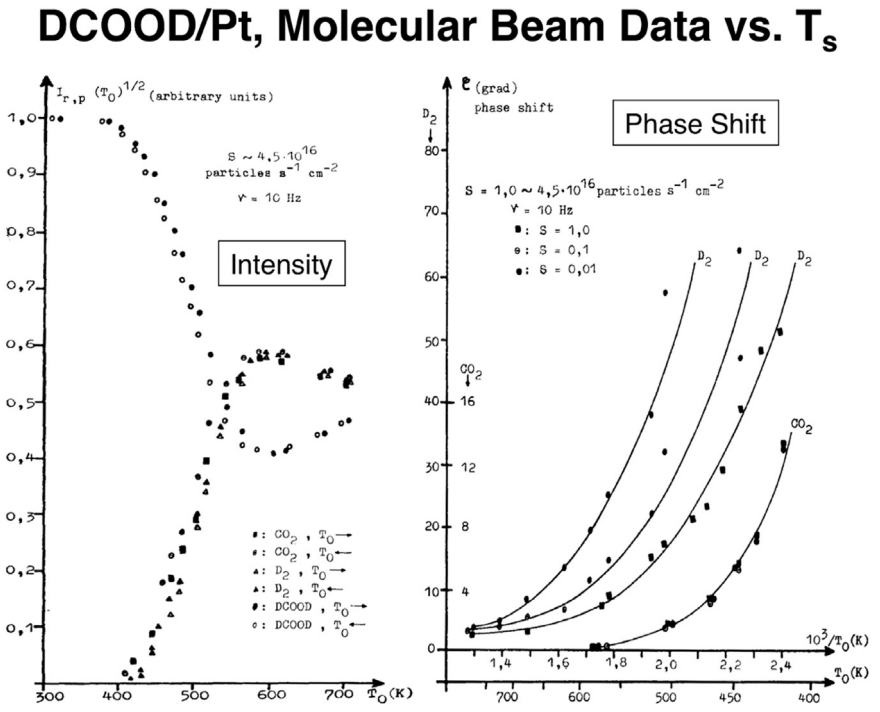

Fig. 26. Results from modulated molecular beam experiments designed to study the thermal conversion of deuterated formic acid, DCOOD, on a polycrystalline Pt surface [329]. Left: Signal intensities for both the reactant (DCOOD) and the products (CO_2 and D_2) as a function of surface temperature, measured as the temperature was ramped either up (solid symbols) or down (open symbols). Conversion starts at 400 K, reaches a maximum at approximately 550 K, and slowly decreases at higher temperatures. Right: Temperature dependence of the phase shifts of the reaction products, provided for three values of the beam flux (labeled S in the figure). The phase shifts are larger for D_2 than for CO_2, and are sensitive to S for the first product but not for the second. These results were used to propose a mechanism where the decomposition of DCOO is monomolecular but the desorption of D_2 is bimolecular. Reproduced with permission from Ref. [329], Copyright 1977 Elsevier.

important to note, however, that even in this regime an initial dissociative step may take place where that alcoholic hydrogen is transferred to an adsorbed oxygen atom to produce alkoxide and hydroxyl surface species (hence the enhancement in adsorption on surfaces predosed with oxygen compared to that seen on the clean substrate). At intermediate temperatures, typically between 300 and 450 K, the alkoxide resulting from that initial activation undergoes a β-hydride elimination step [333,334] to produce atomic hydrogen, which recombines and is ejected into the gas phase as H_2, and an adsorbed aldehyde or ketone, which may desorb or decompose further on the surface. Finally, at higher temperatures, the stoichiometry changes, and no H_2 is produced; all the hydrogen atoms extracted from the organic adsorbates recombine with surface oxygen to produce water. The overall rate of that reaction appears to be limited by the decomposition of the alkoxide species.

The conversion of organic acids on Cu(110) was shown by molecular beam research to share some common features with that of alcohols. The studies by Bowker and coworkers have identified some important mechanistic features [335–337], including the following: (1) oxygen significantly increases the sticking coefficient of the organic acids because of two effects, the facilitation of the formation of weak precursors that can diffuse on the surface until finding an active site, and the promotion of the extraction of the acidic hydrogen to produce the conjugated base (i.e., formate, acetate, etc.) and hydroxyl surface species; (2) further hydrogenation of the hydroxyl species leads to the formation of water, a channel that leads to the removal of surface oxygen atoms; (3) the remaining oxygen (at initial coverages above 0.25 monolayers) remains on the surface (locally compressed into c (6×2) structures, according to scanning tunneling microscopy – STM– experiments); (4) further reactivity is seen at higher temperatures, above 400 K, via the decomposition of the carboxylic surface species, in the case of formic acid to yield CO_2 and H_2; and (5) at even higher temperatures, above 500 K, H_2 is no longer produced, and the hydrogen atoms produced from dehydrogenation of the organic fragments are scavenged by surface hydroxyl to make water.

The kinetics of conversion of oxygenates has also been characterized by Bowker and coworkers on Pd(110). Some similarities with other surfaces have been seen [338], but, in addition, steady-state conversion has been proven possible at high temperatures because of the unique ability of Pd metal to dissolve carbon into the bulk [339,340]. With alcohols and on oxygen-predosed surfaces, two pathways were identified, one that produces CO, CO_2, H_2, and H_2O, as on the other metals, and a second involving CO bond scission. Indeed, methane production was observed with ethanol and 2-propanol [341], and, in combination with $CO+H_2$, from decomposition of acetaldehyde at intermediate temperatures (300–400 K). However, in the latter case, the total dehydrogenation channel was seen to dominate above 400 K, and to be sustainable under steady-state conditions because of the continuous dissolution of carbon into the palladium bulk [342]. The high-temperature transition was also seen on Pd(111), but not with Pd nanoparticles dispersed on a flat support, presumably because those do not have the same capacity to absorb carbon [343].

Finally, a molecular beam experiment has been reported on Pd (111) with $C_2H_5OH+NO+O_2$ mixtures, to test the catalysis of automobile catalytic converters [344]. Maximum NO reduction to N_2, together with CO, CO_2, and H_2O emission, was observed between 500 and 600 K. Beam switching experiments were performed between fuel-rich and fuel-lean compositions, as shown in Fig. 27, to demonstrate that the NO reduction can be managed under net oxidizing conditions [344]. It was found that nitrogen is only produced transiently on the relatively clean Pd surface during oxygen-rich condition, until the slow build up of surface oxygen atoms kills the reaction.

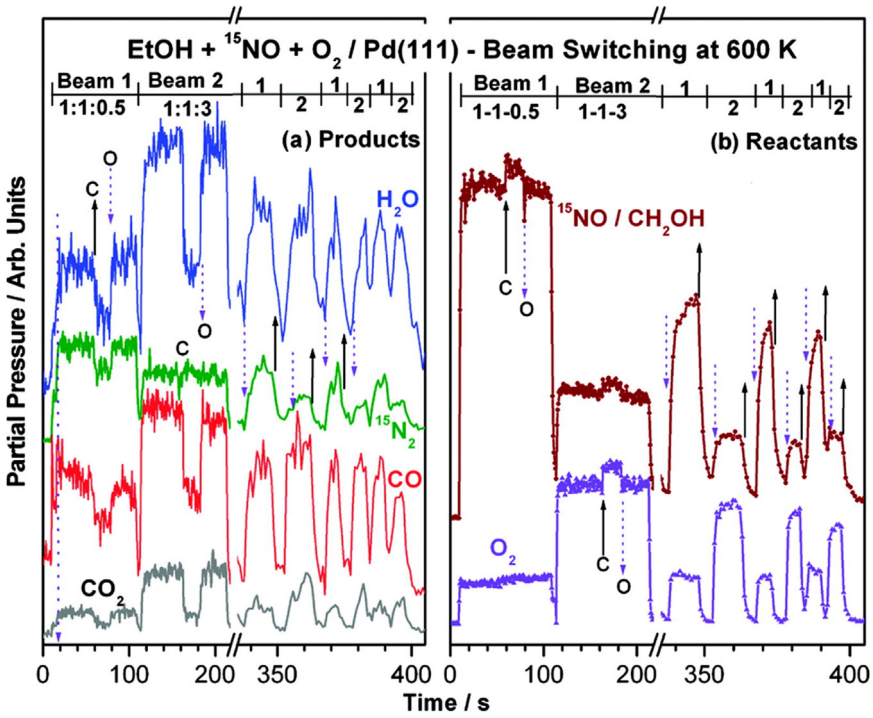

Fig. 27. Typical raw kinetic data obtained from beam switching experiments for the reduction of NO with ethanol (EtOH) in the presence of O_2 on Pd(111) at 600 K, in another study aimed to characterize the scrubbing of exhaust gases from automobile engines [344]. In this example, the traces are shown for all the products observed, namely, CO, CO_2, H_2O, and $^{15}N_2$ (a), as well as for the reactants (O_2, ^{15}NO, EtOH) (b), as a function of time and the composition of the beam, which was switched between EtOH:^{15}N:O_2 ratios of 1:1:0.5 (oxygen-lean, beam 1) and 1:1:3 (oxygen-rich, beam 2). The rate of molecular nitrogen production is high with the oxygen-lean beam, whereas the oxidation products dominate with the oxygen-rich mixture. Moreover, the changes in reactivity are reversible. Reproduced with permission from Ref. [344], Copyright 2009 American Chemical Society.

5.2. Olefin Hydrogenations and Isomerizations

Only a handful of experiments have been carried out using molecular beams to characterize the hydrogenation of unsaturated organic molecules. This may very well be because emulation of such catalytic reactions under vacuum conditions has turned out to be a difficult proposition [345]. With olefin hydrogenations, for instance, it is well known that catalysis takes place not on pristine surfaces but on surfaces covered with a layer of strongly-bonded hydrocarbon fragments [346]. These species, alkylidynes in the case of small olefins [159,347], form immediately during the uptake under UHV at room temperature [348], and block sites for further conversion [349]. Getting around this limitation has proven to be a challenge.

Our research on the chemistry of ethylene on Pt(111) single-crystal surfaces illustrate the benefits and limitations of using molecular beams for the study of olefin conversions [51,345,350–353]. First, it needs to be acknowledged that, with mixtures of olefins and hydrogen or deuterium, several simultaneous reactions are possible, namely, molecular desorption, dehydrogenation to alkylidynes, H-D exchange within the adsorbed molecules, and hydrogenation to alkanes. Moreover, alkylidyne formation, ethylidyne (Pt≡C–CH_3) in the case of ethylene conversion, can only be detected indirectly, via the desorption of molecular hydrogen [13]. Several steps are involved in that process [348,354], possibly including a 1,2-H shift in ethylene to form an ethylidene (Pt=CH–CH_3) intermediate and subsequent fast α-H elimination [355] and H(ads)+H(ads) recombination reactions [356], and therefore caution should be exerted when analyzing the molecular-beam H_2 desorption kinetic data from this system [357]. The one thing that is clear is that there is a delay between the adsorption of ethylene and the production of hydrogen, indicative of the need for the build-up of a critical coverage of hydrocarbons on the surface before other reactions can take place. Also, a small amount of ethane is formed during the decomposition of ethylene to ethylidyne, although the yield of that product is low enough not to affect the kinetics of the latter reaction in any significant way.

Fortunately, it has been determined that, at temperatures below 240 K, the decomposition of ethylene is slow, a fact that has afforded the investigation of the kinetics of the adsorption and hydrogenation steps for ethylene on both clean and hydrogen-covered surfaces independently. At 40 K, ethylene adsorption is in an intrinsic-precursor π-bonded adsorption state, and the probability of sticking increases with coverage [358]. At 95 K, on the other hand, bonding to the surface goes directly into the di-σ-bonded state, and the adsorption probability of ethylene remains constant with increasing coverage for incident trajectories with low parallel momentum but decreases with coverage at high parallel momentum. It would seem that high parallel momentum may contribute to an increased overall scattering probability from a high-energy extrinsic precursor, resulting in a decreased net adsorption probability at higher ethylene coverages [358]. A certain population of weakly-adsorbed species, which, as indicated above, is know to be π bonded to the surface, can also be maintained at coverages near saturation by exposure of the platinum substrate to a constant flux of ethylene molecules [51]. The presence of coadsorbed hydrogen reduces the total ethylene uptake but increases the amount of π-bonded ethylene. The main conclusion from molecular beam studies of this reaction has been that it is this π species that is essential for the hydrogenation of ethylene: the kinetic reaction rate orders were determined to be 1.2 ± 0.3 and 0.8 ± 0.2 for the weakly-adsorbed ethylene and hydrogen surface coverages, respectively (Fig. 28) [51]. It was also observed that the π-bonded ethylene can slowly exchange with the second di-σ state that forms first and bonds more strongly to the surface [15,52,359]. This suggests an adsorption mechanism at

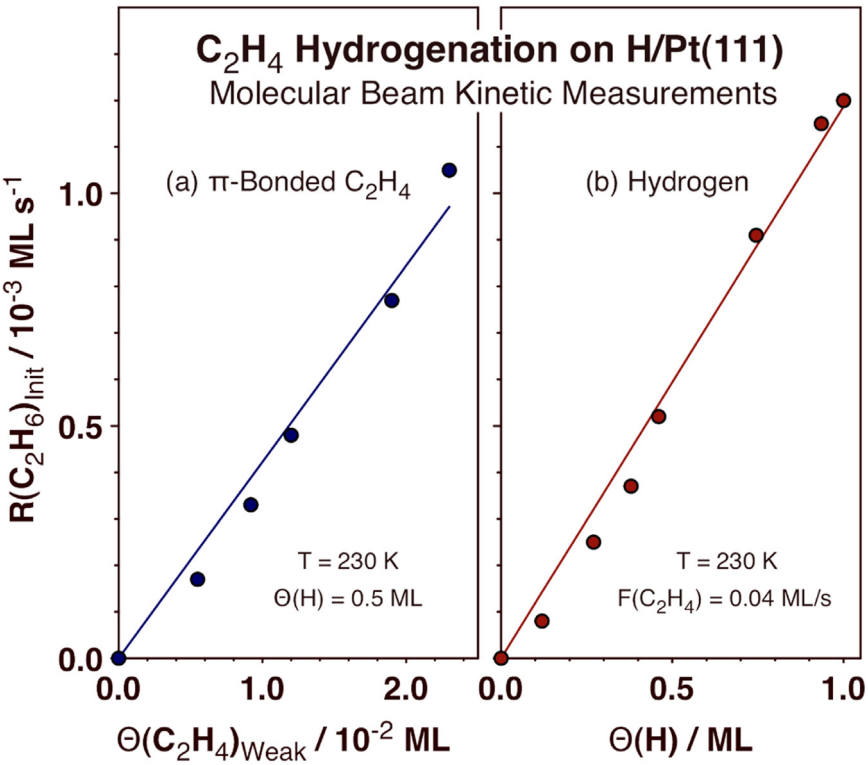

Fig. 28. Kinetic parameters extracted from effusive molecular beam experiments on the hydrogenation of ethylene on Pt(111) [345]. Shown are the linear correlations established for the initial rate of ethane formation, $R(C_2H_6)_{Init}$, as a function of the coverages of π-adsorbed ethylene ($\Theta(C_2H_4)_{Weak}$, a) and atomic hydrogen (Θ(H), b), suggesting that the rate-limiting step may be the first of the two stepwise hydrogenations proposed in the well-known Horiuti-Polanyi mechanism to form an ethyl surface intermediate [49,348]. Reproduced with permission from Ref. [345], Copyright 2013 the Owner Societies.

high coverages via an initial interaction with the few metal atoms left exposed by an imperfect monolayer followed by a collective rearrangement of the neighboring molecules into a new compressed layer. It is a scenario that may account for the behavior seen during catalysis at atmospheric pressures.

A few molecular beam experiments have also been reported for the adsorption and conversion of olefins on palladium single crystals. Tysoe and Lambert showed that, on Pd(111), not only dehydrogenation to H_2 and self-hydrogenation to ethane can be promoted, but also C–C bond formation reactions to make C_4 and C_6 molecules [360]. A C_4H_4 metallocycle was later identified as the intermediate for these products [361–363]. On Pd(110), ethylene decomposition can be sustained under steady-state conditions above 450 K, with continuous hydrogen evolution as C is deposited onto the surface [364]. Studies with molecular beams made out of mixtures of cis-2-butene and hydrogen on Pd(111) showed no sustained hydrogenation but indicated steady-state conversion via cis-trans isomerization and, when D_2 was used, H-D exchange [56]. All this was explained by the availability of surface deuterium atoms for the latter processes but not for the former. On the other hand, the subsurface D needed for the hydrogenation reaction does not appear to be accessible in this system [365]. Freund and coworkers have proposed that the deposition of surface carbon may be a controlling factor in the ability for subsurface hydrogen to diffuse out to the surface and to participate in the hydrogenation reactions [57]. It should be noted that, in this, palladium is a unique case because of its ability to dissolve hydrogen atoms into the bulk, and that no similar behavior has been seen with other transition metals [345].

5.3. Alkane high-temperature oxidations

The steady-state conversion of saturated hydrocarbons on metal surfaces is more difficult to promote, given that those molecules are quite stable and difficult to activate. As discussed in Section 3.3.3, it is possible to observe alkane activation using molecular beams, but usually only if high translational energies or other forms of molecular excitation are used. Nevertheless, alkanes can be converted under catalytic conditions, and in a few instances those reactions have been emulated with molecular beams under UHV.

In one early example, King and coworkers characterized the oxidation of methane on Pt(110) between 400 and 900 K using mixed CH_4+O_2 beams [366]. The only reaction products detected were H_2, CO, and CO_2; curiously, no H_2O evolution was observed. The authors also identified two kinetic regimes, with CO_2 as the main product at temperatures below 550 K and CO dominating above 550 K. By contrast, in results from complementary non-steady-state experiments where submonolayer coverages of CH (ads) were first deposited by CH_4 activation using a molecular beam and oxidation was induced afterward by employing a second O_2 beam, CO_2 and H_2O were both seen to desorb at temperatures as low as 330 K [367]. Hydrogen abstraction by the adsorbed oxygen atoms was ruled out as a possible step for this reaction; instead, the carbon dioxide was proposed to form via an initial CH (ads)+O(ads)→CO(ads)+H(ads) step followed by oxidation of the adsorbed CO with surface oxygen atoms.

In a separate study, it was shown that the partial oxidation of small alkanes, i.e., ethane, propane and butane, mostly produce syn gas ($CO+H_2$), but also ethylene at high temperatures, above 1000 K [368]; similar products were reported with ethylene [369]. Infrared emission spectra recorded from the desorbing species showed that the CO produced is vibrationally excited but rotationally cool, suggesting that the dynamics of CO formation involve a reaction between surface carbon and oxygen atoms without thermal accommodation on the surface. By seeding the

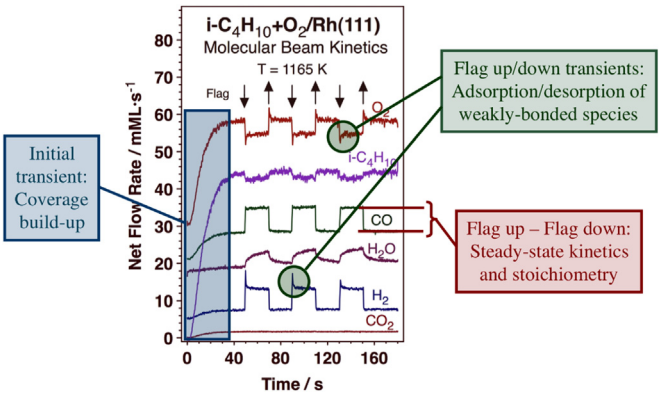

Fig. 29. Isothermal kinetic data for the conversion of a 1:1 isobutane+O_2 mixture, fed using an effusive molecular beam, on a Rh(111) single-crystal surface at 1165 K [373], in an experiment designed to probe short-contact-time catalysis at high temperatures [588]. The evolution of the partial pressures of the reactants (oxygen and isobutane) and products (hydrogen, carbon monoxide, water, and carbon dioxide), which can be used to extract reaction rates after proper analysis, are shown as a function of time. H_2, CO, and H_2O, but not CO_2, are produced, and they are generated in the expected stoichiometric ratios; the first two with rapid kinetics following the activation of the alkane, and water in a slower fashion, via the secondary formation of hydroxo surface intermediates. Highlighted in the figure is the fact that these data can be used to obtain information about both the transient and the steady-state kinetics of the reaction. Adapted with permission from Ref. [373], Copyright 2010 American Chemical Society.

alkane beam to provide additional kinetic energy, the steady-state oxidation of methane and ethane on Pt and Rh foils was found to lead to an enhancement in hydrogen production [370,371]. An explanation was advanced where methoxy and ethoxy intermediates may form on the surface. Threshold temperatures of 1000 and 800 K were measured for methane and ethane oxidation, respectively. Rh was found to be less reactive than Pt, but to require lower oxygen fluxes to produce CO+H_2.

We have also studied the oxidation of alkanes, in our case of methane, propane, isobutane, and hexane, on a Rh(111) surface [13,14,372,373], by using an effusive beam in order to emulate the conditions used in short-contact-time catalysis [374,375]. Typical data from these experiments are shown in Fig. 29. Several mechanistic details were derived from our results, including the following: (1) the steady-state reaction follows a $C_nH_{2n+2}+n/2O_2 \rightarrow nCO+(n+1)H_2$ stoichiometry; (2) a competing minority channel is indicated by the production of a small amount of water; (3) the absence of any CO_2 production argues against a water-shift reaction; (4) the slow transient measured for the formation of water highlights the secondary nature of the surface reaction responsible for its production; (5) the mirroring spikes in the O_2 and H_2 traces seen immediately after blocking and unblocking of the beam point to the formation of other transient species on the surface; and (6) both surface and subsurface atomic oxygen species form during the reaction, but only the more labile surface intermediate is relevant to the catalysis, blocking Rh sites for alkane activation and reacting to form CO and H_2O.

6. Reactions on supported nanoparticles: Materials gap

The overwhelming majority of the kinetic work on reactions on surfaces has been carried out on flat substrates. This is so in great part because single crystals and other simple surfaces offer a unique control of the nature of the surface sites. On the other hand, many of the problems of interest involve rough surfaces, often in the form of small nanoparticles dispersed on a second material. This is particularly true in heterogeneous catalysis, on which much of the reactivity work with molecular beams has been focused. It is not always straightforward to extrapolate the information acquired with experiments on flat surfaces to these more realistic conditions, because nanoparticles not only display many planes and defects but also may have different electronic properties, and may interact with the support and even create new interfacial sites. These potential discrepancies have been discussed extensively in the catalysis community, and are referred to as a "materials gap" [345,376–379]. A few research groups have tried to address the kinetic aspects of the materials gap using molecular beams, as reviewed next.

6.1. CO oxidation

A reasonable body of work exists already on molecular beam measurements of the kinetics of oxidation of carbon monoxide on metal nanoparticles, specifically on Pd nanoparticles dispersed on oxide supports. On alumina films, made via the oxidation of NiAl (100) single-crystal surfaces, the kinetics of CO oxidation on large and ordered Pd particles can in general be described by a homogeneous surface model. However, significant deviations have been observed on small and defect-rich particles, which were initially explained by the development of a small fraction of new sites for weakly CO binding [380] but later ascribed to the inhibition of the dissociative adsorption of O_2 at high CO coverage on the basis of results from transient CO_2 production experiments induced by CO beam switching [381]. Surface adsorbate diffusion was seen to play a particularly important role in determining reaction rates on large, but not on small, Pd nanoparticles [382]. An added complication to the description of this kinetics due to the fast diffusion of oxygen into the bulk was also identified [383,384].

Further research has been performed on Pd nanoparticles dispersed on thin Fe_3O_4 films grown on Pt(111) crystals. At low reaction temperatures, below 450 K, CO oxidation was found to be significantly slower on partially oxidized versus metallic Pd particles, presumably because of the weaker bond of CO on the former surfaces [385]. At higher temperatures, however, Pd oxides can be dynamically formed and decomposed, and can participate in the CO oxidation process. As a consequence, two reaction regimes have been identified as a function of oxygen coverage: a fast CO oxidation on O-precovered metallic Pd, and a slow CO oxidation involving reduction of the Pd oxide phase [386].

On lithographically-made Pd/SiO_2 samples, experiments with two CO and O_2 separate beams were used to show that, under conditions of limited oxygen mobility, the switching behavior between the two kinetic regimes mentioned above is largely driven by the surface mobility of CO [387,388]. The macroscopically observable bi-stability seen with large particles (Fig. 30) vanishes with decreasing particle size because of a fluctuation-induced transition between two kinetic reaction regimes, with a transition rate controlled by both particle size and surface defects [389].

Interfacial sites at the boundary between the metal and the support may play a unique role in catalysis. In one report, on the oxidation of CO with O_2 on Au nanoparticles dispersed on Mg (100), the Henry group determined that oxygen does not dissociate on the gold nanoparticles [390]. Instead, a reaction mechanism was proposed in which CO adsorbs on low-coordinated gold atoms and reacts with oxygen adsorbed molecularly, possibly at the Au/MgO interface.

In measurements of the CO oxidation rate on small size-selected Pd and Au clusters supported on thin MgO films, the cluster coverage was varied independently of the cluster size in order to be able to change the ratio of the CO arriving at the surface via direct versus diffusion flux (reverse spill-over) channels [391,392]. In the case of Pd, the change in reaction rate as a function of cluster coverage was found to be different for Pd_8 versus Pd_{30} clusters: for the small nanoparticles, the reaction probability was

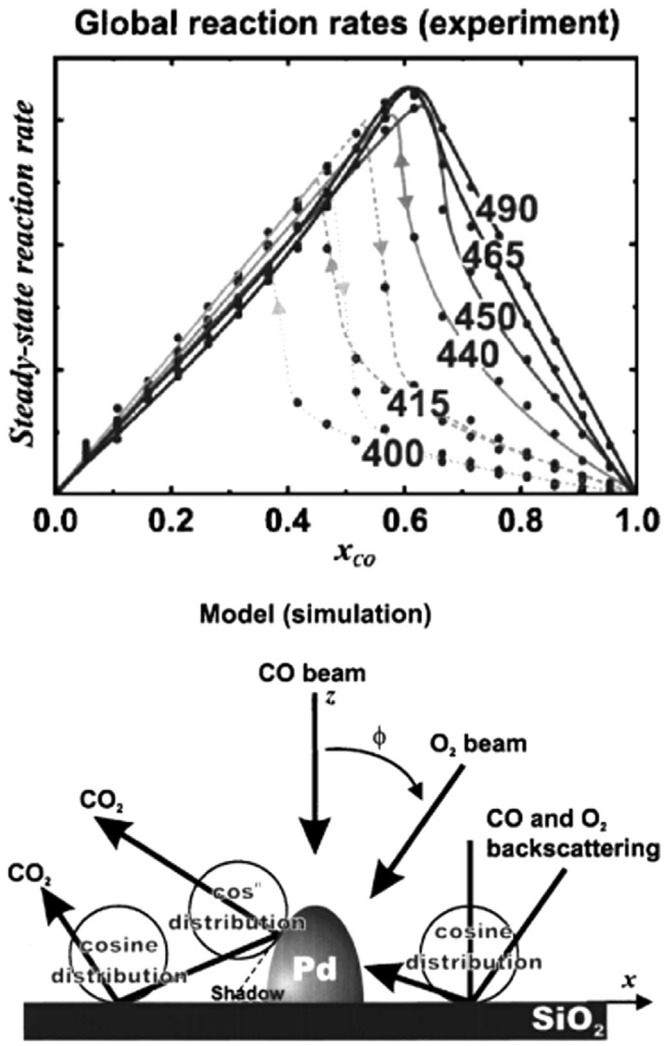

Fig. 30. CO oxidation kinetics on nanolithographically prepared supported Pd model catalysts, measured by using separate molecular beams for the CO and O_2 reactants [388]. Shown are the measured reaction rates as a function of the beam composition (in the form of CO fraction, x_{CO}) for surface temperatures in the range between 400 and 490 K. Especially noteworthy here is the hysteresis seen at temperatures below 440 K, where the reaction is bistable. A general model of the different events considered to interpret the kinetics of this system is included in the bottom. Reproduced with permission from Ref. [388], Copyright 2005 American Institute of Physics.

determined to be independent of the source of the CO, whether directly from the beam or via diffusion, whereas for larger clusters the probability was established to be smaller for CO supplied by reverse spill-over.

As mentioned above, the group of Henry and coworkers has performed some molecular beam kinetic measurements on surfaces consisting of Pd clusters deposited on MgO(100). In a study of the dependence of the rate of CO oxidation with O_2 versus particle size, an effect was observed that was explained in part by spillover of CO from the support [393]. However, this could not fully account for the large rates seen with small Pd clusters, a few nanometers in diameter, in which case a second-strongly bound CO adsorption state was identified below 500 K. The residence time of that state was determined to be about 10 times that known on single crystal surfaces, which was ascribed to adsorption on edge sites [394]. Overall, all these reports point to the increase complexity added to the description of the kinetics of even simple reactions such as carbon monoxide oxidation when supported nanoparticles are used as catalysts. It has already been demonstrated that new factors need to be included in any interpretation of the data, including variations in the electronic properties of the metal versus nanoparticle size, the large number of defects present on the surface, the contribution of new metal-oxide interfacial surface sites, and a different, generally increased, ability of adsorbates to diffuse in and out of the bulk of the nanoparticles.

6.2. NO reduction

With CO+NO mixtures, Henry and coworkers determined that, on Pd nanoparticles dispersed on MgO(100), CO_2 and N_2, and sometimes a little of N_2O, are all produced below 575 K [395,396]. In experiments using a molecular beam of CO and an isotropic pressure of NO, the rate-limiting step for the reaction was determined to be the dissociation of NO at low temperatures and the adsorption of CO at high temperatures [396]. With a reverse arrangement, with a molecular beam of NO plus an isotropic pressure of CO, NO was seen to always dissociate between approximately 550 and 725 K. The steady-state reaction rate reached a maximum that shifted to higher temperature with increasing CO pressure and with decreasing particle size (Fig. 31). At higher temperatures, on the other hand, the reaction was shown to be limited by NO and CO adsorption; the medium-sized particles appear to be the more active under those conditions as well.

In general, the authors of these studies concluded that the intrinsic activity of the metal depends not only on particle size but also on particle shape: the medium-sized particles, which exhibit mainly (111) facets, are more active than the largest particles,

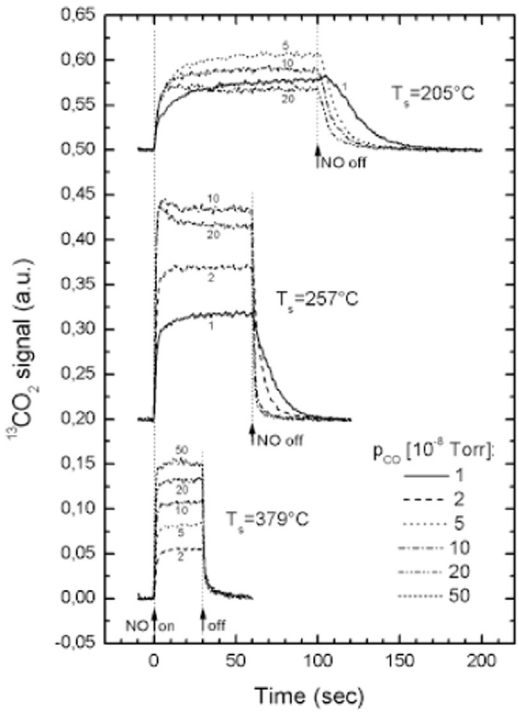

Fig. 31. Transient kinetics for the production of $^{13}CO_2$ during the conversion of ^{13}CO+NO on a Pd/MgO model catalyst (with Pd nanoparticles of 2.8 nm in diameter on average) at various temperatures and with various gas compositions, set by adjusting the ^{13}CO isotropic pressure and using a fixed pulsed NO beam. Three sets of curves are shown, reflecting three types of behavior as a function of temperature. Top: At low temperatures, the time to reach the steady state is long and increases with decreasing ^{13}CO pressure, because the reaction is limited by the (high) total coverage. Center: At 257 °C, where the maximum activity is seen, a transient peak is observed at high ^{13}CO pressures. Bottom: In the high-temperature regime, the time constant of the transient period becomes small and almost independent of the ^{13}CO pressure. Reproduced with permission from Ref. [397], Copyright 2002 IOP Publishing Ltd.

which primarily exhibit (100) planes [396,397]. In experiments with well-defined small clusters, Pd_n with n=4, 8, or 30, N_2 was found to form at relatively low temperatures, about 400 to 450 K. These values are at least 100 K below the temperature measured with Pd single crystals, a change that affords the prevention of poisoning by adsorbed nitrogen adatoms [398].

The kinetics of the decomposition of NO and its reduction by CO have also been characterized on Pd particles dispersed on an alumina film (made by oxidizing NiAl(110)) [17,28]. NO decomposes slowly on that surface at low (100 K) temperatures to form various N_xO_y species, in a process initiated at oxide sites that involves structural changes in the alumina support [399]. However, above 300 K, decomposition on the Pd surfaces takes over. The presence of strongly-bonded nitrogen in the vicinity of edge and defect sites was also found to give rise to an enhanced dissociation probability under conditions of high adsorbate coverages [400].

6.3. Decomposition of oxygenates

A couple of studies have been reported on the thermal decomposition of oxygen-containing organic molecules on supported metal nanoparticles. In one, Bowker and coworkers looked into the decomposition of formic acid on Pd/TiO_2 [401]. On the pure oxide surface, without any metal, only dehydration was seen, with steady-state reaction becoming sustainable above 500 K. Upon the addition of the Pd nanoparticles, however, dehydrogenation was seen to start at about 350 K.

On Pd/Al_2O_3, two competing decomposition pathways were observed [402,403]. Dehydrogenation to CO dominates in this case, but some C–O bond scission proceeds as well, albeit at a much lower rate, leading to the deposition of carbon and hydrocarbon species on the surface. On the basis of steady-state isotope exchange experiments, it was determined that the rate of carbon deposition drops rapidly with increasing carbon coverage, whereas the kinetics of dehydrogenation is hardly affected.

6.4. Hydrocarbon conversion

A couple of reports can be found in the literature on molecular-beam kinetic measurements for the hydrogenation of olefins promoted by supported metal particles. The most extensive study in this category is that of the conversion of 2-butene with hydrogen on Fe_2O_3-supported Pd nanoparticles, characterized by the Freund group. This is an interesting system, because hydrogenation competes with double-bond migration, cis-trans isomerization, and, if deuterium is used instead of hydrogen, H-D exchange (Fig. 32) [404–406]. It was found that, on Pd nanoparticles, those reactions may follow different mechanisms. The key, once again, is that palladium is a unique metal, because it can absorb significant amounts of hydrogen and also allows for carbon to diffuse into the subsurface region [57].

Indeed, with cis- and trans-2-butenes, it was found that selectivity toward cis-trans isomerization versus hydrogenation depends critically on the nature of the carbonaceous deposits that are typically present during reaction on real catalysts [53,407]. At low temperatures, between 190 and 210 K, both reaction pathways were found to proceed on the initially clean surface, faster with cis-2-butene than with the trans isomer [54], but to quickly stop because of poisoning by the carbonaceous layer that builds up on the surface. Above 250 K, in contrast, a sustained catalytic activity for the cis-trans isomerization, but not for the hydrogenation, becomes viable; only if highly dehydrogenated carbonaceous fragments are preadsorbed on the surface it is possible to sustain the hydrogenation catalytically (Fig. 32). Remarkably, deposition of submonolayer amounts of strongly dehydrogenated carbonaceous species on the Pd particles results in a significant decrease of the

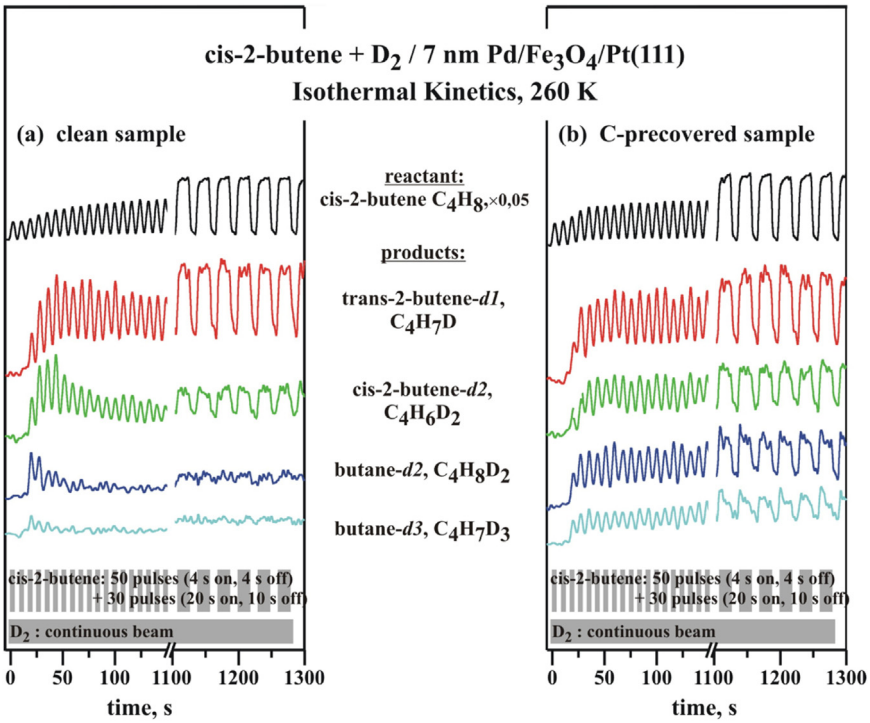

Fig. 32. Results from isothermal pulsed molecular beam experiments on the conversion of cis-2-butene with D_2 at 260 K on initially clean (a) and C-precovered (b) Pd/Fe_3O_4 model catalysts [53]. Shown is the evolution of the reaction rates of the most important compounds involved, namely, the reactant (cis-2-butene), the two primary products from H-D exchange and hydrogenation/deuteration (trans-2-butene-d_1 and butane-d_2, respectively), and the next two secondary products (cis-2-butene-d_2 and butane-d_3), as a function of time. The data highlight the fact that, while on the clean surface only sustained isomerization is possible (left panel), on the surface precovered with carbonaceous deposits steady-state conversion is seen for both isomerization and hydrogenation reactions (right). Adapted with permission from Ref. [53], Copyright 2008 American Chemical Society.

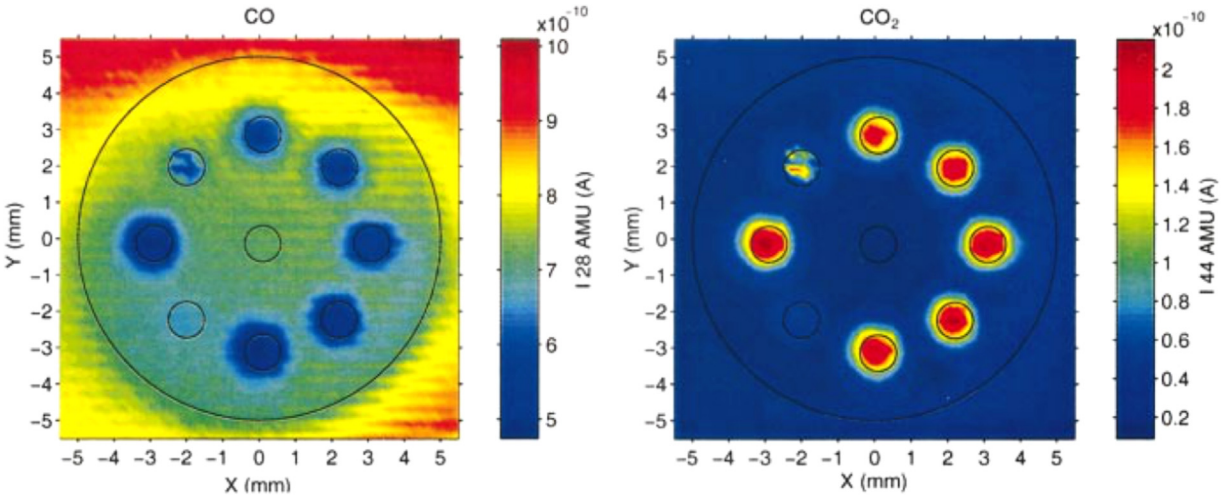

Fig. 33. 3D plots showing the spatial distribution of the CO (left) and CO_2 (right) mass spectrometer signals over an oxidized Al(111) crystal decorated with eight Pd peripheral spots surrounding one Au central spot (all indicated by black circles) during the oxidation of CO with O_2 at 573 K. The experiments were carried out with a scannable double-capillary probe where the reactants are fed through the outside stainless-steel nose (6 mm outside diameter) placed at a distance of 0.2 mm from the surface and the products collected by the inner quartz capillary (0.9 mm outside diameter) positioned 0.05 mm inside the nose. The measured partial pressures, which are color-coded according to the scale provided on the right of the figure, indicate high conversion of CO to CO_2 only on the Pd nanoparticles (two of them, on the left side of the sample, were quite thin and therefore not as reactive as the others). Reproduced with permission from Ref. [417], Copyright 2004 American Institute of Physics. (For interpretation of the references to color in this figure legend, the reader is referred to the web version of this article.)

cis-trans isomerization rate for trans-2-butene, but does not affect the rate of the cis-to-trans conversion.

Codeposited carbon was shown to assist the catalytic and sustained hydrogenation of cis- and trans-2-butenes, both at similar rates [54]. In addition, low-coordination sites were determined to not show higher intrinsic activity for this catalysis. Rather, they display a more effective replenishment of hydrogen from the subsurface under steady-state reaction conditions once they become covered with surface carbon [56]. In the case of the uptake of methane on Pd nanoparticles supported on MgO(100), sticking measurements with a beam directed at normal incidence yielded values about twice as large as those seen on flat Pd(111) surfaces (once the dispersion of the metal particles was taken into account), suggesting an important role for either surface defects on the nanoparticles or the support in this case as well [408].

Palladium shows unique behavior, as discussed above, and is therefore not representative of other metals when it comes to the promotion of olefin conversion reactions. The experiments from the Freund group have yielded quite high reaction probabilities, not typically matched by regular catalysts, not even those based on Pd. Measurements with other metals will be necessary to better understand these systems. We are aware of only one other study in this area, that of the hydrogenation of ethylene on Ni, Pd and Pt nanoparticles of between 1 and 1.5 nm in diameter dispersed on a MgO(100) support [409,410]. Ni nanoparticles were seen to deactivate readily at 300 K, whereas Pd particles are poisoned only after pulsing the beam of the hydrocarbon reactant at 400 K; Pt particles were found to retain hydrogenation activity even after heating to 400 K. The hydrogenation turnover frequency, normalized to the number of particles, was determined to follow the trend Pt > Pd > Ni.

7. Low-probability reactions: Pressure gap

Another difficulty in emulating catalytic reactions is that the low pressures used in UHV surface-science experiments are many orders of magnitude lower than those encounter in typical catalytic processes. This brings about changes that are not fully understood but that are known to go beyond simple collision frequency effects. In any case, most catalytic reactions display significantly low reaction probabilities, with one in a million or less of the reactants colliding on the surface actually undergoing chemical transformation, and such rare events are difficult to probe with low molecular flows [345,411]. This problem is commonly referred to as a "pressure gap" [334,379,412,413]. A few studies with molecular beams have addressed this issue. In fact, some, in particular those related to combinatorial studies, are not described specifically as molecular beam in nature, but still use capillaries and other types of collimated gas streams; we include them in our discussion below as well.

7.1. Single capillary nanoreactors

The simplest approach to the design of directional molecular beams with the high fluxes associated with realistic catalytic pressures is based on single small capillary tubes. The flow of gases through such capillaries and the flux and angular spread of the resulting beams may be difficult to estimate, but several studies have been carried out toward this goal [414,415], and, based on such calculations, a few "nanoreactors" have been designed. In those, the gas is fed to the surface at high fluxes through an appropriate capillary tube, and the products sniff out via a second capillary or another similar conduit and analyzed using mass spectrometry (MS). Examples of this approach come from the groups of Weinberg [416] and Chorkendorff [417,418], who developed setups with concentric capillaries where the outer tube was used to feed the reaction mixture and the inner capillary employed to extract the products for MS analysis. In the initial test of the instrument developed by the latter group, the conversion of $CO+O_2$ was probed on a surface comprised of Pd nanoparticles dispersed on an Al_2O_3/Al(111) thin film. Kinetic runs could be carried out at fluxes equivalent to pressures of up to 1 bar and with a lateral resolution of better than 0.2 mm (Fig. 33).

These instruments have been used to study a number of catalytic reactions. In one case, the dissociative sticking coefficient for H_2 was measured over Pd films deposited on sputtered highly-ordered pyrolytic graphite (HOPG). That sticking probability was found to be about 1.4 times higher on Pd hydride than on metallic Pd but to display similar apparent desorption energies on both

surfaces [419]. More extensive characterization of this reaction on catalysts made out of Pt, Ru, and Rh nanoparticles of varying sizes (between 2 and 5 nm) dispersed on a flat support indicated that the rate of hydrogen exchange (between H_2 and D_2) at 1 bar is higher on Ru and Rh than on Pt, and that it increases with particle diameter for all the metals probed, although less so with Pt [420]. The exchange rate was also found to decrease dramatically with the increase in carbon content that happens upon annealing of the metal films at high temperatures [421]. The H_2+D_2 exchange reaction was found to be faster on Pt+Rh alloys than on either metal alone [422]. In another study, the influence of monoatomic steps and defects on the methanation reaction with a 1 bar $CO+H_2$ gas mixture was evaluated over a Ru(0,1,54) single crystal, which contains one monoatomic step atom for each 27-atom-wide terrace [423]. By using selective site-poisoning with sulfur atoms, it was determined that methanation takes place preferentially on undercoordinated sites such as steps and kinks.

We have also experimented with this type of design. Our initial setup was comprised of two concentric capillaries, with the inner one used as the gas feeder and the outer as the sniffer [14,345]. That arrangement was later simplified to reach our current design, where only one capillary tube is used, to generate a high-flux beam, and where the scattered gas is analyzed by using a mass spectrometer placed within the UHV chamber [424]. Both systems were successfully employed to study the catalytic hydrogenation of ethylene on a polished polycrystalline Pt disk [49,411,424,425]. Steady-state ethylene conversion with probabilities close to unity could be achieved by using beams with ethylene fluxes equivalent to pressures in the mTorr range and high (≥ 100) H_2:C_2H_4 ratios [411,425]. Additional spectroscopic data led to the suggestion that such high reaction probabilities are possible because of the removal of most of the ethylidyne layer known to form during catalysis.

Using isotope labeling, it was also determined that multiple H-D substitutions are possible, as expected based on the well-known reversible stepwise mechanism proposed a long time ago by Horiuti and Polanyi (Fig. 34) [49,424]. In fact, the ethane isotopologue distributions obtained in these experiments reflect a much higher probability for the dehydrogenation of ethyl intermediates back to the olefin, relative to the hydrogenation to ethane, than typically seen in this catalysis. In addition, a second mechanistic pathway was clearly identified responsible for most of the dideuteroethane produced, with a linear dependence of the yield on ethylene flux (Fig. 34). Based on the kinetic parameters extracted from these studies versus deuterium and ethylene fluxes, it was argued that the second route may be a "reverse" Eley-Rideal step between gas-phase ethylene and two deuterium atoms adsorbed on adjacent sites of the platinum surface.

In extended studies with $H_2+D_2+C_2H_4$ mixed beams, it was found that the addition of ethylene to the H_2+D_2 beam leads to a significant decrease in the probability for HD production but that the reaction can still be sustained catalytically under the conditions of our experiments [426]. Three kinetic regimes were identified with increasing partial pressure (or flux) of ethylene in the reaction mixture. The first, seen for mixtures with less than 10 ppm of ethylene, shows a steady-state production of ethane with kinetics similar to those reported from UHV studies, with a rate law dependent linearly on both ethylene partial pressure and hydrogen atom coverage. The surface is mainly covered with hydrogen, and ethane formation occurs primarily via a "reverse" Eley-Rideal mechanism, as mentioned above. A second, intermediate regime is seen for mixtures with up to about 1% of ethylene. In that case, HD production is still relatively fast, albeit the rate decreases slowly with increasing ethylene pressure, but the surface is mostly covered with reversibly-adsorbed ethylene (plus some ethylidyne, $Pt_3{\equiv}C{-}CH_3$), which partially blocks the

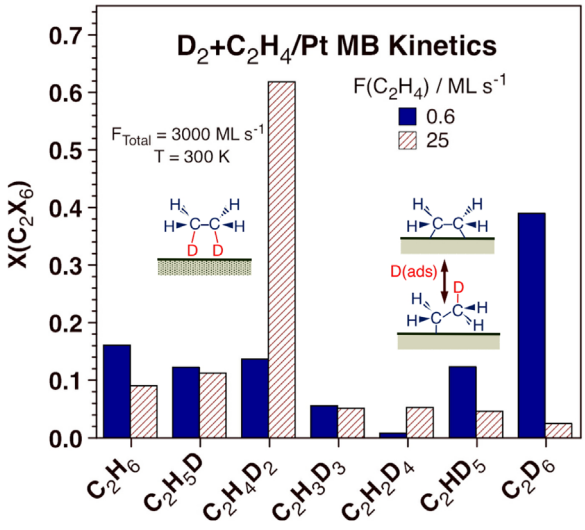

Fig. 34. Distribution of the ethane isotopologues detected from the conversion of $D_2+C_2H_4$ mixtures on a Pt polycrystalline sample at room temperature [49,424]. The reactants were fed by using a single molecular beam with a constant total flux of 3000 ML/s (monolayers per second), high enough to afford sustained steady-state catalysis [411,425]. Data are reported for two different ethylene fluxes, corresponding to two different D_2:C_2H_4 ratios, in order to highlight the two extreme product distributions observed, namely, multiple H–D exchange and extensive multideuterated ethane formation, all the way to C_2D_6, seen with deuterium-rich mixtures (solid blue bars), and (predominantly) direct deuteration to dideuteroethane, which develops as the ethylene partial pressure is increased (hatched red). Reproduced with permission from Ref. [424], Copyright 2016 the Owner Societies.

hydrogen uptake. The probability for ethane formation decreases noticeably in this regime, and the reaction mechanism switches to the stepwise hydrogen incorporation sequence proposed by Horiuti and Polanyi many years ago. Finally, for reaction mixtures with more than 1% of ethylene, the ethylidyne surface layer reaches coverages close to saturation, and controls the HD and ethane formation kinetics via site blocking; this latter regime is the one operational in most catalytic runs. It was also shown that the relative importance of the reversibly-adsorbed ethylene and irreversibly-adsorbed ethylidyne species to the reaction kinetics depends on surface temperature, and that the ethylidyne layer can be removed at temperatures around 500 K to restore the full catalytic activity of the clean Pt surface.

7.2. Combinatorial systems

Kinetic probes based on capillary arrays have also been implemented in connection with catalytic testing of solid surface in high-throughput, or combinatorial, mode. In this application, experiments are not carried out under UHV but rather in ambient environments. Nevertheless, the setup is designed so that a gas mixture is fed in high fluxes via a capillary tube directly to specific spots within the solid, in a way similar to that of the high-flux effusive molecular beam setups discussed in the previous section; the products in this case are collected and analyzed with the aid of a secondary capillary. Several capillary pairs are often arranged in an array for multiple sampling in one go, using either multiple mass spectrometers or a single unit and a gas distribution scheme.

This methodology has been used the most by Weinberg and coworkers at Symyx [427]. They have published several patents describing the evolution of their instrumentation [416,428,429]. Their first version consisted of concentric capillaries, as with the other systems described in the preceding Section 7.1 (Fig. 35, top). With it, the authors evaluated the relative activity of Rh-Pd-Pt-Cu alloys toward CO oxidation as a function of composition [430], the

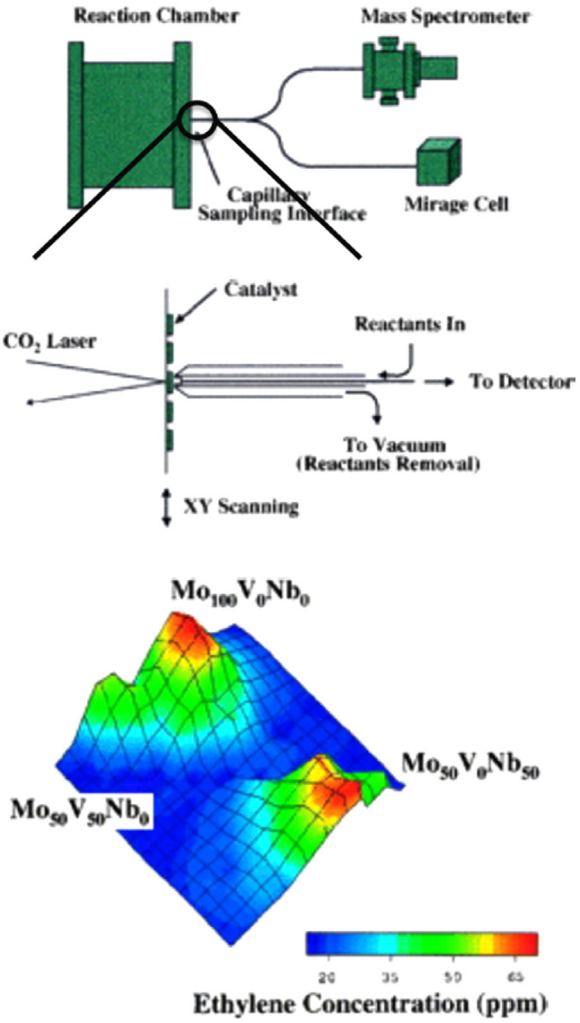

Fig. 35. Top: Schematic depiction of a scanning screening apparatus developed for high-throughput (combinatorial) studies of the activity of flat surface catalysts [432]. The instrument is comprised of three modular subsystems: the reaction chamber (left), the mass spectrometer, for gas detection and analysis (right, top), and a photothermal deflection (PTD) detector. The capillary sampling interface shown in the center of the general diagram, depicted in more detail in the center of the figure, is similar to that described in Fig. 33. Bottom: example of the type of data obtained with this instrument: the production of ethylene from oxidative dehydrogenation of ethane with O_2 (N_2:C_2H_6:O_2 = 5:4:1, P_{Total} = 760 Torr, T_s = 673 K) is mapped for a combinatorial library consisting of molybdenum-vanadium-niobium oxide films of varying compositions, having continuing gradients in V and Mo+Nb content. "Hot" spots in these 3D plots were used to identify catalyst composition prospects for secondary screening. Reproduced with permission from Ref. [432], Copyright 1999 National Academy of Sciences of the United States of America.

performance of supported noble metals and perovskites for low-temperature CO oxidation/light off in cold start automotive emissions conditions, the reactivity of CoCr oxide catalysts for volatile organic compound (VOC) removal, and the catalytic behavior of mixed metal oxides for the selective gas-phase oxidation of propane to acrylic acid and acrylonitrile [431]. Much information on catalytic trends versus surface composition has been derived from such studies. For instance, in an investigation of the trends of mixed Mo-V-Nb-O (Fig. 35, bottom) [432] and V–Al–Nb and Cr–Al–Nb [433] metal oxide libraries toward the promotion of ethane oxidative dehydrogenation to ethylene and CO_2, the authors learned that Nb does not affect the catalytic activity of the V–Al oxides, as it does with Mo–V–Nb oxides.

With a second-generation instrument equipped with multiple probes [434], the selective catalytic reduction of NO with NH_3 mixtures was probed on supported vanadia systems as a function of the nature and composition of the metal precursors, support, and doping, and also on mixed-redox metal oxides and supported base and noble metal systems [435]. The active hits, that is, those showing high NO consumption and N_2 production, were selected for secondary screening. In another study, the methanation of CO and CO_2 was tested over zirconia- and ceria-supported noble and base metal catalysts [436]. Ru, Rh, and Ni were found to promote methanation, whereas Pt was seen to catalyze the reverse water-gas-shift reaction. Methanation activity was also proven to be enhanced by acidic and redox dopants, or suppressed by basic dopants. Studies on the selective low-temperature CO oxidation and VOC removal using mixed CO+propylene feeds revealed novel RuCoCe formulations of the catalyst [437]. For the water–gas shift reaction with real post-reformer feeds containing CO, CO_2, H_2O and H_2, a new synergistic PtFeCe ternary composition was discovered [437].

Both a 16-channel reactor module and a 48-channel fixed bed reactor workstation (comprised of three 16-channel modules) were later developed where the microfluidic flow splitter consisted of one central inlet and 16 identical concentric capillary spirals that radiate out from the center to 16 individual outlets to achieve uniform flow distribution among all reactor channels from a common feed system. These systems have been used for a number of studies, including selective oxidations, oxidative dehydrogenations, ammoxidations, acetoxylations, the conversion of methanol to olefins, hydrogenations, isomerizations, the water-gas shift reaction, and emissions abatement [438].

Recently, Gellman and coworkers have reported another variant of the multiplexed capillary-tube based nanoreactor design for high-throughput testing of solid samples with gradient compositions [439,440]. In their case, the pair of capillaries for gas feeding and sample collection are square and adjacent to each other, and are sealed against the surface by using an appropriate gasket; the full setup was incorporated into a UHV chamber. To date, this system has been used to test the activity of transition-metal alloys toward the isotope scrambling of H_2+D_2 mixtures [47]. It was determined, for instance, that the promotion of H-D scrambling in Pd-Cu alloys decreases with increasing Cu content.

8. Non-catalytic applications

As can be concluded from our review so far, much of the molecular beam studies on the reactivity of gas mixtures on solid surfaces have been geared to develop a better understanding of specific catalytic system. Nevertheless, the technique is also amenable to the investigation of other important processes. In particular, there has been extensive interest in characterizing the kinetics of surface etching and surface oxidation this way, as it relates to microelectronic processing. There are also examples available in the literature on the use of molecular beams for the study of film deposition via chemical means. Together with microcalorimetry, molecular beams have been used to study the energetics of oxide particle formation. Below we briefly survey all this work.

8.1. Surface etching

8.1.1. Silicon surfaces

Several molecular beam studies have focused on etching processes of semiconductor surfaces by gas-phase agents [441–443]. For instance, with Cl_2, anisotropic etching of Si(100) surfaces was demonstrated by taking advantage of the directionality of the beam: the ratio of the etch rates in the vertical versus horizontal directions was shown to be larger than 25 [444]. Silicon removal

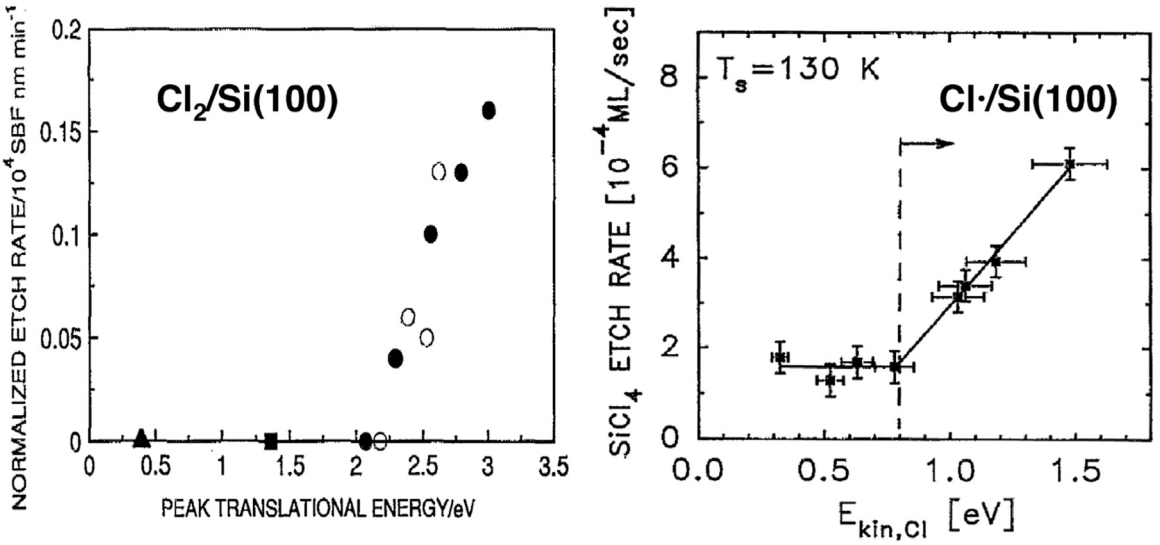

Fig. 36. Left: Translational-energy dependence of the rate of etching of Si(100) surfaces with Cl_2 at a surface temperature of 803 K, measured with a seeded supersonic beam [447]. The values reported by the filled circles were obtained as a function of Cl_2 concentration at a constant nozzle temperature of $T_N = 1183$ K, whereas the open circles indicate the dependence on T_N at a constant Cl_2/He mixing ratio. Reproduced with permission from Ref. [447], Copyright 1993 American Institute of Physics. Right: Similar data from experiments with a hyperthermal atomic (instead of molecular) chlorine beam and a surface temperature of $T_s = 130$ K [446]. Reproduced with permission from Ref. [446], Copyright 1994 American Institute of Physics. In both cases a threshold energy was identify for the start of the etching process. Importantly, though, the rates are orders of magnitude faster, start at lower kinetic energies of the reactant, and occur at much lower surface temperatures with the atomic chlorine beam.

was proven to be chemical in nature, not just the result of physical sputtering (with $SiCl_4$ being the main product [445,446]), and the ratio of the etch rates for polycrystalline Si versus SiO_2 surfaces was shown to be larger than 1000. A kinetic energy threshold was observed for the start of the etching (Fig. 36, left), but the etch rate enhancement was not attributed to the formation of Cl radicals or to vibrationally excited Cl_2 molecules [447,448]. Two thermal desorption processes were identified, with activation energies of 2.8 and 0.9 eV, corresponding to gas etching with collision-induced desorption of weakly-bound $SiCl_4$ and translational-energy-induced etching, respectively [446,449].

The effect of surface structure on etching was investigated by using pristine Si(100) and Si(111) wafers as well as a Si(100) surface damaged by Ar^+ ion bombarded to create surface defects [450]. Similar etch rates were measured on Si(100) and Si(111), with the major products being $SiCl_4$ at surface temperatures below 500 K and $SiCl_2$ at surface temperatures above 600 K; some SiCl was also detected above 1100 K. When the etch rate is reaction limited, higher etch rate can be obtained with atomic chlorine than with molecular chlorine, whereas in the adsorption limited regime the etch rate is primarily determined by the surface temperature. Higher translational excitation of both atomic and molecular chlorine results in higher etch rates, especially on defective Si(100) surfaces.

Fluorine-containing etching agents have in general shown higher activity than their chlorine counterparts. In an early molecular beam study, the etching of Si(100) wafers with hot SF_6 was shown to be enhanced by vibrational excitation of the incoming molecules [451,452]. It has also been shown that, at low energies, both XeF_2 and F_2 adsorb dissociatively and with high probability but only on the dangling bonds of Si [453]. Using a He atom diffraction technique, it was established that fluorination initially creates a degree of disorder on the surface but that order is restored once monolayer coverage is reached. After monolayer saturation F_2 ceases to react with the surface, whereas XeF_2 continues to deposit fluorine by reacting with the Si–Si dimer and with the lattice bonds. The dose dependence of the fluorine content was shown to not follow a single exponential behavior, but to rather increase rapidly in the early stages of the uptake but much more slowly thereafter [454]. This behavior was explained by the rapid development of a monolayer of SiF_x surface species in the initial regime followed by the slow formation of a steady-state multilayer of $SiF–SiF_2–SiF_3$ and $SiF_2–SiF_3$ chains. In terms of the temperature dependence of the etching process, with XeF_2 the initial reaction probability initially decreases from 100% at 150 K to 20% around 400 K, possibly a reflection of a precursor-mediated mechanism, but then increases again at temperatures above 600 K, up to 45% at 900 K, presumably because of the desorption of SiF_2 species [455]. At room temperature, the high etch rate of silicon single-crystal surfaces with fluorine versus chlorine is due to the higher rate of formation of volatile products with the former etching agent [450].

Etching of silicon surfaces has also been studied by using atomic chlorine and atomic fluorine beam sources. The dynamics of these impinging atoms may be complex, possibly involving significant multiple-bounce scattering and trapping desorption [456]. At high temperatures the etching reactions are the same as with the molecular species, at least with Cl_2, but at lower temperatures the main desorption product is $SiCl_2$, with some $SiCl_4$ or Si_2Cl_6 being formed as well [457]. This atomic-Cl etching can be enhanced by increasing the translational energy of the chlorine atoms (Fig. 36, right), and reaches rates several hundred times greater than those possible with molecular beam [458]. Atomic recombination of Cl, Br, and F atoms has been shown to follow pseudo-first order kinetics, suggesting that a two-step process is operational in which the first halogen atom adsorbs into a relatively strongly-bonded chemisorbed state and the second reacts with it either directly or after physisorbing onto the halogenated surface [459].

Regarding Si etching with ClF_3 beams, it has been reported that those molecules are not, by themselves, capable of promoting silicon removal at room temperature [460]. Nevertheless, etch rates of 40 μm/min or higher were measured even at room temperature because of the formation of more reactive ClF_3 clusters. Selectivity for the etching of Si versus the removal of SiO_2 or a photoresist was estimated at a minimum rate ratio of 1:1000. Anisotropic etching was seen as well, with an aspect ratio of 10 or higher favoring the direction of the beam.

8.1.2. *Gallium arsenide surfaces*

With GaAs, the main product of chlorine etching is $GaCl_3$. The

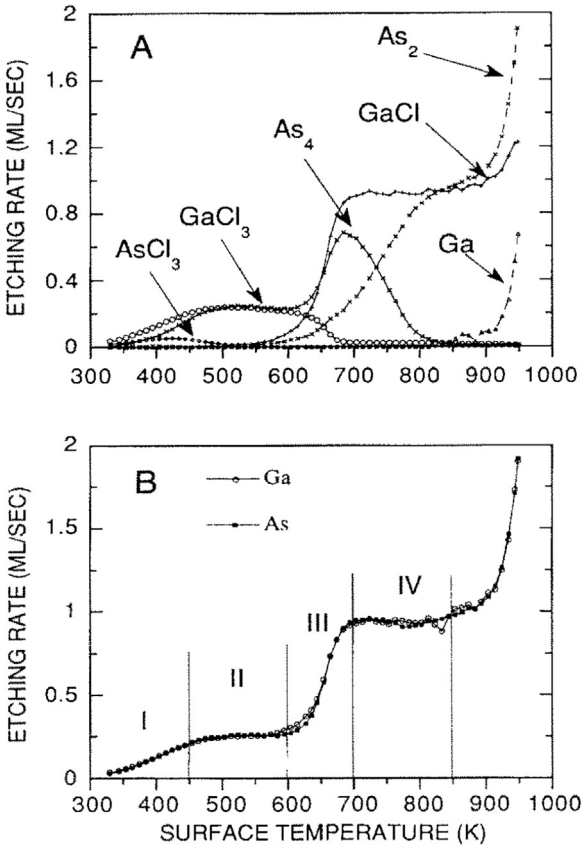

Fig. 37. Data from studies of the dry etching of GaAs(100) with Cl_2 using modulated supersonic molecular beams. Top: Dependence of the etching rate on surface temperature, reported together with an identification of the main desorbing products. Bottom: Independent total absolute etching rates for Ga (open circles) and As (solid squares). The wide variations seen in the gas composition of the ejected products as a function of temperature (top panel) attest to the complex multichannel mechanism of the etching process, yet the data in the lower panel indicate that etching is stoichiometric under all conditions. Reproduced with permission from Ref. [463], Copyright 1993 Elsevier Science Publishers B.V.

reaction was shown to be precursor mediated, and to not exhibit any activation barriers for the desorption of the product [461,462]. The chlorine surface coverage during steady state was estimated to be in the monolayer regime between 350 and 650 K, but close to zero above 700 K [463]. Analysis of the angular distribution of GaCl, which is ejected from the surface at higher temperatures ($T > 650$ K), points to two surface reaction channels: one where accommodation and desorption of the incident Cl_2 occurs readily, and a second with delayed chemical conversion [464]. Other products have been detected as well, including $AsCl_3$, As_4, and As_2 [465], all ejected with close-to-cosine angular distributions but with measurable time delays [443]. Nevertheless, the ratio of the etching rates of Ga and As is independent of the surface temperature and within the range expected from stoichiometry (Fig. 37) [465]. The mode of As removal with Cl_2 beams changes with surface temperature, with surface diffusion becoming important at surface temperatures above 400 K [465]. Anisotropic etching is also seen with GaAs, as with Si [466].

Etching with HCl instead of Cl_2 shows similar reaction characteristics, including the dominance of GaCl production, the cosine angular distribution of the products, and the time delays mentioned above [467,468]. However, etching of GaAs with HC1, unlike Cl_2 (which etches GaAs at room temperature), does not lead to measurable GaAs etching below 670 K [469]. Between 670 and 870 K some As_2 desorbs with the main GaCl product, and above 850 K gas-phase Ga is also detected, in an etching regime limited by As removal [469].

GaAs(001)$-(2\times4)$ etching with CH_3Cl has been shown to follow two reaction channels, as reported above for other systems: a trapping/desorption pathway, dominant with low-energy beams, and a direct inelastic scattering channel that develops for high incident energies [470].

8.1.3. Others

Etching of a few other surfaces has been probed with the aid of molecular beams. In one case, polycrystalline aluminum nitride has been made to react with an effusive beam of XeF_2 [471,472]. The reaction was shown to start at a surface temperature of 700 K via the formation of AlF_3(ads), and sustained desorption to begin above $T_s = 800$ K, at which point N_2 and AlF_3 desorb from the surface. The etching probability increases monotonically with sample temperature until reaching a value of approximately half of the incoming XeF_2 by 920 K.

8.2. Surface oxidation

Surface oxidation is an integral part of microelectronic processing, in particular to develop thin dielectric oxides on top of semiconductor surfaces. Thin oxides usually form naturally, certainly on silicon surfaces, but a more controlled build up of such layers is necessary for practical applications [473,474]. This can be accomplished via exposure of the surface to either molecular oxygen or to a form of activated oxygen such as atomic oxygen (from plasmas) or ozone. Molecular beams have been used to study some kinetic aspects of these processes.

8.2.1. Silicon surfaces

Exposure of silicon to molecular oxygen leads to a combination of silicon oxide thin-film growth and etching. The initial sticking and activation of O_2 appears to be precursor-mediated with low-energy beams [475], transitioning to direct adsorption as the incident energy is increased [476,477]. The first mechanism is structure sensitive, being twice as fast on the unreconstructed (1×1) Si(111) surface compared to the well-known (7×7) reconstructed phase that prevails at room temperature [478,479], but that difference disappears at high beam energies, as the direct dissociative adsorption pathway takes over [480,481]. Molecular oxygen reacts with silicon surfaces, with both Si(100) and Si(111), via two stable surface intermediates that are formed sequentially. The second of those intermediates is identical to that formed by the reaction with atomic oxygen, and leads to SiO desorption above 1010 K (Fig. 38) [475,482,483]. The first intermediate, with O_2, has been proposed to consist of a peroxy radical or a peroxide bridge [484].

Surface oxidation can be catalyzed by the addition of alkali metals. Sticking coefficient measurements of O_2 on Cs-predosed Si (100) surfaces, using molecular beams, identified two different kinds of cesium sites, and determined that the initial sticking probability increases linearly with the coverage of each kind of cesium site [485]. The data showed that the effect of cesium is local, and that an oxygen-cesium bond is formed during the reaction that passivates the cesium.

Silicon oxidation can also be carried out by using oxygen-atom beams. In addition to the work by the Engstrom group cited above [484,486], this has also been reported by Madix and Susu in a study that indicated that etching with such atomic species is at least one order of magnitude faster than with O_2 [487]. Those authors also found that the reactivity is independent of the orientation of the crystal plane.

8.2.2. Germanium surfaces

Madix and Susu have reported lower reactivity on germanium

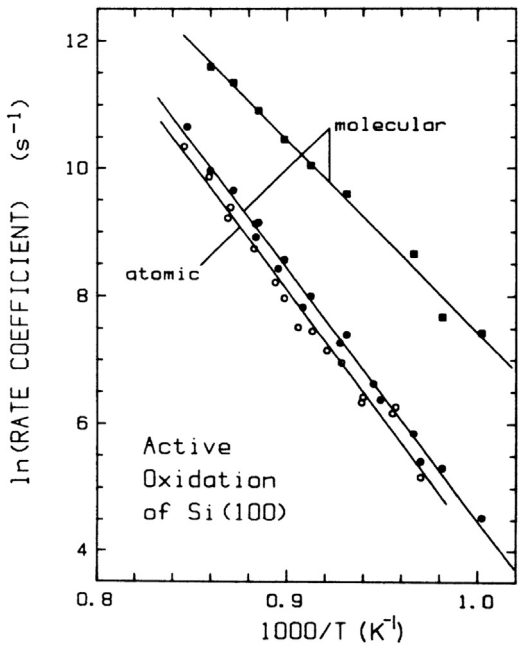

Fig. 38. Arrhenius plot of the reaction rate coefficients for the formation of SiO (g) from reaction of a Si(100) surface with either atomic (open circles) or molecular (solid symbols) oxygen as a function of surface temperature [486]. Two sets of data are provided for the latter, for the slow (solid circles) and fast (solid squares) steps identified in this study. Overall oxidation is faster with O_2 that with O·, but some oxygen dissociation followed by atomic-oxygen oxidation is also operational in the former case. Reproduced with permission from Ref. [486], Copyright 1990 The American Physical Society.

surfaces, about 40% of that seen on silicon [487,488]. At low temperatures the sticking coefficient decreases with temperature, the signature of a precursor-mediated adsorption process [442], and an increase in sticking at glancing angles of incidence is seen, consistent with a rise in trapping probability [489]. On the other hand, a direct adsorption channel becomes increasingly more efficient at higher temperatures [490]. These observations are in many ways qualitatively similar to those reported for the adsorption dynamics of oxygen on silicon. On clean Ge(100), oxygen scatters primarily by a direct inelastic mechanism, presumably on defect sites, but considerable trapping occurs on oxygen-covered surfaces [490]. The only species observed in the gas phase in this system has been GeO (g), which desorbs with a cosine spatial distribution indicative of full energy accommodation with the surface [489]. At low coverages desorption was seen to follow first-order kinetics with an activation energy of approximately 250 kJ/mol, whereas at higher coverages zero-order kinetics prevails, with the same activation energy. These results have been explained in terms of a model where GeO desorbs mainly from oxygenated ledge sites; the transition to zero-order desorption kinetics occurs once those sites are saturated. An intermediate oxidation step analogous to that reported on silicon is suspected in the reaction with germanium as well [491].

Nitrogen oxides can also be used as oxidants for these surfaces. In fact, this has turned out to be an efficient way to etch semiconductor surfaces, almost as good as by using molecular oxygen. On Ge(111), for example, the reaction probability with NO was measured to be about 1/4 of that with O_2 [491]. A more recent molecular beam study of the dynamics of the reaction of NO_2 on Ge(111) highlighted some deviations from a Boltzmann distribution in the desorbing NO product, indicating rapid bond scission and NO ejection before any significant energy accommodation with the surface can take place [102].

8.3. Film deposition

Another type of surface reactions of importance in microelectronics fabrication is that of the deposition of thin solid films. This may be done by chemical means, by chemical vapor deposition (CVD) or, as introduced more recently, by atomic layer deposition (ALD) [492–494]. In these processes, a chosen precursor is made to react with a second agent, a small molecule such as H_2, NH_3, or O_2 that acts as a reducing, oxidizing, or ligand displacement agent. The reactions are separated in time in ALD, but may involve the same basic surface chemistry in both cases. The relevant steps have in some cases been investigated using molecular beams, as discussed below. Another more standard methodology for film growth is molecular beam epitaxy (MBE), where the different elements to be deposited on the surface are provided by beams of vapors of the appropriate elements [495–497]. That technique falls outside the bounds of this review, but a few selected examples of such approach are also provided below.

8.3.1. Silicon surfaces

The deposition of silicon via the decomposition of silane or disilane precursors has been one of the first CVD processes studied with the aid of molecular beams. The initial research focused on assessing the viability of this approach [442,498–504]. The reaction was found to be second order in silane flux and to produce traces of disilane when starting from silane, suggesting the formation of an initial SiH_3(ads) intermediate [498,499]. Based on additional results using deuterium labeling, a second SiH_2(ads) intermediate was proposed [505], and a third SiH(ads) species was later added to the picture as well [506].

Much of the more recent work on the characterization of the kinetics of CVD processes with molecular beams has been carried out by the Engstrom group [507]. In an early study with Si_2H_6 on Si (100) and Si(111), they found that the probability for dissociative adsorption depends linearly on the translational energy of the incident beam [508], and in a cosine-square fashion as a function of incident angle [509]. In addition, the reaction on the (111) surface shows sensitivity to the surface reconstruction from a (7×7) to a (1×1) lattice that occurs above 1100 K (Fig. 39) [505,509]. It was concluded that both the dangling bond density and the effective corrugation of the surface are important in determining the reaction probability. Two reaction mechanisms were identified: (1) a complete pyrolysis to form two adsorbed Si atoms and gas-phase hydrogen, a step that increases in prominence with increasing incident kinetic energy; and (2) a reaction forming one adsorbed Si atom and gas-phase hydrogen and SiH_4 (from a chemisorbed intermediate) [510]. The relative prominence of these two channels was found to be sensitive to the structure of the surface: only complete pyrolysis was observed on the clean Si (100)-(2×1) and Si(111)-(1×1) surfaces, whereas silane production was also detected on the Si(111)-(7×7) surface and on the Si (100)-(2×1) surface in the presence of a finite coverage of either adsorbed hydrogen or phosphorus atoms.

With SiH_4, the dependence of its sticking coefficient on incident energy was estimated to be exponential [511]. On Si(100), there is also a weak dependence on substrate temperature, and on Si(111) an additional increase in sticking probability is observed in connection with the reconstruction from the (7×7) to the (1×1) phases. Experiments with SiD_4 revealed a modest kinetic isotope effect, a result inconsistent with activation via tunneling. Results from comparative studies of the reaction probability with SiH_4 versus Si_2H_6 on the Si(111)-(7×7) surface as a function of incident kinetic energy suggested a similar decomposition mechanism for the two molecules, namely, Si–H bond activation; SiH_4(g) was proposed to be formed via unimolecular thermal decomposition of an adsorbed Si_2H_5(ads) species [510].

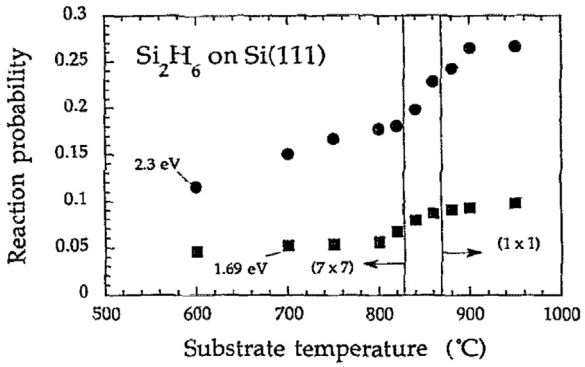

Fig. 39. Reaction probabilities for Si_2H_6 dissociative chemisorption on Si(111) as a function of substrate temperature for two incident energies of the supersonic molecular beam [508]. Higher reaction probabilities are seen with both higher kinetic energies and higher surface temperatures. Perhaps more strikingly, a sharp transition is seen between approximately 1100 and 1140 K, ascribed to a significant change in surface reactivity upon the removal of the well-known (7×7) reconstruction of the Si(111) surface [478,479]; the high-temperature, unreconstructed (1×1) phase has more silicon dangling bonds and is, consequently, more reactive. Reproduced with permission from Ref. [508], Copyright 1993 American Institute of Physics.

Epitaxial silicon thin-film deposition using Si_2H_6 has also been explored on silicon oxide [512]. The incubation period associated with polycrystalline Si deposition on SiO_2 was found to decrease with both increasing substrate temperature and increasing incident beam kinetic energy. Other molecules have been deposited as well. For instance, the deposition of SiC thin films on Si(100) has been demonstrated by using high-energy ($E_i = 2.0$ eV) SiH_3CH_3 beams [512]. In another example, phosphine has been used to add phosphorous to the surface. The initial probability of reaction for PH_3 on Si(111)-(7×7) was found to decrease with increasing substrate temperature and with increasing kinetic energy of the incident beam, a signature of precursor-mediated dissociation [513]. It also increases sharply, by a factor of approximately 4 to 5, upon transition from the reconstructed (7×7) to the unreconstructed (1×1) surfaces, and exhibits an autocatalytic behavior consistent with a mechanism in which submonolayer coverages of P(ads) are capable of lifting the (7×7) reconstruction [514]. The reaction probabilities of PH_3, SiH_4, and Si_2H_6 on Si(111)-(7×7) all follow Langmuir kinetics assuming the blocking of two sites per P adsorbed atom, and in the case of the silane it passes through a maximum with increasing P(ads) coverage. Finally, treatment of the Si(100) surface with atomic hydrogen appears to cap the dangling bonds and to passivate the surface toward any subsequent silane uptake [515].

8.3.2. Germanium surfaces

Similar experiments have been carried out with GeH_4 and Ge_2H_6 on Ge(100) and Ge(111), to deposit germanium films. At sufficiently large incident kinetic energies ($E_i \geq 1$ eV) both germanium precursors were found to react by direct dissociative chemisorption, with reaction probabilities increasing approximately exponentially with increasing (scaled) incident kinetic energy [516]. At moderate kinetic energies ($E_i \sim 0.4$ eV), however, the reaction probability of Ge_2H_6 on Ge(100) (but not on Ge(111)) decreases with either increasing substrate temperature or incident kinetic energy, as expected for a precursor-mediated mechanism. Conversion of Ge_2H_6 on either surface does not seem to involve a GeH_4 intermediate. Similar behavior was reported for the same precursors on Si(100) and Si(111) substrates, except that the Si surfaces are much more reactive, by as much as a factor of 10, than their Ge counterparts [517]. The Ge hydrides were also found to be moderately more reactive, by a factor of approximately 2, than the Si hydrides. The reactivity of ~2 monolayers-thick Ge films grown on Si(100) were found to exhibit a reactivity intermediate between Si(100) and Ge(100), whereas on Si(111) the Ge epitaxial layer is less reactive than the pure surfaces of either Si or Ge.

Nucleation of Si and $Si_{1-x}Ge_x$ thin films on Si or SiO_2 surfaces using Si_2H_6 or GeH_4 have been tested with molecular beams as well [518]. The time associated with the start of the formation of stable islands was found to depend strongly on both the kinetic energy of the incident molecular precursors and the substrate temperature, and, after island coalescence, the morphology of the resulting thin films was determined to depend primarily on substrate temperature, with smoother films being grown at substrate temperatures below 875 K. Addition of atomic hydrogen, via a separate coincidental beam, was shown to increase the incubation time, especially at substrate temperatures below 900 K, suggesting that hydrogen atoms adsorbed on the Si-like sites on SiO_2 can effectively block the nucleation of Si. The addition of Ge to the surface increases the incubation time but lessens the effect of hydrogen.

8.3.3. Gallium arsenide surfaces

For the growth of GaAs films, the most common precursors used in chemical deposition processes are arsine (AsH_3) for As and one of the following compounds for Ga: trimethylgallium (TMGa, $(CH_3)_3Ga$), triethylgallium (TEGa, $(C_2H_5)_3Ga$), or diethylgallium chloride (DEGaCl, $(C_2H_5)_2GaCl$) [519,520]. This is a more complex system because it requires two precursors, needs careful monitoring of stoichiometry, and may show several different termination surfaces. Some molecular beam work has been designed to address these and other kinetic issues [521–525]. For instance, by monitoring the residence times and sticking coefficients using time-resolved molecular beams, the adsorption of all three gallium precursors on the As-rich GaAs(100)-c(2×8) surface was shown to be precursor mediated [526]. In the same vein, the sticking of TMGa on relaxed and reconstructed versions of GaAs (100), (110), and (111) surfaces was estimated to proceed mostly through a precursor as well (the possible exception being the GaAs(100)-(1×6) surface, Fig. 40) [523,527,528].

With the gallium precursors, the trends observed for the structure dependence of the depth of the energy well that describes the precursor state, estimated from the temperature dependence of the surface residence time during scattering, was explained in terms of the charge distribution in the relaxed or reconstructed surface structures, whereas the energy barrier height to chemisorption was interpreted as reflecting the stability of those same structures. In this context, the higher suppression of TMGa decomposition on the (2×2)-reconstructed GaAs(111)B may be due to the absence of localized charge at the topmost As atoms. It was speculated that it is the adsorbed methyl groups rather than the surface Ga that play the key role in the inactivation of a Ga-stabilized surface [529]. At least on GaAs(100), CH_3 was found to be the major reaction product, its desorption facilitated by an arsine ambient; no CH_4 or C_2H_6 desorption was detected [530–532], but some $GaCH_3$ was seen at high Ga coverages [533]. With TEGa the surface chemistry is quite similar: the products include hydrogen and a small amount of ethyl radicals, even though the desorption of ethylene, the product from β-hydride elimination, becomes dominant [534], and As termination of the surface facilitates decomposition [535]. The β-hydride elimination channel has also been observed with triisobutylgallium and tritertbutylgallium [536].

Less work seems to be available on the chemistry of the arsenic precursors. Besides arsine and As_2 and As_4 [530,531,537–539], a few other compounds have been tested. At room temperature, tertbutylarsine was found to chemisorb on the arsenic-rich c(4×4) and gallium-rich (4×6) surfaces, but not on the arsenic-rich (2×4) structure, of GaAs(001), presumably via a

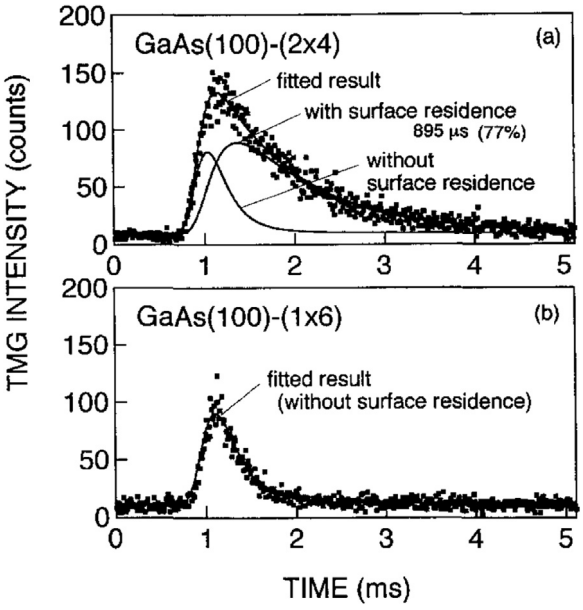

Fig. 40. Time-of-arrival spectra for trimethylgallium scattered from (2 × 4) (a, top) and (1 × 6) (b, bottom) reconstructed GaAs(100) surfaces at 546 K [523]. Also shown are fits to two components, originating from direct scattering (no surface residence time) and from molecules that spend a finite residence time on the surface. For the less stable Ga-rich (1 × 6) surface the spectrum is well reproduced by a single component, for scattering without surface residence, whereas on the more stable (2 × 4) substrate a second delayed component is apparent. Reproduced with permission from Ref. [523], Copyright 1997 Elsevier Science B.V.

precursor-mediated mechanism [540,541]. The angular dependence of the reflected molecules was explained by trapping/desorption and direct inelastic scattering processes. The adsorption energy estimated from the results of these experiments were consistent with a model based on the surface reconstruction of each surface.

8.3.4. Other Materials

Molecular beams have been used to test the deposition of other materials, including semiconductors [495,496], semiconductor oxides [497,542], ferroelectric materials [543,544], and other dielectric materials [545]. In many of those studies the use of the beams have just been the means to provide high fluxes of reactants, but in others the extra energy of supersonic beams have been employed to promote deposition mechanisms not available by normal thermal activation [442]. It is beyond the objective of this review to provide a discussion of deposition technologies; our focus here is on the use of molecular beams for the study of reaction mechanisms on solid surfaces. Nevertheless, some of the work in the area of molecular beam deposition has added to our knowledge of the corresponding surface chemistry involved. Below we provide a few examples.

As with GaAs deposition, other analogous III-V semiconductors can be prepared by chemical means using triethyl complexes and ammonia. On a GaN(0001)/AlN/6H–SiC composite substrate, TEGa supersonic jets have been used to deposit homoepitaxial α-GaN quasi-2D islands with irregular perimeters [546–548]. The growth rate was shown to exhibit linear dependences on both TEGa and NH_3 fluxes, consistent with a Langmuir-Hinshelwood mechanism. The Ga incorporation efficiency is lower with high-energy TEGa beams, a result consistent with dissociative chemisorption.

Silicon carbide films have also been made using molecular beams. In one case, hot C_2H_2 has been dosed on Si(100) for this purpose [549]. The growth rate of the film was found to be proportional to the beam flux under low beam-flux condition, but to decrease at high temperatures because of carbon poisoning. The kinetics of deposition is modified in complex ways because of a preferential pyramidally-shaped corrosion along the (111) facet; SiC was seen to form on the etched sites. With methylsilane, the use of thermal beams leads to film growth only via reaction of out-diffused silicon atoms with the incoming precursor species, a process that is self limiting and stops after a few layers. At moderately higher kinetic energies, on the other hand, a second growth mechanism opens up that is not thickness-limited [550]. Complex morphological changes on the surface and preferential etching were identified in this case as well.

A different application of molecular beams in this category is for the deposition of organic layers, often also in connection with microelectronics applications. The studies on the growth of pentacene thin films provide an example of this work. The effect of surface defects was characterized by using two Ag(111) surfaces with different average step distances [551]. While the initial stage of the growth was found to be similar on the two different surfaces regardless of the pentacene kinetic energy and the substrate temperature, the thicker films show different structural and thermal properties. On SiO_2, the rate of growth was seen to accelerate at high incident-beam energies, moving from the submonolayer to the multilayer regime because of molecular insertion events into the topmost layer of the pentacene thin film [552]. These insertions were deemed possible on terrace sites but to be more likely at step edges. With diindenoperylene (DIP) on SiO_2, the initial adsorption is precursor mediated, but after monolayer saturation the adsorption probability increases, particularly at the highest incident kinetic energies [553].

8.3.5. Atomic Layer Deposition (ALD)

Molecular beams have also been used to investigate the surface chemistry of some of the precursors used in CVD and ALD depositions of different materials, including diffusion barriers and metal interconnects. As an example of the first, we can cite our own work on the reactivity of pentakis(dimethylamido)tantalum ($Ta[N(CH_3)_2]_5$, PDMAT), by itself and with ammonia as a co-reactant, on a Ta substrate [494,554]. The main desorbing species detected include not only the expected dimethylamine, $HN(CH_3)_2$, and the β-hydride elimination product, $H_2C{=}NCH_3$ (which displays slower transient kinetics than the rest), but also H_2, CH_4, C_2H_4, and HCN (Fig. 41). Thermal conversion on the surface was found to start at 450 K. Addition of ammonia to the reaction mixture was shown to lead to an enhancement in hydrogenation to the amine at the expense of methane formation, but only at temperatures above approximately 550 K. Isotope labeling was used to establish that the hydrogenation of the amido groups involves hydrogen atoms from the ammonia; methane formation, on the other hand, occurs via intramolecular hydrogen transfer instead.

In a related ALD study, on the deposition of TiN on SiO_2 using tetrakis(dimethylamido)titanium ($Ti[N(CH_3)_2]_4$, TDMAT) and NH_3, the effect of surface modification with self-assembled monolayers (SAMs) on the film deposition was tested [555,556]. On the bare oxide surface, the reaction probability was found to vary only weakly with either incident kinetic energy or the angle of incidence of the molecular beam, in a behavior that could be described as precursor-mediated [557]. For organic layers possessing unreactive end groups such as methyl moieties, the thickness of the film deposited per cycle is strongly attenuated, and growth is in the form of islands nucleated around defects within the adlayer. Because the reactivity decreases continuously with increasing incident energy while increasing with increasing incidence angle, it was proposed that the titanium precursor is first trapped on the surface and then diffuses through the SAM until reacting with residual hydroxyl surface groups at the SAM/SiO_2 interface. For organic layers with reactive end groups such as $-NH_2$ and $-OH$

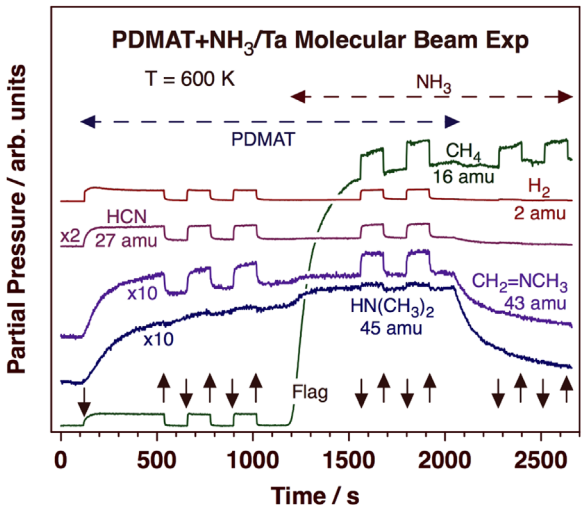

Fig. 41. Typical isothermal kinetic curves from experiments with effusive molecular beams of pentakis(dimethylamido)tantalum (PDMAT) and ammonia on a Ta foil at 600 K [554]. The traces for the evolution of the partial pressures of all the detectable products, namely, methane (CH_4), hydrogen (H_2), hydrogen cyanide (HCN), N-methyl methyleneimine ($CH_2{=}NCH_3$), and dimethylamine ($HN(CH_3)_2$), are shown as a function of time during all stages of the experiment, which include alternating exposures of the surface to PDMAT alone (t = 100–1200 s), PDMAT + NH_3 mixtures (t = 1200–2100 s), and NH_3 alone (t = 2100–2700 s). Blocking and unblocking of the beam, indicated by the up- and down-pointing arrows, respectively, was done periodically to check on the contributions from the steady-state reaction to the signal and to study the transients right before and right after exposure of the surface to the gases. Adapted with permission from Ref. [554], Copyright 2011 American Chemical Society.

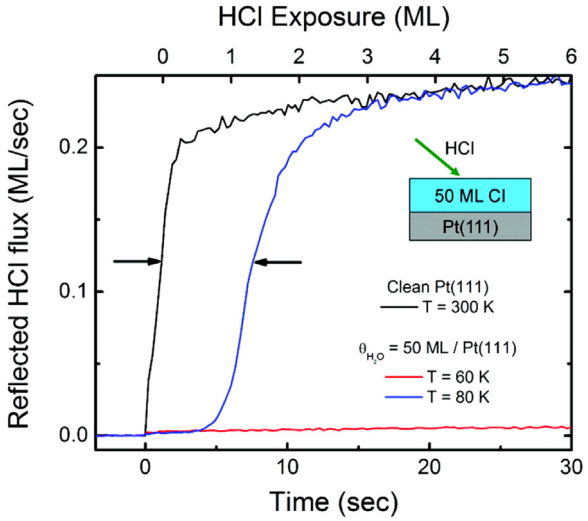

Fig. 42. Intensity of the HCl molecules scattered from a 50 monolayer-thick (ML) crystalline ice film grown on a Pt(111) surface exposed to a HCl effusive beam impinging at 45°, as measured by using a King and Wells setup [562]. The flux reflected by the clean Pt(111) at 300 K (black trace) is provided as reference, to illustrate the profile expected from total scattering from the surface. Two other traces are displayed, for HCl exposure at 60 (red trace) and 80 K (blue trace). In both cases the signal does not change much right after the start of the exposure (t = 0 s), indicating unit sticking probability, but the reflected flux increases sharply after 5 s of exposure of the ice film at 80 K, indicating the point of saturation of the HCl monolayer on ice. At 60 K, by contrast, HCl condenses, and the sticking coefficient remains at unity even after long exposures. Reproduced with permission from Ref. [562], Copyright 2011 American Chemical Society. (For interpretation of the references to color in this figure legend, the reader is referred to the web version of this article.)

growth is also attenuated, but to a lesser extent. The inhibition is even less pronounced if the temperature is raised, a result that suggests some degradation of the interfacial layer leading to the exposure of new adsorption sites on the surface. A second direct mechanism also opens up at sufficiently high incident energies.

There is also a report on a molecular beam study of the ALD of copper films, used for interconnects, on TiN and SiO_2 substrates using hexafluroacetylacetonate copper(I) trimethylvinylsilane and molecular hydrogen [558]. Film deposition starts at specific nucleation centers. With the aid of electron microscopy, it was determined that on SiO_2 the Cu nuclei density reaches a maximum near 5×10^{10} cm^{-2}, nearly independently of substrate temperature, whereas on TiN surfaces the maximum nuclei density is strongly dependent on temperature and varies by nearly two orders of magnitude between approximately 425 and 535 K.

8.4. Others

Finally, we mention a few cases where molecular beams have been used to study the chemistry of surface processes for applications other than catalysis of microelectronics processing. As with the examples discussed in the previous Section, the beams can be used as a tool for film deposition, or they can be employed to characterize the ensuing the surface chemistry. In a few cases, both elements are considered in the reported studies.

In one example, Kay and coworkers have used molecular beams to both prepare ice films and characterize them in terms of their porosity and their ability to adsob and/or absorb different gases [559]. Below 110 K, the incident energy of the water molecules in the beam was found to have no effect on the structure of the initial phase of the resulting ice film or on its crystallization kinetics. This is still the case above 110 K, but under those circumstances the surface temperature does matter, as when a crystalline ice template is used. These results suggest that the crystallization of amorphous solid water (ASW) requires the cooperative motion of several water molecules. The condensation coefficient for N_2 on those films was found to be essentially unity until near saturation, independent of the ASW film thickness, indicating that molecular transport within the porous films is rapid [560]. By following the uptake of N_2 versus exposure, it was shown that the porosity of the ice films can be controlled by tuning the angle of incidence of the water molecules during deposition [561]. With HCl, the initial sticking coefficient on the ice films was found to always be unity below 60 K, but to diminish significantly once a monolayer builds up on the surface at 80 K (Fig. 42) [562].

In a different type of application, Campbell and coworkers have combined molecular beams with microcalorimetry to characterize the energetics of the initial stages of deposition of metals on oxide surfaces [563–565]. Sticking probabilities are usually quite high, close to unity, but the heats of adsorption vary with coverage. For instance, in the case of Pb deposition on NiAl(110) at 300 K, the heat of adsorption starts at 249 ± 10 kJ/mol on the clean surface but, because of the repulsive interactions between Pb adatoms, decreases within the first layer until reaching the value of the heat of sublimation of bulk Pb (195 kJ/mol) [566]. In contrast, Au deposition on CeO_{2-x}(111) thin films exhibits initial heats of adsorption lower than the bulk heat of sublimation, displaying variable values depending on the value of x (which reflects the stoichiometry of the underlying oxide). This behavior was explained on the basis of the Au particles binding preferentially on oxygen vacancies [567].

Similar studies have been performed on other systems, including Cu/CeO_{2-x}(111) [568,569] and Ag/F_3O_4(111) [570]. Some important trends have been identified as a function of the nature of both the oxide used as the substrate and the metal being deposited (Fig. 43) [571–573]. For instance, with late transition metals, deposition on oxides typically leads to growth in the form of 3D nanoparticles. The number of clusters per unit area increases initially with coverage but usually saturates after a few percent of

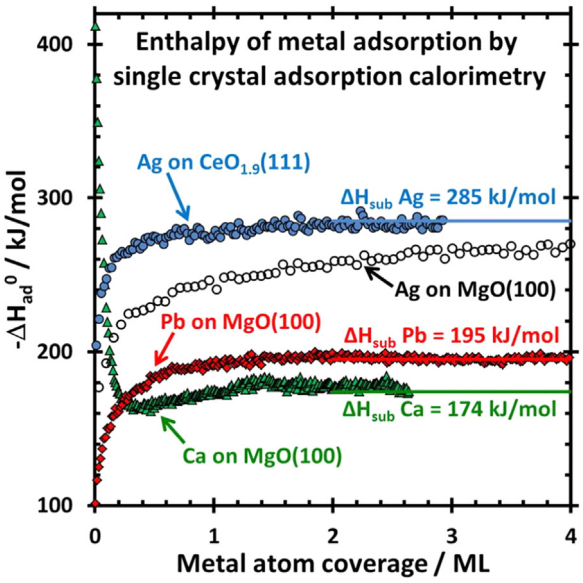

Fig. 43. Evolution of the heats of adsorption of several metals (Ag, Pb, Ca) on single-crystal oxides ($CeO_{1.9}$(111), MgO(100)) at 300 K as a function of metal coverage, determined by using an instrument that combines microcalorimetric measurements with molecular beam dosing (Fig. 5b) [573]. In the initial stages of the uptake the values of the heats of adsorption vary with coverage, reflecting different energy contributions from metal-metal versus metal-oxide bonding, but those asymptotically approach the bulk heats of sublimation (indicated by the horizontal lines) after the build up of multilayer films. Reproduced with permission from Ref. [573], Copyright 2013 American Chemical Society.

a monolayer, after which the clusters grow in size at nearly fixed number density until they coalesce. In such cases, the heat of metal adsorption typically starts out low and increases with coverage as the cluster size grows. Overall, the strength of the attachment to the oxide is dominated by the number of metal-metal bonds as well as the strength of metal/oxide interfacial bonding.

9. Concluding remarks

In this review we have surveyed the use of molecular beams for the study of the kinetics of chemical reactions on solid surfaces. The main characteristic of molecular beams is their directionality, a property that affords the design of experiments where surfaces may be exposed to high fluxes of reactant gases while maintaining the surrounding ultrahigh vacuum conditions used in modern surface-science studies to exert control over the cleanliness of the substrate and the operation of surface-sensitive techniques. In combination with mass spectrometry detection, this makes molecular beams uniquely suited for the measurements of the rates of surface reactions under both transient and steady-state conditions. Virtually no other technique is available for the acquisition of this type of information. Its isothermal nature makes the molecular beam approach much more powerful from the kinetic point of view than temperature-programmed desorption (TPD), a technique more commonly used in surface-science laboratories.

The additional control over kinetic energy provided by supersonic beams, together with the external ways available to tune the energetics of other degrees of freedom (vibrational, rotational) within the reacting molecules in the beam, have been amply exploited to look into the details of the dynamics of adsorption, desorption, and surface conversion steps. This work has been seminal in developing a detailed molecular-level picture of such surface dynamics. It is thanks to the early molecular beam research on adsorption of simple molecules that we now have a fairly complete picture of the potential energy surfaces that describe the interactions of molecules with solids and understand the details of the transfer of energy between molecules from the gas phase and surfaces that results in either adsorption or scattering, elastically or, more often, inelastically. Chemisorption through weakly-bonded precursor states, lateral diffusion across the surface until adsorption on specific surface sites occurs, differences in sticking probabilities between terraces and defects, and the dynamics of bond activation in dissociative adsorption events, are all now much better understood thanks to this type of molecular beam investigations.

Bimolecular reactions on surfaces add another level of complexity to the study of the dynamics and kinetics of surface processes using molecular beams. In addition to understanding the dynamics of adsorption and activation of each of the reactants, a need arises to also explain how both reactants interact with each other and how they convert into products. At the center of many of the discussions in this case is the issue of where exactly the interaction between the reactants takes place: on the surface, between two adsorbed species (the Langmuir-Hinshelwood mechanism), or at the interface, as an incoming gas molecule impacts on a second species already adsorbed on the surface (an Eley-Rideal pathway). Evidence from molecular beam experiments has been indispensible to establish the overwhelming prevalence of the first route as well as to identify the few exceptions where the second takes place. Other mechanistic details of bimolecular reactions, especially when those involve multiple steps, have also been elucidated in many instances with the aid of molecular beams.

The level of complexity of the problems tackled with molecular beams has increased over time. Studies on simple reactions such as CO and H_2 oxidations and NO reduction have been extended to systems involving larger organic molecules such as alcohols, organic acids, olefins, and alkanes, among others. The main interest driving these advances has been the desire to better understand heterogeneous catalysis, and that has also required moving away from the use of simple surfaces such as single crystals into more representative models like nanoparticles dispersed on the surfaces of the oxides typically used as catalyst supports. Another theme that has received some consideration is the fact that most catalytic reactions are not high-probability events, and are therefore not easy to emulate unless molecular beams with high fluxes are used. This issue, which is closely related to the so-called "pressure gap" often discussed among researchers in the fields of surface science and catalysis, has been tackled by a few groups already, but still needs to be fully addressed.

Molecular beams have also found use in the study of other problems of practical applications. In this review we have highlighted the extensive work that has been published on the molecular beam characterization of reactions associated with the processing of semiconductor surfaces for microelectronics manufacturing. Much understanding has been developed by using molecular beams in terms of the chemistry of etching and oxidation of those surfaces as well as on the details of the deposition of thin films by chemical means. A few other subjects have been addressed with molecular beams, although here the examples are more limited.

On the whole, it can be said that molecular beams have played a unique and invaluable role in the study of the dynamics and chemical kinetics of reactions on solid surfaces. We owe much to this type of research when it comes to a molecular-level understanding of surface interactions and reactions with gas-phase molecules. On the other hand, it would seem that the golden era of molecular beams in surface-science studies is in the past. Certainly, much of what has been discussed here relates to experiments carried out several decades ago. It could be said, for instance, that the picture that we have nowadays of the dynamics of

adsorption processes relies heavily on studies carried out last century. Some molecular beam work is still ongoing in this area, but not nearly with the same intensity as in years past. It is worth pausing and questioning why this may be.

One answer may very well be that we now have at least an outline of the basic mechanisms associated with adsorption and surface reaction steps, and therefore do not need to continue working in this area with the same vigor as before. This may be true for relatively simple systems, but certainly not for all cases. There is always the possibility of addressing ever more complex surface reaction. These may involve larger and more varied reactants, for instance, molecules that may potentially react by following a series of competitive parallel pathways. The complexity of the surfaces may be increased as well, by adding several elements or a higher degree of topographic variety. Tackling bigger challenges can be envision too, to, for instance, try to emulate reactions in liquid-solid interfaces [574]. The frontiers of kinetic studies in surface chemistry are still quite open.

It may be argued that molecular beam experiments are expensive; the cost may no longer be justifiable. Indeed, modern surface-science instrumentation in general is costly, relatively sophisticated, and difficult to operate, but this is the case in other fields as well. In the end, it comes down to balancing the cost with the potential benefits. Our own biased assessment is that there are still major fundamental questions in surface chemistry highly relevant to modern and important practical applications in need of proper answers. Heterogeneous catalysis is evolving to address more complex chemical systems with a higher degree of selectivity, and new systems inspired on novel nanotechnologies are being introduced to this end [575–579]. New applications in the microelectronics industry such as film growth using chemical means need to address new stringent topographic requirements and the demand for selective surface chemistry to be used in patterning [493,580–583]. Other areas, such as energy conversion and storage, involve at their core central surface chemistry issues [584]. Surface science in general, and molecular beams in particular, should be useful to address these new topics for years and decades to come.

It should also be said that sophisticated supersonic beams with particular excitation and angle-resolved detection schemes have been crucial to extract dynamic information from adsorption and desorption processes but are not required for most chemically-oriented mechanistic studies. In fact, simpler effusive beam arrangements may be better suited to address questions of stoichiometry and selectivity in catalytic processes with complex molecules, for instance. Perhaps something as simple and cheap as a capillary-array based doser may be sufficient to investigate this type of problems. We argue that, chemists at least, should think of retaking this approach to address the problems evolving from the new technologies associated with catalysis, microelectronics applications, energy processing, tribology, electrochemistry, and other areas.

One does need to be aware of the limitations of molecular-beam kinetic measurements, which include the requirement to detect desorbing products; this means that they cannot directly probe any process occurring on the solid surface. There is also the issue of sensitivity: so far, it has been difficult to probe the kinetics of low-probability reactions with molecular beams. In principle mass spectrometry can detect quite low partial pressures of gases and discriminate among different compounds by virtue of their masses (or their cracking patterns in more complex cases [14]), but in practice high partial pressures of background gases, scattering of molecules from surfaces other than the ones being studied, and interference among the cracking patterns of several reactants and products, all reduce the sensitivity of these experiments to perhaps 1% or so of total pressure [17]. This point is crucial, because even so-called facile catalytic reactions typically exhibit reaction probabilities on the order of one conversion per million collisions or less [345]. Luckily, there may be some strategies available to improve sensitivity, such as the use of more selective gas-phase detection methods (e.g., laser ionization techniques), or the application of time-resolved surface detection, even if these may increase cost. On the whole, we believe that the benefits of the knowledge that can be extracted from molecular beam experiments vastly outweigh any shortcomings the technique may have. More researches should engage in this type of work.

Acknowledgements

Financial support for this work has been provided by Grants from the U.S. Department of Energy (DE-SC0008703) and the U.S. National Science Foundation (CHE-1359668).

References

[1] P. Casavecchia, Rep. Prog. Phys. 63 (2000) 355–414.
[2] S.L. Bernasek, G.A. Somorjai, Prog. Surf. Sci. 5 (1975) 377–439.
[3] J.A. Barker, D.J. Auerbach, Surf. Sci. Rep. 4 (1985) 1–99.
[4] C.R. Arumainayagam, R.J. Madix, Prog. Surf. Sci. 38 (1991) 1–102.
[5] K.D. Rendulic, A. Winkler, Surf. Sci. 299 (1994) 261–276.
[6] M.J. Cardillo, Surf. Sci. 299–300 (1994) 277–283.
[7] C.T. Rettner, D.J. Auerbach, J.C. Tully, A.W. Kleyn, J. Phys. Chem. 100 (1996) 13021–13033.
[8] J.C. Tully, Annu. Rev. Phys. Chem. 51 (2000) 153–178.
[9] A.W. Kleyn, Chem. Soc. Rev. 32 (2003) 87–95.
[10] L.B.F. Juurlink, D.R. Killelea, A.L. Utz, Prog. Surf. Sci. 84 (2009) 69–134.
[11] D.C. Jacobs, J. Phys.: Condens. Matter 7 (1995) 1023–1045.
[12] G.O. Sitz, Rep. Prog. Phys. 65 (2002) 1165–1193.
[13] F. Zaera, Int. Rev. Phys. Chem. 21 (2002) 433–471.
[14] J. Wilson, H. Guo, R. Morales, E. Podgornov, I. Lee, F. Zaera, Phys. Chem. Chem. Phys. 9 (2007) 3830–3852.
[15] F. Zaera, in: J. Reedijk, K. Poeppelmeier (Eds.), Comprehensive Inorganic Chemistry II, Oxford, UK, 2013, pp. 39–74.
[16] C.R. Henry, Surf. Sci. Rep. 31 (1998) 235–325.
[17] J. Libuda, H.J. Freund, Surf. Sci. Rep. 57 (2005) 157–298.
[18] G.A. Somorjai, J.Y. Park, Chem. Soc. Rev. 37 (2008) 2155–2162.
[19] T. Matsushima, Prog. Surf. Sci. 82 (2007) 435–477.
[20] P.R. McCabe, L.B.F. Juurlink, A.L. Utz, Rev. Sci. Instrum. 71 (2000) 42–53.
[21] H.C. Chang, W.H. Weinberg, Surf. Sci. 65 (1977) 153–164.
[22] R.J. M.P. D'Evelyn, Madix, Surf. Sci. Rep. 3 (1983) 413–495.
[23] B.N. Eldridge, M.L. Yu, Rev. Sci. Instrum. 58 (1987) 1014–1026.
[24] F. Pradère, M. Château, M. Benslimane, M. Bierry, M. Châtelet, D. Clèment, A. Guilbaud, J.C. Jeannot, A. De Martino, H. Vach, Rev. Sci. Instrum. 65 (1994) 161–173.
[25] S.T. Ceyer, W.J. Siekhaus, G.A. Somorjai, J. Vac. Sci. Technol. 19 (1981) 726–732.
[26] D.F. Padowitz, K.A. Peterlinz, S.J. Sibener, Langmuir 7 (1991) 2566–2673.
[27] G. Scoles, D. Bassi, U. Buck, D.C. Laine (Eds.), Atomic and Molecular Beam Methods, 1, Oxford University Press, New York, 1988.
[28] J. Libuda, Surf. Sci. 587 (2005) 55–68.
[29] M. Bowker, P.D.A. Pudney, C.J. Barnes, J. Vac. Sci. Technol. A 8 (1990) 816–820.
[30] C.T. Campbell, S.M. Valone, J. Vac. Sci. Technol. A 3 (1985) 408–411.
[31] H.P. Steinrück, K.D. Rendulic, Vacuum 36 (1986) 213–215.
[32] A. Winkler, J.T. Yates Jr., J. Vac. Sci. Technol. A 6 (1988) 2929–2932.
[33] D.M. Murphy, J. Vac. Sci. Technol. A 7 (1989) 3075–3091.
[34] J.M. Guevremont, S. Sheldon, F. Zaera, Rev. Sci. Instrum. 71 (2000) 3869–3881.
[35] V.P. Clausing, Z. Phys. 66 (1930) 471–476.
[36] H.C.W. Beijerinck, N.F. Verster, J. Appl. Phys. 46 (1975) 2083–2091.
[37] D.R. Olander, V. Kruger, J. Appl. Phys. 41 (1970) 2769–2776.
[38] C.S. Gopinath, F. Zaera, J. Catal. 200 (2001) 270–287.
[39] K. Roy, R. Jain, C.S. Gopinath, ACS Catal. 4 (2014) 1801–1811.
[40] J.F. Duncan, G.B. Cook, Isotopes in Chemistry, Clarendon Press, Oxford, 1968.
[41] T.I. Taylor, in: P.H. Emmett (Ed.), Catalysis, New York, 1957, pp. 257–403.
[42] A. Ozaki, Isotopic Studies of Heterogeneous Catalysis, Kodansha/Academic Press, Tokyo and New York, 1977.
[43] L.C.S. Melander, W.H. Saunders Jr., Reaction Rates of Isotopic Molecules, Wiley, New York, 1980.
[44] T.V.W. Janssens, G. Jin, F. Zaera, J. Am. Chem. Soc. 119 (1997) 1169–1170.
[45] S.L. Bernasek, G.A. Somorjai, J. Chem. Phys. 62 (1974) 3149–3161.
[46] T. Engel, G. Ertl, in: D.A. King, D.P. Woodruff (Eds.), The Chemical Physics of Solid Surfaces and Heterogeneous Catalysis, Amsterdam, 1982, pp. 195–216.
[47] G. Gumuslu, P. Kondratyuk, J.R. Boes, B. Morreale, J.B. Miller, J.R. Kitchin, A.

J. Gellman, ACS Catal. 5 (2015) 3137–3147.
[48] I. Lee, J. Hong, F. Zaera, J. Phys. Chem. C 115 (2011) 982–989.
[49] Y. Dong, M. Ebrahimi, A. Tillekaratne, F. Zaera, J. Phys. Chem. Lett. 7 (2016) 2439–2443.
[50] P.D.A. Pudney, S.A. Francis, R.W. Joyner, M. Bowker, J. Catal. 131 (1991) 104–114.
[51] H. Öfner, F. Zaera, J. Phys. Chem. B 101 (1997) 396–408.
[52] H. Öfner, F. Zaera, J. Am. Chem. Soc. 124 (2002) 10982–10983.
[53] B. Brandt, J.-H. Fischer, W. Ludwig, J. Libuda, F. Zaera, S. Schauermann, H.-J. Freund, J. Phys. Chem. C 112 (2008) 11408–11420.
[54] B. Brandt, W. Ludwig, J.H. Fischer, J. Libuda, F. Zaera, S. Schauermann, J. Catal. 265 (2009) 191–198.
[55] K.M. Neyman, S. Schauermann, Angew. Chem. Int. Ed. 49 (2010) 4743–4746.
[56] W. Ludwig, A. Savara, S. Schauermann, H.-J. Freund, ChemPhysChem 11 (2010) 2319–2322.
[57] S. Schauermann, N. Nilius, S. Shaikhutdinov, H.-J. Freund, Acc. Chem. Res. 46 (2012) 1673–1681.
[58] F. Zaera, C.S. Gopinath, Chem. Phys. Lett. 332 (2000) 209–214.
[59] D. Tibiletti, A. Goguet, D. Reid, F.C. Meunier, R. Burch, Catal. Today 113 (2006) 94–101.
[60] F. Zaera, C.S. Gopinath, Phys. Chem. Chem. Phys. 5 (2003) 646–654.
[61] P.A. Redhead, Vacuum 12 (1962) 203–211.
[62] D.A. King, Surf. Sci. 47 (1975) 384–402.
[63] D. Menzel, in: R. Gomer (Ed.), Interactions on Metal Surfaces, New York, 1975, pp. 102–143.
[64] Y.X. Li, M. Bowker, J. Catal. 142 (1993) 630–640.
[65] F. Zaera, C.S. Gopinath, J. Chem. Phys. 111 (1999) 8088–8097.
[66] F. Zaera, S. Wehner, C.S. Gopinath, J.L. Sales, V. Gargiulo, G. Zgrablich, J. Phys. Chem. B 105 (2001) 7771–7774.
[67] F. Zaera, C.S. Gopinath, J. Chem. Phys. 116 (2002) 1128–1136.
[68] F. Zaera, J. Liu, M. Xu, J. Chem. Phys. 106 (1997) 4204–4215.
[69] C.S. Gopinath, F. Zaera, J. Catal. 186 (1999) 387–404.
[70] M. Rocca, U. Valbusa, A. Gussoni, G. Maloberti, L. Racca, Rev. Sci. Instrum. 62 (1991) 2172–2176.
[71] J. Libuda, I. Meusel, J. Hartmann, H.-J. Freund, Rev. Sci. Instrum. 71 (2000) 4395–4408.
[72] T. Dellwig, J. Hartmann, J. Libuda, I. Meusel, G. Rupprechter, H. Unterhalt, H. J. Freund, J. Mol. Catal. A: Chem. 162 (2000) 51–66.
[73] J. Libuda, H.J. Freund, J. Phys. Chem. B 106 (2002) 4901–4915.
[74] C.E. Borroni-Bird, D.A. King, Rev. Sci. Instrum. 62 (1991) 2177–2185.
[75] A. Stuck, C.E. Wartnaby, Y.Y. Yeo, J.T. Stuckless, N. Al-Sarraf, D.A. King, Surf. Sci. 349 (1996) 229–240.
[76] W.A. Brown, R. Kose, D.A. King, Chem. Rev. 98 (1998) 797–831.
[77] N. Al-Sarraf, J.T. Stuckless, C.E. Wartnaby, D.A. King, Surf. Sci. 283 (1993) 427–437.
[78] J.T. Stuckless, N. Al-Sarraf, C. Wartnaby, D.A. King, J. Chem. Phys. 99 (1993) 2202–2212.
[79] Y.Y. Yeo, L. Vattuone, D.A. King, J. Chem. Phys. 104 (1996) 3810–3821.
[80] J.T. Stuckless, C.E. Wartnaby, N. Al-Sarra, S.J.B. Dixon-Warren, M. Kovar, D. A. King, J. Chem. Phys. 106 (1997) 2012–2030.
[81] Y.Y. Yeo, L. Vattuone, D.A. King, J. Chem. Phys. 106 (1997) 392–401.
[82] R. Kose, D.A. King, Chem. Phys. Lett. 313 (1999) 1–6.
[83] A.D. Karmazyn, V. Fiorin, S.J. Jenkins, D.A. King, Surf. Sci. 538 (2003) 171–183.
[84] V. Fiorin, D. Borthwick, D.A. King, Surf. Sci. 603 (2009) 1360–1364.
[85] Y.Y. Yeo, A. Stuck, C.E. Wartnaby, R. Kose, D.A. King, J. Mol. Catal. A: Chem. 131 (1998) 31–38.
[86] W.A. Brown, R. Kose, D.A. King, Surf. Sci. 440 (1999) 271–278.
[87] L. Vattuone, Y.Y. Yeo, R. Kose, D.A. King, Surf. Sci. 447 (2000) 1–14.
[88] J.T. Stuckless, N.A. Frei, C.T. Campbell, Rev. Sci. Instrum. 69 (1998) 2427–2438.
[89] M.C. Crowe, C.T. Campbell, Annu. Rev. Anal. Chem. 4 (2011) 41–58.
[90] J.-H. Fischer-Wolfarth, J. Hartmann, J.A. Farmer, J.M. Flores-Camacho, C. T. Campbell, S. Schauermann, H.-J. Freund, Rev. Sci. Instrum. 82 (2011) 024102.
[91] S. Schauermann, T.L. Silbaugh, C.T. Campbell, Chem. Rec. 14 (2014) 759–774.
[92] D.A. King, CRC Crit. Rev. Solid State Mater. Sci. 7 (1978) 167–208.
[93] G.A. Somorjai, Chemistry in Two Dimensions: Surfaces, Cornell University Press, Ithaca, 1981.
[94] G. Comsa, R. David, Surf. Sci. Rep. 5 (1985) 145–198.
[95] C.T. Rettner, M.N.R. Ashfold (Eds.), Dynamics of Gas-Surface Interactions, The Royal Society of Chemistry, Cambridge, 1991.
[96] D.P. Woodruff, T.A. Delchar, Modern Techniques of Surface Science, Cambridge University Press, Cambridge, 1994.
[97] M. Bowker, Appl. Catal. A 160 (1997) 89–98.
[98] J.E. Lennard-Jones, Trans. Faraday Soc. 28 (1932) 333–359.
[99] A. Zangwill, Physics at Surfaces, Cambridge University Press, Cambridge, 1988.
[100] H.P. Steinrück, R.J. Madix, Surf. Sci. 185 (1987) 36–52.
[101] H.J. Robota, W. Vielhaber, M.C. Lin, J. Segner, G. Ertl, Surf. Sci. 155 (1985) 101–120.
[102] A. Mödl, H. Robota, J. Segner, W. Vielhaber, M.C. Lin, G. Ertl, Surf. Sci. 169 (1986) L341–L347.
[103] D.A. King, M.G. Wells, Surf. Sci. 29 (1972) 454–482.
[104] D.A. King, M.G. Wells, Proc. R. Soc. Lond. A: Math. Phys. Eng. Sci. 339 (1974) 245–269.
[105] K.D. Rendulic, G. Anger, A. Winkler, Surf. Sci. 208 (1989) 404–424.
[106] C.T. Rettner, L.A. DeLouise, D.J. Auerbach, J. Chem. Phys. 85 (1986) 1131–1149.
[107] M.D. Williams, D.S. Bethune, A.C. Luntz, J. Chem. Phys. 88 (1988) 2843–2845.
[108] A.V. Hamza, H.P. Steinruck, R.J. Madix, J. Chem. Phys. 86 (1987) 6506–6514.
[109] G. Anger, A. Winkler, K.D. Rendulic, Surf. Sci. 220 (1989) 1–17.
[110] K. Christmann, Surf. Sci. Rep. 9 (1988) 1–163.
[111] U. Harten, J.P. Toennies, C. Wöll, J. Chem. Phys. 85 (1986) 2249–2258.
[112] P.G. Jessop, R.H. Morris, Coord. Chem. Rev. 121 (1992) 155–284.
[113] J. Wang, C.Y. Fan, Q. Sun, K. Reuter, K. Jacobi, M. Scheffler, G. Ertl, Angew. Chem. Int. Ed. 42 (2003) 2151–2154.
[114] G.J. Kubas, Chem. Rev. 107 (2007) 4152–4205.
[115] I.M.N. Groot, H. Ueta, M.J.T.C. van der Niet, A.W. Kleyn, L.B.F. Juurlink, J. Chem. Phys. 127 (2007) 244701.
[116] H.P. Steinrück, K.D. Rendulic, A. Winkler, Surf. Sci. 154 (1985) 99–108.
[117] M. Salmeron, R.J. Gale, G.A. Somorjai, J. Chem. Phys. 67 (1977) 5324–5334.
[118] B. Poelsema, K. Lenz, G. Comsa, J. Chem. Phys. 134 (2011) 074703.
[119] J.N. Russell, S.M. Gates, J.T. Yates, J. Chem. Phys. 85 (1986) 6792–6802.
[120] K.D. Rendulic, A. Winkler, H.P. Steinrück, Surf. Sci. 185 (1987) 469–478.
[121] M. Balooch, M.J. Cardillo, D.R. Miller, R.E. Stickney, Surf. Sci. 46 (1974) 358–392.
[122] M.J. Cardillo, M. Balooch, R.E. Stickney, Surf. Sci. 50 (1975) 263–278.
[123] W.A. Diño, H. Kasai, A. Okiji, Prog. Surf. Sci. 63 (2000) 63–134.
[124] B.E. Hayden, C.L.A. Lamont, Surf. Sci. 243 (1991) 31–42.
[125] H.A. Michelsen, C.T. Rettner, D.J. Auerbach, R.N. Zare, J. Chem. Phys. 98 (1993) 8294–8307.
[126] S.M. McClure, M.I. Reichman, D.C. Seets, P.D. Nolan, G.O. Sitz, C.B. Mullins (in), Chem. Phys. Solid Surfaces (2003) 109–142.
[127] M. Dürr, U. Höfer, Surf. Sci. Rep. 61 (2006) 465–526.
[128] A.C. Luntz, M.D. Williams, D.S. Bethune, J. Chem. Phys. 89 (1988) 4381–4395.
[129] C.T. Rettner, C.B. Mullins, J. Chem. Phys. 94 (1991) 1626–1635.
[130] P. Sjövall, P. Uvdal, J. Vac. Sci. Technol. A 16 (1998) 943–947.
[131] P. Brault, H. Range, J.P. Toennies, J. Chem. Phys. 106 (1997) 8876–8889.
[132] L. Vattuone, M. Rocca, C. Boragno, U. Valbusa, J. Chem. Phys. 101 (1994) 713–725.
[133] D.J. Auerbach, H.E. Pfnür, C.T. Rettner, J.E. Schlaegel, J. Lee, R.J. Madix, J. Chem. Phys. 81 (1984) 2515–2516.
[134] J. Lee, R.J. Madix, J.E. Schlaegel, D.J. Auerbach, Surf. Sci. 143 (1984) 626–638.
[135] H.E. Pfnür, C.T. Rettner, J. Lee, R.J. Madix, D.J. Auerbach, J. Chem. Phys. 85 (1986) 7452–7466.
[136] C.T. Rettner, H. Stein, E.K. Schweizer, J. Chem. Phys. 89 (1988) 3337–3341.
[137] C.T. Rettner, E.K. Schweizer, H. Stein, J. Chem. Phys. 93 (1990) 1442–1454.
[138] P.D. Szuromi, J.R. Engstrom, W.H. Weinberg, J. Phys. Chem. 89 (1985) 2497–5002.
[139] C.T. Rettner, H.E. Pfnür, D.J. Auerbach, Phys. Rev. Lett. 54 (1985) 2716.
[140] S.T. Ceyer, J.D. Beckerle, M.B. Lee, S.L. Tang, Q.Y. Yang, M.A. Hines, J. Vac. Sci. Technol. A 5 (1987) 501–507.
[141] A.V. Hamza, R.J. Madix, Surf. Sci. 179 (1987) 25–46.
[142] M.B. Lee, Q.Y. Yang, S.T. Ceyer, J. Chem. Phys. 87 (1987) 2724–2741.
[143] S.T. Ceyer, Annu. Rev. Phys. Chem. 39 (1988) 479–510.
[144] J.R. Engstrom, D.W. Goodman, W.H. Weinberg, J. Am. Chem. Soc. 110 (1988) 8305–8319.
[145] C.R. Arumainayagam, M.C. McMaster, G.R. Schoofs, R.J. Madix, Surf. Sci. 222 (1989) 213–246.
[146] C.R. Arumainayagam, M.C. McMaster, R.J. Madix, Surf. Sci. 237 (1990) L424–L431.
[147] M.C. McMaster, R.J. Madix, Surf. Sci. 275 (1992) 265–280.
[148] M.C. McMaster, R.J. Madix, Surf. Sci. 294 (1993) 420–428.
[149] M.C. McMaster, R.J. Madix, J. Chem. Phys. 98 (1993) 9963–9976.
[150] W.H. Weinberg, Langmuir 9 (1993) 655–662.
[151] D. Kelly, W.H. Weinberg, J. Chem. Phys. 105 (1996) 271–278.
[152] R.W. Verhoef, D. Kelly, C.B. Mullins, W.H. Weinberg, Surf. Sci. 325 (1995) 93–101.
[153] D. Kelly, W.H. Weinberg, J. Chem. Phys. 105 (1996) 7171–7176.
[154] D. Kelly, W.H. Weinberg, J. Chem. Phys. 105 (1996) 11313–11318.
[155] J.F. Weaver, M.A. Krzyzowski, R.J. Madix, Surf. Sci. 393 (1997) 150–161.
[156] J.F. Weaver, M.A. Krzyzowski, R.J. Madix, J. Chem. Phys. 112 (2000) 396–407.
[157] J.F. Weaver, M. Ikai, A. Carlsson, R.J. Madix, Surf. Sci. 470 (2001) 226–242.
[158] J.F. Weaver, A.F. Carlsson, R.J. Madix, Surf. Sci. Rep. 50 (2003) 107–199.
[159] F. Zaera, Chem. Rev. 95 (1995) 2651–2693.
[160] G.R. Schoofs, C.R. Arumainayagam, M.C. McMaster, R.J. Madix, Surf. Sci. 215 (1989) 1–28.
[161] M. Valden, J. Pere, N. Xiang, M. Pessa, Chem. Phys. Lett. 257 (1996) 289–296.
[162] C.N. Stewart, G. Ehrlich, J. Chem. Phys. 62 (1975) 4672–4782.
[163] P.M. Holmblad, J. Wambach, I. Chorkendorff, J. Chem. Phys. 102 (1995) 8255–8263.
[164] H. Yang, J.L. Whitten, J. Chem. Phys. 96 (1992) 5529–5537.
[165] H. Burghgraef, A.P.J. Jansen, R.A. van Santen, Surf. Sci. 324 (1995) 345–356.
[166] R.W. Verhoef, D. Kelly, C.B. Mullins, W.H. Weinberg, Surf. Sci. 311 (1994) 196–213.
[167] V.A. Ukraintsev, I. Harrison, J. Chem. Phys. 101 (1994) 1564–1581.
[168] C.B. Mullins, W.H. Weinberg, J. Chem. Phys. 92 (1990) 3986–3988.
[169] A.C. Luntz, D.S. Bethune, J. Chem. Phys. 90 (1989) 1274.
[170] C.T. Reeves, D.C. Seets, C.B. Mullins, J. Mol. Catal. A: Chem. 167 (2001) 207–215.
[171] A. Gross, J. Chem. Phys. 102 (1995) 5045–5058.
[172] S. Titmuss, A. Wander, D.A. King, Chem. Rev. 96 (1996) 1291–1306.
[173] G. Comelli, V.R. Dhanak, M. Kiskinova, K.C. Prince, R. Rosei, Surf. Sci. Rep. 32 (1998) 165–231.

[174] A. Hopkinson, D.A. King, Chem. Phys. 177 (1993) 433–452.
[175] S.J. Dixon-Warren, A.T. Pasteur, D.A. King, J. Chem. Phys. 103 (1995) 2261–2271.
[176] A.T. Pasteur, S.J. Dixon-Warren, D.A. King, J. Chem. Phys. 103 (1995) 2251–2260.
[177] T. Ali, A.V. Walker, B. Klötzer, D.A. King, Surf. Sci. 414 (1998) 304–314.
[178] S.L. Bernasek, W.J. Siekhaus, G.A. Somorjai, Phys. Rev. Lett. 30 (1973) 1202–1204.
[179] R.J. Gale, M. Salmeron, G.A. Somorjai, Phys. Rev. Lett. 38 (1977) 1027–1029.
[180] M. Salmerón, R.J. Gale, G.A. Somorjai, J. Chem. Phys. 70 (1979) 2807–2818.
[181] T.H. Lin, G.A. Somorjai, J. Chem. Phys. 81 (1984) 704–709.
[182] A.T. Gee, B.E. Hayden, C. Mormiche, T.S. Nunney, J. Chem. Phys. 112 (2000) 7660–7668.
[183] I.M.N. Groot, K.J.P. Schouten, A.W. Kleyn, L.B.F. Juurlink, J. Chem. Phys. 129 (2008) 224707.
[184] R.A. Olsen, L.B.F. Juurlink, in: R. Díez Muiño, H.F. Busnengo (Eds.), Dynamics of Gas-Surface Interactions: Atomic-level Understanding of Scattering Processes at Surfaces, Berlin, 2013, pp. 101–129.
[185] B. Poelsema, L.K. Verheij, G. Comsa, Surf. Sci. 152 (1985) 496–504.
[186] C. Hahn, J. Shan, Y. Liu, O. Berg, A.W. Kleijn, L.B.F. Juurlink, J. Chem. Phys. 136 (2012) 114201.
[187] I.M.N. Groot, A.W. Kleyn, L.B.F. Juurlink, J. Phys. Chem. C 117 (2013) 9266–9274.
[188] H.P. Steinrück, M. Luger, A. Winkler, K.D. Rendulic, Phys. Rev. B 32 (1985) 5032–5037.
[189] H. Karner, M. Luger, H.P. Steinrück, A. Winkler, K.D. Rendulic, Surf. Sci. 163 (1985) L641–L644.
[190] K.D. Rendulic, A. Winkler, Int. J. Mod. Phys. B 3 (1989) 941–972.
[191] A.T. Yinnon, R. Kosloff, R.B. Gerber, B. Poelsema, G. Comsa, J. Chem. Phys. 88 (1988) 3722–3731.
[192] B. Poelsema, G. Comsa, Faraday Discuss. Chem. Soc. 80 (1985) 247–256.
[193] B. Poelsema, R.L. Palmer, G. Comsa, Surf. Sci. 123 (1982) 152–164.
[194] T.H. Lin, G.A. Somorjai, Surf. Sci. 107 (1981) 573–585.
[195] A.T. Gee, B.E. Hayden, J. Chem. Phys. 113 (2000) 10333–10343.
[196] P. Gambardella, Ž. Šljivančanin, B. Hammer, M. Blanc, K. Kuhnke, K. Kern, Phys. Rev. Lett. 87 (2001) 056103.
[197] A.T. Gee, B.E. Hayden, C. Mormiche, A.W. Kleyn, B. Riedmüller, J. Chem. Phys. 118 (2003) 3334–3341.
[198] H. Hou, Y. Huang, S.J. Gulding, C.T. Rettner, D.J. Auerbach, A.M. Wodtke, Science 284 (1999) 1647–1650.
[199] R.W. Verhoef, D. Kelly, C.B. Mullins, W.H. Weinberg, Surf. Sci. 291 (1993) L719–L724.
[200] L.B.F. Juurlink, P.R. McCabe, R.R. Smith, C.L. DiCologero, A.L. Utz, Phys. Rev. Lett. 83 (1999) 868–871.
[201] L.B.F. Juurlink, R.R. Smith, A.L. Utz, J. Phys. Chem. B 104 (2000) 3327–3336.
[202] J.D. Beckerle, Q.Y. Yang, A.D. Johnson, S.T. Ceyer, J. Chem. Phys. 86 (1987) 7236–7237.
[203] J.D. Beckerle, A.D. Johnson, Q.Y. Yang, S.T. Ceyer, J. Chem. Phys. 91 (1989) 5756–5777.
[204] L. Vattuone, L. Savio, F. Pirani, D. Cappelletti, M. Okada, M. Rocca, Prog. Surf. Sci. 85 (2010) 92–160.
[205] M. Okada, Chem. Rec. 14 (2014) 775–790.
[206] A.T. Pasteur, S.J. Dixon-Warren, Q. Ge, D.A. King, J. Chem. Phys. 106 (1997) 8896–8904.
[207] M. Gostein, G.O. Sitz, J. Chem. Phys. 106 (1997) 7378–7390.
[208] S. Jaatinen, J. Blomqvist, P. Salo, A. Puisto, M. Alatalo, M. Hirsimäki, M. Ahonen, M. Valden, Phys. Rev. B 75 (2007) 075402.
[209] M.G. Tenner, E.W. Kuipers, W.Y. Langhout, A.W. Kleyn, G. Nicolasen, S. Stolte, Surf. Sci. 236 (1990) 151–168.
[210] M. Kurahashi, Y. Yamauchi, Phys. Rev. Lett. 110 (2013) 246102.
[211] M. Kurahashi, Prog. Surf. Sci. 91 (2016) 29–55.
[212] O. Michio, M. Kousuke, G. Seishiro, K. Toshio, Jpn. J. Appl. Phys. 44 (2005) 8580.
[213] T.J. Curtiss, R.B. Bernstein, Chem. Phys. Lett. 161 (1989) 212–218.
[214] T.J. Curtiss, R.S. Mackay, R.B. Bernstein, J. Chem. Phys. 93 (1990) 7387–7405.
[215] D. Cappelletti, A. Gerbi, F. Pirani, M. Rocca, M. Scotoni, L. Vattuone, U. Valbusa, Phys. Scr. 73 (2006) C20.
[216] G. Doyen, in: W. Schommers, P.V. Blanckenhagen (Eds.), Topics in Current Physics, Berlin, 1987, pp. 301–346.
[217] T.E. Madey, Surf. Sci. 33 (1972) 355–376.
[218] J. Liu, M. Xu, T. Nordmeyer, F. Zaera, J. Phys. Chem. 99 (1995) 6167–6175.
[219] I. Langmuir, J. Am. Chem. Soc. 40 (1918) 1361–1402.
[220] J.M. Thomas, W.J. Thomas, Introduction to the Principles of Heterogeneous Catalysis, Academic Press, London, 1967.
[221] P. Kisliuk, J. Phys. Chem. Solids 3 (1957) 95–101.
[222] M.A. Morris, M. Bowker, D.A. King, in: C.H. Bamford, C.F.H. Tipper, R.G. Compton (Eds.), Comprehensive Chemical Kinetics, Amsterdam, 1984, pp. 1–179.
[223] M.P. D'Evelyn, H.-P. Steinrück, R.J. Madix, Surf. Sci. 180 (1987) 47–76.
[224] C.R. Arumainayagam, M.C. McMaster, R.J. Madix, J. Phys. Chem. 95 (1991) 2461–2465.
[225] A. Gerbi, L. Vattuone, L. Savio, M. Rocca, J. Chem. Phys. 122 (2005) 134701.
[226] A.F. Carlsson, R.J. Madix, Surf. Sci. 479 (2001) 98–108.
[227] V.P. Zhdanov, Surf. Sci. 111 (1981) 63–79.
[228] J.N. Russell, I. Chorkendorff, A.M. Lanzillotto, M.D. Alvey, J.T. Yates, J. Chem. Phys. 85 (1986) 6186–6191.
[229] K.A. Peterlinz, T.J. Curtiss, S.J. Sibener, J. Chem. Phys. 95 (1991) 6972–6985.
[230] K.J. Wu, S.D. Kevan, J. Chem. Phys. 95 (1991) 5355–5363.
[231] S.D. Kevan, J. Mol. Catal. A: Chem. 131 (1998) 19–30.
[232] G. Zgrablich, J.L. Sales, R. Unac, V.P. Zhdanov, Surf. Sci. 290 (1993) 163–171.
[233] F. Zaera, Acc. Chem. Res. 35 (2002) 129–136.
[234] M. Silverberg, A. Ben-Shaul, J. Chem. Phys. 87 (1987) 3178–3194.
[235] T. Nordmeyer, F. Zaera, Chem. Phys. Lett. 183 (1991) 195–198.
[236] O.M. Becker, J. Chem. Phys. 96 (1992) 5488–5496.
[237] A.P.J. Jansen, Comput. Phys. Commun. 86 (1995) 1–12.
[238] J.L. Riccardo, W.A. Steele, A.J.R. Cuesta, G. Zgrablich, Langmuir 13 (1997) 1064–1072.
[239] E.W. Hansen, M. Neurock, Chem. Eng. Sci. 54 (1999) 3411–3421.
[240] V.P. Zhdanov, Surf. Sci. Rep. 45 (2002) 231–326.
[241] A. Chatterjee, D.G. Vlachos, J. Comp. Aided Mater. Des. 14 (2007) 253–308.
[242] B. Temel, H. Meskine, K. Reuter, M. Scheffler, H. Metiu, J. Chem. Phys. 126 (2007).
[243] H. Jónsson, Proc. Natl. Acad. Sci. USA 108 (2011) 944–949.
[244] D. Stacchiola, L. Burkholder, W.T. Tysoe, J. Am. Chem. Soc. 124 (2002) 8984–8989.
[245] D. Stacchiola, L. Burkholder, T. Zheng, M. Weinert, W.T. Tysoe, J. Phys. Chem. B 109 (2005) 851–856.
[246] I. Lee, F. Zaera, J. Phys. Chem. B 109 (2005) 12920–12926.
[247] I. Lee, F. Zaera, J. Am. Chem. Soc. 128 (2006) 8890–8898.
[248] I. Lee, Z. Ma, S. Kaneko, F. Zaera, J. Am. Chem. Soc. 130 (2008) 14597–14604.
[249] S. Karakalos, T.J. Lawton, F.R. Lucci, E.C.H. Sykes, F. Zaera, J. Phys. Chem. C 117 (2013) 18588–18594.
[250] A.D. Gordon, S. Karakalos, F. Zaera, Surf. Sci. 629 (2014) 3–10.
[251] M. Bowker, D.A. King, J. Chem. Soc. Faraday Trans. 1 (75) (1979) 2100–2115.
[252] S. Karakalos, J. Hong, F. Zaera, Angew. Chem. Int. Ed., 55, (2016) 6225–6228.
[253] S. Karakalos, F. Zaera, J. Phys. Chem. C 119 (2015) 13785–13790.
[254] T. Engel, G. Ertl, in: D.D. Eley, H. Pines, P.B. Weisz (Eds.), Adv. Catal., New York, 1979, pp. 1–78.
[255] T. Engel, G. Ertl, in: D.A. King, D.P. Woodruff (Eds.), The Chemical Physics of Solid Surfaces and Heterogeneous Catalysis, Amsterdam, 1982, pp. 73–93.
[256] J.A. Fair, R.J. Madix, J. Chem. Phys. 73 (1980) 3486–3491.
[257] C.T. Campbell, G. Ertl, H. Kuipers, J. Segner, J. Chem. Phys. 73 (1980) 5862–5873.
[258] M. Bowker, Q. Guo, R.W. Joyner, Surf. Sci. 280 (1993) 50–62.
[259] T. Engel, G. Ertl, J. Chem. Phys. 69 (1978) 1267–1281.
[260] T. Engel, G. Ertl, Chem. Phys. Lett. 54 (1978) 95–98.
[261] A. Böttcher, H. Niehus, S. Schwegmann, H. Over, G. Ertl, J. Phys. Chem. B 101 (1997) 11185–11191.
[262] R.L. Palmer, J.N. Smith, J. Chem. Phys. 60 (1974) 1453–1463.
[263] C.A. Becker, J.P. Cowin, L. Wharton, D.J. Auerbach, J. Chem. Phys. 67 (1977) 3394–3395.
[264] M. Bowker, Q. Guo, Y. Li, R.W. Joyner, Catal. Lett. 18 (1993) 119–123.
[265] I.Z. Jones, R.A. Bennett, M. Bowker, Surf. Sci. 439 (1999) 235–248.
[266] J. Segner, C.T. Campbell, G. Doyen, G. Ertl, Surf. Sci. 138 (1984) 505–523.
[267] J.L. Gland, E.B. Kollin, J. Chem. Phys. 78 (1983) 963–974.
[268] E.M. Stuve, R.J. Madix, C.R. Brundle, Surf. Sci. 146 (1984) 155–178.
[269] H. Conrad, G. Ertl, J. Küppers, Surf. Sci. 76 (1978) 323–342.
[270] J. Liu, M. Xu, F. Zaera, Catal. Lett. 37 (1996) 9–13.
[271] M. Xu, J. Liu, F. Zaera, J. Chem. Phys. 104 (1996) 8825–8828.
[272] S. Nagarajan, K. Thirunavukkarasu, C.S. Gopinath, J. Phys. Chem. C 113 (2009) 7385–7397.
[273] K. Thirunavukkarasu, S. Nagarajan, C.S. Gopinath, Appl. Surf. Sci. 256 (2009) 443–448.
[274] C.S. Gopinath, K. Roy, S. Nagarajan, ChemCatChem 7 (2015) 588–594.
[275] R.A. Bennett, I.Z. Jones, M. Bowker, Top. Catal. 42 (2007) 373–376.
[276] G. Ertl, Surf. Sci. 152 (1985) 328–337.
[277] D.A. King, in: G.F. Froment, K.C. Waugh (Eds.), Stud. Surf. Sci. Catal., 1997, pp. 79–89.
[278] V.V. Gorodetskii, A.V. Matveev, E.A. Podgornov, F. Zaera, Top. Catal. 32 (2005) 17–28.
[279] N. Pacia, J.A. Dumesic, J. Catal. 41 (1976) 155–167.
[280] J.N. Smith, R.L. Palmer, J. Chem. Phys. 56 (1972) 13–20.
[281] G.E. Gdowski, R.J. Madix, Surf. Sci. 119 (1982) 184–206.
[282] D.F. Padowitz, S.J. Sibener, Surf. Sci. 254 (1991) 125–143.
[283] B.E. Hayden, C.L.A. Lamont, J. Phys. : Condens. Matter 1 (1989) SB33.
[284] T. Engel, H. Kuipers, Surf. Sci. 90 (1979) 181–196.
[285] S.T. Ceyer, W.L. Guthrie, T.H. Lin, G.A. Somorjai, J. Chem. Phys. 78 (1983) 6982–6991.
[286] H. Permana, K.Y.S. Ng, C.H.F. Peden, S.J. Schmieg, D.K. Lambert, D.N. Belton, J. Catal. 164 (1996) 194–206.
[287] G.S. Herman, C.H.F. Peden, S.J. Schmieg, D.N. Belton, Catal. Lett. 62 (1999) 131–138.
[288] C. Hess, E. Ozensoy, D.W. Goodman, J. Phys. Chem. B 107 (2003) 2759–2764.
[289] W.A. Brown, R.K. Sharma, D.A. King, S. Haq, J. Phys. Chem. 100 (1996) 12559–12568.
[290] M. Brandt, H. Müller, G. Zagatta, N. Böwering, U. Heinzmann, Surf. Sci. 352–354 (1996) 290–294.
[291] M. Brandt, G. Zagatta, N. Böwering, U. Heinzmann, Surf. Sci. 385 (1997) 346–356.
[292] F. Zaera, Surf. Sci. 500 (2002) 947–965.
[293] M. Aryafar, F. Zaera, J. Catal. 175 (1998) 316–327.
[294] F. Zaera, C.S. Gopinath, J. Mol. Catal. A: Chem. 167 (2001) 23–31.

[295] F. Zaera, Prog. Surf. Sci. 69 (2001) 1–98.
[296] C.S. Gopinath, F. Zaera, J. Phys. Chem. B 104 (2000) 3194–3203.
[297] F. Zaera, J. Phys. Chem. B 106 (2002) 4043–4052.
[298] F. Zaera, J. Phys.: Condens. Matter 16 (2004) S2299–S2310.
[299] V. Bustos, C.S. Gopinath, R. Uñac, F. Zaera, G. Zgrablich, J. Chem. Phys. 114 (2001) 10927–10931.
[300] V. Bustos, R. Uñac, F. Zaera, G. Zgrablich, J. Chem. Phys. 118 (2003) 9372–9379.
[301] L.A. Avalos, V. Bustos, R. Uñac, F. Zaera, G. Zgrablich, J. Mol. Catal. A: Chem. 228 (2005) 89–95.
[302] L.A. Avalos, V. Bustos, R. Uñac, F. Zaera, G. Zgrablich, J. Phys. Chem. B 110 (2006) 24964–24971.
[303] F. Zaera, J.L. Sales, M.V. Gargiulo, M. Ciacera, G. Zgrablich, J. Phys. Chem. C 111 (2007) 7795–7800.
[304] S. Wehner, M.T. Paffett, F. Zaera, J. Phys. Chem. B 108 (2004) 18683–18692.
[305] R.O. Uñac, V. Bustos, J. Wilson, G. Zgrablich, F. Zaera, J. Chem. Phys. 125 (2006) 074705.
[306] M. Bowker, Q. Guo, R.W. Joyner, Catal. Today 10 (1991) 409–412.
[307] M. Bowker, Q. Guo, Y. Li, R.W. Joyner, J. Chem. Soc. Faraday Trans. 91 (1995) 3663–3670.
[308] Y. Li, M. Bowker, Surf. Sci. 348 (1996) 67–76.
[309] K. Thirunavukkarasu, K. Thirumoorthy, J. Libuda, C.S. Gopinath, J. Phys. Chem. B 109 (2005) 13272.
[310] K. Thirunavukkarasu, K. Thirumoorthy, J. Libuda, C.S. Gopinath, J. Phys. Chem. B 109 (2005) 13283.
[311] S. Nagarajan, K. Thirunavukkarasu, C.S. Gopinath, J. Phys. Chem. C 115 (2011) 21299–21310.
[312] R.G. Sharpe, M. Bowker, Surf. Sci. 360 (1996) 21–30.
[313] M. Bowker, R.A. Bennett, I.Z. Jones, Top. Catal. 28 (2004) 25–30.
[314] H. Uetsuka, N. Mizutani, H. Hayashi, H. Onishi, K. Kunimori, Catal. Lett. 69 (2000) 165–168.
[315] D.A. Hoffman, J.B. Hudson, Surf. Sci. 180 (1987) 77–88.
[316] F. Steinbach, J. Schütte, Surf. Sci. 88 (1979) 498–516.
[317] S.N. Foner, R.L. Hudson, J. Chem. Phys. 80 (1984) 518–523.
[318] W.L. Guthrie, J.D. Sokol, G.A. Somorjai, Surf. Sci. 109 (1981) 390–418.
[319] J.M. Bradley, A. Hopkinson, D.A. King, Surf. Sci. 371 (1997) 255–263.
[320] M. Asscher, W.L. Guthrie, T.H. Lin, G.A. Somorjai, J. Phys. Chem. 88 (1984) 3233–3238.
[321] J.M. Bradley, A. Hopkinson, D.A. King, J. Phys. Chem. 99 (1995) 17032–17042.
[322] K. Roy, C.S. Gopinath, ChemCatChem 6 (2014) 531–537.
[323] K. Roy, R. Jain, M.K. Ghosalya, K. Prabhakar Reddy, C.S. Gopinath, Comptes Rendus Chim. 19 (2016) 1363–1369.
[324] F. Steinbach, H.-J. Spengler, Surf. Sci. 104 (1981) 318–340.
[325] G.E. Gdowski, J.A. Fair, R.J. Madix, Surf. Sci. 127 (1983) 541–554.
[326] I.E. Wachs, R.J. Madix, Surf. Sci. 65 (1977) 287–313.
[327] I.E. Wachs, R.J. Madix, J. Catal. 61 (1980) 310–315.
[328] S.C. Dahlberg, G.A. Fisk, R.R. Rye, J. Catal. 36 (1975) 224–234.
[329] F. Steinbach, V. Hausen, Surf. Sci. 62 (1977) 504–518.
[330] J.N. Russell Jr., I. Chorkendorf, J.T. Yates Jr., Surf. Sci. 183 (1987) 316–330.
[331] S.M. Francis, F.M. Leibsle, S. Haq, N. Xiang, M. Bowker, Surf. Sci. 315 (1994) 284–292.
[332] M. Bowker, Top. Catal. 3 (1996) 461–468.
[333] M.K. Weldon, C.M. Friend, Chem. Rev. 96 (1996) 1391–1412.
[334] Z. Ma, F. Zaera, Surf. Sci. Rep. 61 (2006) 229–281.
[335] M. Bowker, R.A. Bennett, S. Poulston, P. Stone, Catal. Lett. 56 (1998) 77–83.
[336] M. Bowker, S. Poulston, R.A. Bennett, P. Stone, A.H. Jones, S. Haq, P. Hollins, J. Mol. Catal. A: Chem. 131 (1998) 185.
[337] T.G.A. Youngs, S. Haq, M. Bowker, Surf. Sci. 602 (2008) 1775–1782.
[338] M. Bowker, L. Gilbert, J. Counsell, C. Morgan, J. Phys. Chem. C 114 (2010) 17142–17147.
[339] M. Bowker, C. Morgan, J. Couves, Surf. Sci. 555 (2004) 145–156.
[340] C. Morgan, M. Bowker, Surf. Sci. 603 (2009) 54–59.
[341] R.P. Holroyd, M. Bowker, Surf. Sci. 377 (1997) 786–790.
[342] M. Bowker, R. Holroyd, N. Perkins, J. Bhantoo, J. Counsell, A. Carley, C. Morgan, Surf. Sci. 601 (2007) 3651–3660.
[343] M. Bowker, L. Cookson, J. Bhantoo, A. Carley, E. Hayden, L. Gilbert, C. Morgan, J. Counsell, P. Yaseneva, Appl. Catal. A 391 (2011) 394–399.
[344] S. Nagarajan, K. Thirunavukkarasu, C.S. Gopinath, J. Counsell, L. Gilbert, M. Bowker, J. Phys. Chem. C 113 (2009) 9814–9819.
[345] F. Zaera, Phys. Chem. Chem. Phys. 15 (2013) 11988–12003.
[346] F. Zaera, Catal. Lett. 91 (2003) 1–10.
[347] F. Zaera, Top. Catal. 34 (2005) 129–141.
[348] F. Zaera, Langmuir 12 (1996) 88–94.
[349] J. Simonovis, A. Tillekaratne, F. Zaera, J. Phys. Chem. C (2017).
[350] F. Zaera, Isr. J. Chem. 38 (1998) 293–311.
[351] F. Zaera, T.V.W. Janssens, H. Öfner, Surf. Sci. 368 (1996) 371–376.
[352] F. Zaera, Mol. Phys. 100 (2002) 3065–3073.
[353] F. Zaera, Appl. Catal. A 229 (2002) 75–91.
[354] F. Zaera, C.R. French, J. Am. Chem. Soc. 121 (1999) 2236–2243.
[355] T.V.W. Janssens, F. Zaera, J. Phys. Chem. 100 (1996) 14118.
[356] K. Christmann, G. Ertl, T. Pignet, Surf. Sci. 54 (1976) 365–392.
[357] T.V.W. Janssens, F. Zaera, Surf. Sci. 344 (1995) 77–84.
[358] A.F. Carlsson, R.J. Madix, J. Chem. Phys. 115 (2001) 8074–8082.
[359] F. Zaera, Chem. Rec. 5 (2005) 133–144.
[360] W.T. Tysoe, G.L. Nyberg, R.M. Lambert, J. Phys. Chem. 88 (1984) 1960–1963.
[361] H. Hoffmann, F. Zaera, R.M. Ormerod, R.M. Lambert, L.P. Wang, W.T. Tysoe, Surf. Sci. 232 (1990) 259–265.
[362] H. Hoffmann, F. Zaera, R.M. Ormerod, R.M. Lambert, J.M. Yao, D.K. Saldin, L. P. Wang, D.W. Bennett, W.T. Tysoe, Surf. Sci. 268 (1992) 1–10.
[363] R.M. Ormerod, R.M. Lambert, H. Hoffmann, F. Zaera, J.M. Yao, D.K. Saldin, L. P. Wang, D.W. Bennett, W.T. Tysoe, Surf. Sci. 295 (1993) 277–286.
[364] M. Bowker, C. Morgan, N. Perkins, R. Holroyd, E. Fourre, F. Grillo, A. MacDowall, J. Phys. Chem. B 109 (2005) 2377–2386.
[365] S. Ohno, M. Wilde, K. Mukai, J. Yoshinobu, K. Fukutani, J. Phys. Chem. C 120 (2016) 11481–11489.
[366] A.V. Walker, D.A. King, J. Phys. Chem. B 104 (2000) 6462–6467.
[367] D.T.P. Watson, J.J.W. Harris, D.A. King, Surf. Sci. 505 (2002) 58–70.
[368] K. Kunimori, T. Iwade, H. Uetsuka, J. Electron Spectrosc. Relat. Phenom. 64–65 (1993) 451–459.
[369] H. Uetsuka, K. Watanabe, T. Iwade, K. Kunimori, J. Chem. Soc. Faraday Trans. 91 (1995) 1801–1804.
[370] T. Sasaki, K. Nakao, K. Tomishige, K. Kunimori, Chem. Commun. (2006) 3821–3823.
[371] T. Sasaki, K. Nakao, K. Tomishige, K. Kunimori, Appl. Catal. A 328 (2007) 140–149.
[372] J.N. Wilson, R.A. Pedigo, F. Zaera, J. Am. Chem. Soc. 130 (2008) 15796–15797.
[373] J.N. Wilson, F. Zaera, J. Phys. Chem. C 114 (2010) 16946–16954.
[374] K.A. Williams, R. Horn, L.D. Schmidt, AIChE J. 53 (2007) 2097–2113.
[375] L. Bobrova, N. Vernikovskaya, V. Sadykov, Catal. Today 144 (2009) 185–200.
[376] T.P. St Clair, D.W. Goodman, Top. Catal. 13 (2000) 5–19.
[377] H.J. Freund, N. Ernst, T. Risse, H. Hamann, G. Rupprechter, Phys. Status Solidi 187 (2001) 257–274.
[378] A. Molenbroek, S. Helveg, H. Topsøe, B. Clausen, Top. Catal. 52 (2009) 1303–1311.
[379] F. Gao, D.W. Goodman, Annu. Rev. Phys. Chem. 63 (2012) 265–286.
[380] J. Hoffmann, I. Meusel, J. Hartmann, J. Libuda, H.J. Freund, J. Catal. 204 (2001) 378–392.
[381] J. Libuda, I. Meusel, J. Hoffmann, J. Hartmann, L. Piccolo, C.R. Henry, H. J. Freund, J. Chem. Phys. 114 (2001) 4669–4684.
[382] V. Johánek, M. Laurin, J. Hoffmann, S. Schauermann, A.W. Grant, B. Kasemo, J. Libuda, H.J. Freund, Surf. Sci. 561 (2004) L218–L224.
[383] J. Hoffmann, S. Schauermann, J. Hartmann, V.P. Zhdanov, B. Kasemo, J. Libuda, H.J. Freund, Chem. Phys. Lett. 354 (2002) 403–408.
[384] M. Baumer, J. Libuda, K.M. Neyman, N. Rosch, G. Rupprechter, H.-J. Freund, Phys. Chem. Chem. Phys. 9 (2007) 3541–3558.
[385] T. Schalow, B. Brandt, M. Laurin, S. Schauermann, J. Libuda, H.J. Freund, J. Catal. 242 (2006) 58–70.
[386] B. Brandt, T. Schalow, M. Laurin, S. Schauermann, J. Libuda, H.J. Freund, J. Phys. Chem. C 111 (2007) 938–949.
[387] M. Laurin, V. Johánek, A.W. Grant, B. Kasemo, J. Libuda, H.-J. Freund, J. Chem. Phys. 122 (2005) 084713.
[388] M. Laurin, V. Johánek, A.W. Grant, B. Kasemo, J. Libuda, H.J. Freund, J. Chem. Phys. 123 (2005) 054701.
[389] V. Johánek, M. Laurin, A.W. Grant, B. Kasemo, C.R. Henry, J. Libuda, Science 304 (2004) 1639–1644.
[390] O. Meerson, G. Sitja, C.R. Henry, Eur. Phys. J. D 34 (2005) 119–124.
[391] M.A. Röttgen, S. Abbet, K. Judai, J.-M. Antonietti, A.S. Wörz, M. Arenz, C. R. Henry, U. Heiz, J. Am. Chem. Soc. 129 (2007) 9635–9639.
[392] U. Heiz, E.L. Bullock, J. Mater. Chem. 14 (2004) 564–577.
[393] C. Becker, C.R. Henry, Surf. Sci. 352 (1996) 457–462.
[394] L. Piccolo, C. Becker, C.R. Henry, Eur. Phys. J. D – At. Mol. Opt. Plasma Phys. 9 (1999) 415–419.
[395] L. Piccolo, C.R. Henry, Appl. Surf. Sci. 162 (2000) 670–678.
[396] L. Piccolo, C.R. Henry, J. Mol. Catal. A: Chem. 167 (2001) 181–190.
[397] G. Prévot, O. Meerson, L. Piccolo, C.R. Henry, J. Phys.: Condens. Matter 14 (2002) 4251–4269.
[398] K. Judai, S. Abbet, A.S. Wörz, U. Heiz, C.R. Henry, J. Am. Chem. Soc. 126 (2004) 2732–2737.
[399] S. Schauermann, V. Johánek, M. Laurin, J. Libuda, H.J. Freund, Phys. Chem. Chem. Phys. 5 (2003) 5139.
[400] V. Johánek, S. Schauermann, M. Laurin, C.S. Gopinath, J. Libuda, H.J. Freund, J. Phys. Chem. B 108 (2004) 14244–14254.
[401] M. Bowker, P. Stone, R. Bennett, N. Perkins, Surf. Sci. 511 (2002) 435–448.
[402] S. Schauermann, J. Hoffmann, V. Johánek, J. Hartmann, J. Libuda, H.-J. Freund, Angew. Chem. Int. Ed. 41 (2002) 2532–2535.
[403] S. Schauermann, J. Hoffmann, V. Johánek, J. Hartmann, J. Libuda, H.-J. Freund, Catal. Lett. 84 (2002) 209–217.
[404] I. Lee, F. Delbecq, R. Morales, M.A. Albiter, F. Zaera, Nat. Mater. 8 (2009) 132–138.
[405] I. Lee, F. Zaera, J. Catal. 269 (2010) 359–366.
[406] I. Lee, F. Zaera, Top. Catal. 56 (2013) 1284–1298.
[407] M. Wilde, K. Fukutani, W. Ludwig, B. Brandt, J.H. Fischer, S. Schauermann, H. J. Freund, Angew. Chem. Int. Ed. 47 (2008) 9289–9293.
[408] S.L. Tait, Z. Dohnálek, C.T. Campbell, B.D. Kay, Surf. Sci. 591 (2005) 90–107.
[409] A.S. Crampton, M.D. Rotzer, C.J. Ridge, F.F. Schweinberger, U. Heiz, B. Yoon, U. Landman, Nat. Commun. 7 (2016).
[410] A.S. Crampton, M.D. Rötzer, F.F. Schweinberger, B. Yoon, U. Landman, U. Heiz, J. Catal. 333 (2016) 51–58.
[411] M. Ebrahimi, J.P. Simonovis, F. Zaera, J. Phys. Chem. Lett. 5 (2014) 2121–2125.
[412] P. Stoltze, J.K. Nørskov, Phys. Rev. Lett. 55 (1985) 2502–2505.
[413] G.A. Somorjai, Y. Li, Proc. Natl. Acad. Sci. USA 108 (2011) 917–924.
[414] B. Kasemo, Rev. Sci. Instrum. 50 (1979) 1602–1604.

[415] M.V. Kurepa, C.B. Lucas, J. Appl. Phys. 52 (1981) 664–669.
[416] W.H. Weinberg, E.W. McFarland, P. Cong, S. Guan, Mass Spectrometers and Methods for Rapid Screening of Libraries of Different Materials, USA, 1999.
[417] M. Johansson, J.H. Jørgensen, I. Chorkendorff, Rev. Sci. Instrum. 75 (2004) 2082–2093.
[418] M. Johansson, T. Johannessen, J.H. Jørgensen, I. Chorkendorff, Appl. Surf. Sci. 252 (2006) 3673–3685.
[419] M. Johansson, E. Skúlason, G. Nielsen, S. Murphy, R.M. Nielsen, I. Chorkendorff, Surf. Sci. 604 (2010) 718–729.
[420] E.M. Fiordaliso, S. Murphy, R.M. Nielsen, S. Dahl, I. Chorkendorff, Surf. Sci. 606 (2012) 263–272.
[421] E.M. Fiordaliso, S. Dahl, I. Chorkendorff, J. Phys. Chem. C 116 (2012) 5773–5780.
[422] E.M. Fiordaliso, S. Dahl, I. Chorkendorff, J. Phys. Chem. C 115 (2011) 25351–25358.
[423] S.B. Vendelbo, M. Johansson, J.H. Nielsen, I. Chorkendorff, Phys. Chem. Chem. Phys. 13 (2011) 4486–4493.
[424] Y. Dong, M. Ebrahimi, A. Tillekaratne, J.P. Simonovis, F. Zaera, Phys. Chem. Chem. Phys., 18, 2016, 19248-19258.
[425] A. Tilekaratne, J.P. Simonovis, M.F. López Fagúndez, M. Ebrahimi, F. Zaera, ACS Catal. 2 (2012) 2259–2268.
[426] Y. Dong, F. Zaera, Catal. Sci. Technol. (2017), submitted for publication.
[427] B. Jandeleit, D.J. Schaefer, T.S. Powers, H.W. Turner, W.H. Weinberg, Angew. Chem. Int. Ed. 38 (1999) 2494–2532.
[428] P.G. Schultz, X. Xiang, I. Goldwasser, Combinatorial screening of inorganic and organometallic materials USA, Symyx Technologies, Inc. (Santa Clara, CA), The Regents of University of California (Oakland, CA), 2002. US Patent No. 6,410,331.
[429] I. Willson, Richard C., Catalyst Testing Process with in Situ Synthesis, USA, University of Houston, Texas (Houston, TX), 2003. US Patent No. 6,514,764.
[430] P. Cong, R.D. Doolen, Q. Fan, D.M. Giaquinta, S. Guan, E.W. McFarland, D. M. Poojary, K. Self, H.W. Turner, W.H. Weinberg, Angew. Chem. Int. Ed. 38 (1999) 484–488.
[431] A. Guram, A. Hagemeyer, C.G. Lugmair, H.W. Turner, A.F. Volpe, W. H. Weinberg, K. Yaccato, Adv. Synth. Catal. 346 (2004) 215–230.
[432] P. Cong, A. Dehestani, R. Doolen, D.M. Giaquinta, S. Guan, V. Markov, D. Poojary, K. Self, H. Turner, W.H. Weinberg, Proc. Natl. Acad. Sci. USA 96 (1999) 11077–11080.
[433] Y. Liu, P. Cong, R.D. Doolen, H.W. Turner, W.H. Weinberg, Catal. Today 61 (2000) 87–92.
[434] A. Hagemeyer, A. Lesik, G. Streukens, A.F. Volpe Jr, H.W. Turner, W.H. Weinberg, K. Yaccato, C. Brooks, Comb. Chem. High Throughput Screening,10 2007, 135-147.
[435] K. Yaccato, A. Hagemeyer, A. Lesik, A. Volpe, H. Weinberg, Top. Catal. 30 (2004) 127–132.
[436] K. Yaccato, R. Carhart, A. Hagemeyer, A. Lesik, P. Strasser, A.F. Volpe Jr, H. Turner, H. Weinberg, R.K. Grasselli, C. Brooks, Appl. Catal. A 296 (2005) 30–48.
[437] C. Brooks, et al., Top. Catal. 38 (2006) 195–209.
[438] H.W. Turner, A.F. Volpe Jr, W.H. Weinberg, Surf. Sci. 603 (2009) 1763–1769.
[439] P. Kondratyuk, G. Gumuslu, S. Shukla, J.B. Miller, B.D. Morreale, A.J. Gellman, J. Catal. 300 (2013) 55–62.
[440] J.R. Kitchin, A.J. Gellman, AIChE J. 62 (2016) 3826–3835.
[441] R.J. Madix, J.A. Schwarz, Surf. Sci. 24 (1971) 264–287.
[442] M.L. Yu, L.A. DeLouise, Surf. Sci. Rep. 19 (1994) 285–380.
[443] P. Bond, P.N. Brier, J. Fletcher, W.J. Jia, H. Price, P.A. Gorry, Surf. Sci. 418 (1998) 181–209.
[444] K. Suzuki, S. Hiraoka, S. Nishimatsu, J. Appl. Phys. 64 (1988) 3697–3705.
[445] K. Suzuki, S. Hiraoka, J. Appl. Phys. 77 (1995) 6624–6629.
[446] A. Szabó, P.D. Farrall, T. Engel, J. Appl. Phys. 75 (1994) 3623–3626.
[447] Y. Teraoka, I. Nishiyama, Appl. Phys. Lett. 63 (1993) 3355–3357.
[448] G.C. Weaver, S.R. Leone, Surf. Sci. 328 (1995) 197–214.
[449] T. Yuden, N. Iwao, Jpn. J. Appl. Phys. 33 (1994) 2240.
[450] A. Szabò, T. Engel, J. Vac. Sci. Technol. A 12 (1994) 648–657.
[451] S. Keizo, N. Ken, N. Shigeru, O. Osami, Jpn. J. Appl. Phys. 25 (1986) L373.
[452] S. Keizo, N. Ken, N. Shigeru, O. Osami, Jpn. J. Appl. Phys. 26 (1987) 166.
[453] J.R. Holt, R.C. Hefty, M.R. Tate, S.T. Ceyer, J. Phys. Chem. B 106 (2002) 8399–8406.
[454] M.J.M. Vugts, M.F.A. Eurlings, L.J.F. Hermans, H.C.W. Beijerinck, J. Vac. Sci. Technol. A 14 (1996) 2780–2789.
[455] M.J.M. Vugts, G.L.J. Verschueren, M.F.A. Eurlings, L.J.F. Hermans, H.C. W. Beijerinck, J. Vac. Sci. Technol. A 14 (1996) 2766–2774.
[456] G.S. Hwang, C.M. Anderson, M.J. Gordon, T.A. Moore, T.K. Minton, K.P. Giapis, Phys. Rev. Lett. 77 (1996) 3049–3052.
[457] K. Kazuhiro, M. Jiro, H. Kei, Jpn. J. Appl. Phys. 33 (1994) 2252.
[458] Y. Teraoka, I. Nishiyama, J. Appl. Phys. 79 (1996) 4397–4401.
[459] G.P. Kota, J.W. Coburn, D.B. Graves, J. Appl. Phys. 85 (1999) 74–86.
[460] K. Kunihiko, Y. Yu, S. Takehiko, S. Toshio, N. Satoshi, A. Takaaki, M. Jiro, Appl. Phys. Express 3 (2010) 126501.
[461] L.A. DeLouise, J. Chem. Phys. 94 (1991) 1528–1542.
[462] L.A. DeLouise, J. Vac. Sci. Technol. A 9 (1991) 1732–1736.
[463] S. Chaochin, X. Ming, D. Zi-Guo, M.F. Vernon, B.E. Bent, Surf. Sci. 282 (1993) 357–370.
[464] P. Bond, P.N. Brier, J. Fletcher, P.A. Gorry, M.E. Pemble, Chem. Phys. Lett. 208 (1993) 269–275.
[465] Hq Hou, Z. Zhang, S. Chen, C. Su, W. Yan, M. Vernon, Appl. Phys. Lett. 55 (1989) 801–803.
[466] J.H. Schmid, T. Tiedje, R. Mar, A. Ballestad, Phys. Rev. B 70 (2004) 045315.
[467] J. Essex-Lopresti, W. Jia, S. Munro, P.A. Gorry, Phys. Chem. Chem. Phys. 2 (2000) 925–933.
[468] H. Fang, J. Eng, C. Su, S. Vemuri, I.P. Herman, B.E. Bent, Langmuir 14 (1998) 1375–1378.
[469] C. Su, Z.G. Dai, W. Luo, D.H. Sun, M.F. Vernon, B.E. Bent, Surf. Sci. 312 (1994) 181–197.
[470] M. Ozeki, M. Tomikawa, N. Onitsuka, Mater. Sci. Eng.: B 165 (2009) 107–110.
[471] W. Morimichi, I. Takashi, A. Keijiro, N. Shogo, I. Takahiro, S. Hiroaki, S. Kyoichi, S. Kosuke, Jpn. J. Appl. Phys. 42 (2003) L356.
[472] M. Watanabe, Y. Mori, T. Ishikawa, H. Sakai, T. Iida, K. Akiyama, S. Narita, K. Sawabe, K. Shobatake, J. Vac. Sci. Technol. A 23 (2005) 1647–1656.
[473] T. Engel, Surf. Sci. Rep. 18 (1993) 93–144.
[474] Y.J. Chabal (Ed.), Fundamental Aspects of Silicon Oxidation, Springer-Verlag, Berlin, 2001.
[475] M.P. D'Evelyn, M.M. Nelson, T. Engel, Surf. Sci. 186 (1987) 75–114.
[476] T. Miyake, S. Soeki, H. Kato, T. Nakamura, A. Namiki, H. Kamba, T. Suzaki, Phys. Rev. B 42 (1990) 11801–11807.
[477] T. Miyake, S. Soeki, H. Kato, T. Nakamura, A. Namiki, H. Kamba, T. Suzaki, Surf. Sci. 242 (1991) 386–393.
[478] W.A. Harrison, Surf. Sci. 55 (1976) 1–19.
[479] G. Binnig, H. Rohrer, C. Gerber, E. Weibel, Phys. Rev. Lett. 50 (1983) 120–123.
[480] U. Memmert, M.L. Yu, Chem. Phys. Lett. 164 (1989) 552–556.
[481] U. Memmert, Y. Ming L, Surf. Sci. 245 (1991) L185–L189.
[482] M.L. Yu, B.N. Eldridge, Phys. Rev. Lett. 58 (1987) 1691–1694.
[483] K. Ohkubo, Y. Igari, S. Tomoda, I. Kusunoki, Surf. Sci. 260 (1992) 44–52.
[484] J.R. Engstrom, D.J. Bonser, M.M. Nelson, T. Engel, Surf. Sci. 256 (1991) 317–343.
[485] H.-J. Ernst, M.L. Yu, Phys. Rev. B 41 (1990) 12953–12956.
[486] J.R. Engstrom, T. Engel, Phys. Rev. B 41 (1990) 1038–1041.
[487] R.J. Madix, A.A. Susu, Surf. Sci. 20 (1970) 377–400.
[488] R.J. Madix, R. Parks, A.A. Susu, J.A. Schwarz, Surf. Sci. 24 (1971) 288–301.
[489] D.A. Hansen, J.B. Hudson, Surf. Sci. 292 (1993) 17–32.
[490] D.A. Hansen, J.B. Hudson, Surf. Sci. 254 (1991) 222–234.
[491] K. Sugiyama, Y. Igari, I. Kusunoki, Surf. Sci. 283 (1993) 64–69.
[492] M. Leskelä, M. Ritala, Angew. Chem. Int. Ed. 42 (2003) 5548–5554.
[493] S.M. George, Chem. Rev. 110 (2010) 111–131.
[494] F. Zaera, Coord. Chem. Rev., 257, (2013) 3177–3191.
[495] E.H.C. Parker (Ed.), The Technology and Physics of Molecular Beam Epitaxy, Springer, New York, 1985.
[496] M.A. Herman, H. Sitter, Molecular Beam Epitaxy: Fundamentals and Current Status, Springer-Verlag, Berlin, 1996.
[497] J.R. Arthur, Surf. Sci. 500 (2002) 189–217.
[498] B.A. Joyce, J.H. Neave, B.E. Watts, Surf. Sci. 15 (1969) 1–13.
[499] B.A. Joyce, Rep. Prog. Phys. 37 (1974) 363.
[500] H. Hirayama, T. Tatsumi, A. Ogura, N. Aizaki, Appl. Phys. Lett. 51 (1987) 2213–2215.
[501] R.J. Buss, P. Ho, W.G. Breiland, M.E. Coltrin, J. Appl. Phys. 63 (1988) 2808–2819.
[502] S.M. Gates, Surf. Sci. 195 (1988) 307–329.
[503] H. Hirayama, T. Tatsumi, N. Aizaki, Appl. Phys. Lett. 52 (1988) 1484–1486.
[504] J.M. Jasinski, S.M. Gates, Acc. Chem. Res. 24 (1991) 9–15.
[505] M.K. Farnaam, D.R. Olander, Surf. Sci. 145 (1984) 390–406.
[506] S.K. Kulkarni, S.M. Gates, B.A. Scott, H.H. Sawin, Surf. Sci. 239 (1990) 13–25.
[507] L.Q. Xia, M.E. Jones, N. Maity, J.R. Engstrom, J. Vac. Sci. Technol. A 13 (1995) 2651–2664.
[508] J.R. Engstrom, L.Q. Xia, M.J. Furjanic, D.A. Hansen, Appl. Phys. Lett. 63 (1993) 1821–1823.
[509] J.R. Engstrom, D.A. Hansen, M.J. Furjanic, L.Q. Xia, J. Chem. Phys. 99 (1993) 4051–4054.
[510] L.Q. Xia, M.E. Jones, N. Maity, J.R. Engstrom, J. Chem. Phys. 103 (1995) 1691–1701.
[511] M.E. Jones, L.Q. Xia, N. Maity, J.R. Engstrom, Chem. Phys. Lett. 229 (1994) 401–407.
[512] S.E. Roadman, N. Maity, J.N. Carter, J.R. Engstrom, J. Vac. Sci. Technol. A 16 (1998) 3423–3433.
[513] N. Maity, L.Q. Xia, S.E. Roadman, J.R. Engstrom, Surf. Sci. 344 (1995) 203–220.
[514] N. Maity, L.Q. Xia, S.E. Roadman, J.R. Engstrom, Surf. Sci. 344 (1995) L1201–L1206.
[515] Y.J. Zheng, J.R. Engstrom, J. Zhang, A. Schellinger, B.A. Joyce, Surf. Sci. 470 (2000) 131–140.
[516] M.E. Jones, S.E. Roadman, A.M. Lam, G. Eres, J.R. Engstrom, J. Chem. Phys. 105 (1996) 7140–7151.
[517] A.M. Lam, Y.J. Zheng, J.R. Engstrom, Surf. Sci. 393 (1997) 205–221.
[518] T.W. Schroeder, A.M. Lam, P.F. Ma, J.R. Engstrom, J. Vac. Sci. Technol. A 22 (2004) 578–593.
[519] H.M. Manasevit, W.I. Simpson, J. Electrochem. Soc. 116 (1969) 1725–1732.
[520] G.B. Stringfellow, Organometallic Vapor-Phase Epitax: Theory and Practice, Academic Press, New York, 1998.
[521] T. Martin, C.R. Whitehouse, J. Cryst. Growth 105 (1990) 57–68.
[522] S. Masahiro, Y. Seikoh, Jpn. J. Appl. Phys. 33 (1994) L884.
[523] M. Sasaki, S. Yoshida, Appl. Surf. Sci. 121 (1997) 73–79.
[524] G. Eres, Crit. Rev. Solid State Mater. Sci. 23 (1998) 275–322.
[525] M. Ohashi, M. Ozeki, J. Cui, Rev. Sci. Instrum. 70 (1999) 4037–4043.
[526] R. Souda, M.L. Yu, Surf. Sci. 280 (1993) 115–124.

[527] M. Sasaki, S. Yoshida, Surf. Sci. 315 (1994) L964–L968.
[528] M. Sasaki, S. Yoshida, Surf. Sci. 356 (1996) 233–246.
[529] M. Sasaki, S. Yoshida, Appl. Surf. Sci. 82 (1994) 269–275.
[530] U. Memmert, M.L. Yu, Appl. Phys. Lett. 56 (1990) 1883–1885.
[531] E.M. Gibson, C.T. Foxon, J. Zhang, B.A. Joyce, J. Cryst. Growth 105 (1990) 81–86.
[532] J.R. Creighton, K.R. Lykke, V.A. Shamamian, B.D. Kay, Appl. Phys. Lett. 57 (1990) 279–281.
[533] M.L. Yu, J. Appl. Phys. 73 (1993) 716–725.
[534] N.I. Buchan, M.L. Yu, Surf. Sci. 280 (1993) 383–392.
[535] B.A. Banse, J.R. Creighton, Surf. Sci. 257 (1991) 221–229.
[536] J.S. Foord, N.K. Singh, E.T. FitzGerald, G.J. Davies, A.C. Jones, J. Cryst. Growth 120 (1992) 103–113.
[537] J.R. Arthur Jr., J. Appl. Phys. 39 (1968) 4032–4034.
[538] J.R. Arthur, Surf. Sci. 43 (1974) 449–461.
[539] B. Galiana, M. Benedicto, L. Díez-Merino, S. Lorbek, G. Hlawacek, C. Teichert, P. Tejedor, J. Chem. Phys. 139 (2013) 164712.
[540] J. Cui, M. Ozeki, M. Ohashi, Appl. Phys. Lett. 70 (1997) 2177–2179.
[541] M. Ozeki, J. Cui, M. Ohashi, Appl. Surf. Sci. 112 (1997) 110–117.
[542] B. Jalan, P. Moetakef, S. Stemmer, Appl. Phys. Lett. 95 (2009) 032906.
[543] Shogo Imada, Takuya Kuraoka, Eisuke Tokumitsu, Hiroshi Ishiwara, Jpn. J. Appl. Phys. 40 (2001) 666.
[544] J.H. Lee, et al., Nat. Mater. 13 (2014) 879–883.
[545] Z. Yu, et al., J. Vac. Sci. Technol. B18 (2000) 1653–1657.
[546] B.A. Ferguson, C.B. Mullins, J. Cryst. Growth 178 (1997) 134–146.
[547] A.J. McGinnis, D. Thomson, R.F. Davis, E. Chen, A. Michel, H.H. Lamb, Surf. Sci. 494 (2001) 28–42.
[548] A.J. McGinnis, D. Thomson, A. Banks, E. Preble, R.F. Davis, H.H. Lamb, J. Vac. Sci. Technol. A 21 (2003) 294–301.
[549] I. Kusunoki, M. Hiroi, T. Sato, Y. Igari, S. Tomoda, Appl. Surf. Sci. 45 (1990) 171–187.
[550] E.C. Sanchez, S.J. Sibener, J. Phys. Chem. B 106 (2002) 8019–8028.
[551] M.F. Danışman, L. Casalis, G. Scoles, Phys. Rev. B 72 (2005) 085404.
[552] J.E. Goose, A. Killampalli, P. Clancy, J.R. Engstrom, J. Phys. Chem. C 113 (2009) 6068–6073.
[553] T.V. Desai, S. Hong, A.R. Woll, K.J. Hughes, A.P. Kaushik, P. Clancy, J. R. Engstrom, J. Chem. Phys. 134 (2011) 224702.
[554] T. Kim, F. Zaera, J. Phys. Chem. C 115 (2011) 8240–8247.
[555] A. Dube, M. Sharma, P.F. Ma, J.R. Engstrom, Appl. Phys. Lett. 89 (2006) 164108.
[556] A. Dube, M. Sharma, P.F. Ma, P.A. Ercius, D.A. Muller, J.R. Engstrom, J. Phys. Chem. C 111 (2007) 11045–11058.
[557] P.F. Ma, A. Dube, A.S. Killampalli, J.R. Engstrom, J. Chem. Phys. 125 (2006) 034706.
[558] P.F. Ma, T.W. Schroeder, J.R. Engstrom, Appl. Phys. Lett. 80 (2002) 2604–2606.
[559] R. Scott Smith, T. Zubkov, B.D. Kay, J. Chem. Phys. 124 (2006) 114710.
[560] T. Zubkov, R.S. Smith, T.R. Engstrom, B.D. Kay, J. Chem. Phys. 127 (2007) 184707.
[561] R.S. Smith, T. Zubkov, Z. Dohnálek, B.D. Kay, J. Phys. Chem. B 113 (2009) 4000–4007.
[562] P. Ayotte, P. Marchand, J.L. Daschbach, R.S. Smith, B.D. Kay, J. Phys. Chem. A 115 (2011) 6002–6014.
[563] C.T. Campbell, O. Lytken, Surf. Sci. 603 (2009) 1365–1372.
[564] J.R.V. Sellers, T.E. James, S.L. Hemmingson, J.A. Farmer, C.T. Campbell, Rev. Sci. Instrum. 84 (2013) 123901.
[565] C.T. Campbell, J.R.V. Sellers, Chem. Rev. 113 (2013) 4106–4135.
[566] J.F. Zhu, S.F. Diaz, L.R. Heeb, C.T. Campbell, Surf. Sci. 574 (2005) 34–42.
[567] S.L. Hemmingson, T.E. James, G.M. Feeley, A.M. Tilson, C.T. Campbell, J. Phys. Chem. C 120 (2016) 12113–12124.
[568] T.E. James, S.L. Hemmingson, T. Ito, C.T. Campbell, J. Phys. Chem. C 119 (2015) 17209–17217.
[569] T.E. James, S.L. Hemmingson, C.T. Campbell, ACS Catal. 5 (2015) 5673–5678.
[570] J.C. Sharp, Y.X. Yao, C.T. Campbell, J. Phys. Chem. C 117 (2013) 24932–24936.
[571] J.A. Farmer, C.T. Campbell, Science 329 (2010) 933–936.
[572] C.T. Campbell, J.C. Sharp, Y.X. Yao, E.M. Karp, T.L. Silbaugh, Faraday Discuss. 152 (2011) 227–239.
[573] C.T. Campbell, Acc. Chem. Res. 46 (2013) 1712–1719.
[574] F. Zaera, Chem. Rev. 112 (2012) 2920–2986.
[575] M.J. Climent, A. Corma, S. Iborra, Chem. Rev. 111 (2010) 1072–1133.
[576] C. Detavernier, J. Dendooven, S. Pulinthanathu Sree, K.F. Ludwig, J.A. Martens, Chem. Soc. Rev. 40 (2011) 5242–5253.
[577] F. Zaera, Chem. Soc. Rev. 42 (2013) 2746–2762.
[578] F. Zaera, ChemSusChem 6 (2013) 1797–1820.
[579] E. Gross, G.A. Somorjai, J. Catal. 328 (2015) 91–101.
[580] M. Leskelä, M. Ritala, O. Nilsen, MRS Bull. 36 (2011) 877–884.
[581] F. Zaera, J. Phys. Chem. Lett. 3 (2012) 1301–1309.
[582] A.J.M. Mackus, A.A. Bol, W.M.M. Kessels, Nanoscale 6 (2014) 10941–10960.
[583] R.W. Johnson, A. Hultqvist, S.F. Bent, Mater. Today 17 (2014) 236–246.
[584] J.W. Elam, N.P. Dasgupta, F.B. Prinz, MRS Bull. 36 (2011) 899–906.
[585] G.A. Somorjai, Surf. Sci. 89 (1979) 496–524.
[586] G.A. Somorjai, J. Phys. Chem. 94 (1990) 1013–1023.
[587] A. Gerbi, L. Vattuone, M. Rocca, U. Valbusa, F. Pirani, D. Cappelletti, F. Vecchiocattivi, J. Chem. Phys. 123 (2005) 224709.
[588] K.A. Williams, L.D. Schmidt, Appl. Catal. A 299 (2006) 30–45.